contrary to the generally accepted double paracrine loop.
In addition, invasion/chemotaxis of cancer cells into 3D matrigel was determined using LOC devices. Results showed that normal and cancer cells can be quantitatively differentiated based on their invasion/chemotaxis phenotypes as determined by confocal fluorescence microscopy imaging.
What's more, a LOC device and method was optimized to evaluate extravasation of normal and cancer cells. Results showed that normal and cancer cells can be quantitatively differentiated based on their extravasation phenotypes as determined by confocal fluorescence microscopy imaging.
Furthermore, using LOC devices, homing choices of breast cancer and liver cancer cells were determined. As expected, the former and the latter preferred lung and liver, respectively. Current work using patient derived circulating tumor cells suggests homing choices can be predicted using LOC devices comprising microenvironments mimicking target tissues.
Finally, a novel anti-cancer drug candidate was tested with 3D tri-culture in LOC devices comprising breast cancer cells, normal epithelial cells and macrophages. Results showed that the novel drug caused 60% less cell death in normal cells compared to the widely used drug doxorubicin in 3D tri-culture whereas both drugs had a similar effect on cell death in 3D mono-culture.
Taken together these results demonstrate the importance of 3D cell culture in LOC devices for physiologically relevant results that can be translated to the clinic.
Keywords: cancer, lab-on-a-chip, invasion, chemotaxis, metastasis.

IS-44

MICROFLUIDIC SYSTEMS FOR STEM CELL AND ORGANOID CULTURE

Sinan Güven
Izmir Biomedicine and Genome Center, İzmir, Turkey

In vitro microphysiological platforms can host and maturate stem cell derived engineered human tissues. Such platforms provide novel research venues for life sciences by mimicking the native tissue architecture, biophysical environment and functionality. Advances in stem cell research enable the in vitro recapitulation of human organogenesis and let the generation of functional tissue models called organoids. Today, combination of on-chip microfluidic systems with stem cell technologies create many organ models such as lung, gut, brain, liver, kidney and stomach, which can be connected to form human-on-a-chip systems. Translation of these platforms to clinical settings promises effective disease models, test beds for toxicology and diagnosis. This talk covers fundamental aspects of on-chip system design and integration with stem cell research.
Keywords: induced pluripotent stem cell, organoid, microfluidic system, organ-on-a-chip, bioengineering

ORAL PRESENTATION FULL TEXTS & ABSTRACTS

OP-01

INVESTIGATION OF EPIDERMAL GROWTH FACTOR RECEPTOR (*EGFR*) PATHWAY RELATED, EXOSOMAL MIRNAS IN NON-SMALL CELL LUNG CANCER (NSCLC) CASES

Altug Koc[1, 2], Levent Pelit[3], Asim Leblebici[2], Gizem Calibasi Kocal[2], Haydar Soydane Karakus[4], Ceyda Aldag[4], Tuncay Goksel[4], Yasemin Basbinar[2]
[1]Department of Medical Genetics, Faculty of Medicine, Dokuz Eylul University Izmir, Turkey
[2]Department of Translational Oncology, Institute of Oncology, Dokuz Eylul University Izmir, Turkey
[3]Department of Chemistry, Faculty of Science, Ege University, Izmir, Turkey
[4]Department of Pulmonary Medicine, Faculty of Medicine, Ege University, Izmir, Turkey

OBJECTIVES: Recently, *EGFR* gene and its related pathways become an important issue for precision medicine practice in NSCLC cases. In the presence of activating somatic mutations of *EGFR* gene, which synthesize a thyrosine kinase, targeted use of "thyrosine kinase inhibitors" ameliorates the "progression free survival" rates. Exosomes are microvesicles that have content similar to tumor itself. DNA content of exosomes is used in the studies of somatic mutations. Recent efforts revealed the possible association between *EGFR* pathways related miRNAs and the somatic mutations. In the presented study, exosomes are used for liquid biopsy approach.
MATERIALS AND METHODS: We wish to investigate, exosomal *EGFR* pathway related 4 miRNAs (miR-30b, miR-30c, miR-221-3p, miR-22-3p and miR-1288 as control) which are defined in literature previously and if possible their correlation with somatic mutations and clinical findings. Thirty-two samples from distinct NSCLC cases are analyzed. Exosomes are derived from peripheral blood plasma of the patients; miRNA extraction, cDNA synthesis, real-time quantitative PCR are done and Δ/Δ Ct method is used for relative quantification.
RESULTS: The control miR1288 is expressed in all of the samples except one. Two of the miRNAs (miR-30b, miR-221-3p) produce weak PCR curves but because of inadequate amount of isolated miRNA, they are discarded from the study. The rest of the miRNAs (miR-30c, miR-22-3p) produced PCR curves.
CONCLUSIONS: The exosomal miR-30c, miR-22-3p are successfully derived from plasma of NSCLC cases and they seems to be potential biomarkers for these patients.
Keywords: *EGFR*, exosome, miRNA, Non-small Cell Lung Cancer (NSCLC)

INTRODUCTION
All over the world, the lung cancer is the leading one among cancer deaths. According to the World Health Organization data, about 2 million new lung cancer cases are diagnosed each year [1]. In our country, the incidence of lung cancer is 29,314. More than 90% of these cases are males and their mean age is 60 years. About 47% of the cases are in advanced stage of disease at the time of diagnosis. Majority of them (80,7%) are Non-Small Cell Lung Cancer (NSCLC) [24531 patients (63.0%]. New treatment strategies targeting the tumor genotype enables the precision medicine. The major biomarkers for the NSCLC are the driver mutations of *EGFR, ALK, MET, ROS1* and *KRAS* genes. Epidermal Growth Factor Receptor (*EGFR*) gene mutations are seen in 15% of the NSCLC cases. The deletions of exon 19 and L858R mutation in *EGFR* gene increase the tyrosine kinase activity this gene. The drugs (erlotinib, gefitinib, afatinib) targeting these mutations are increases "progression free survival" [3]. The secondary *EGFR* mutations (T790M) are responsible for the acquired drug resistance in the 50% of the cases [4MET gene amplification is reported to occur in a subset of adenocarcinomas. Although somatic mutations of MET in lung adenocarcinomas are rare, all but one of those reported so far entail a splice mutation deleting the juxtamembrane domain for binding the c-Cbl E3-ligase; normally such binding leads to ubiquitination and receptor degradation, and loss of this domain leads to MET activation. The purpose of this study was to clarify in the role of MET activation in lung carcinogenesis. MATERIALS AND METHODS MET gene copy number was determined by real-time quantitative polymerase chain reaction in 187 of the patients with lung cancer and the MET gene splice mutation deleting the juxtamembrane domain was examined by direct sequencing in 262. The results were correlated with various clinical and pathologic features including mutations of the epidermal growth factor receptor, KRAS, and HER2 genes. RESULTS All the instances of MET activation occurred in patients with adenocarcinomas. The

prevalences of MET gene amplification and splice mutations were 1.4% (2 of 148]. Investigation of *EGFR* mutations becomes the routine practice in advanced stage NSCLC cases.

The liquid biopsy, as a new term, refers to four main approaches: Cell-free DNA (cfDNA) [Circulating tumor DNA (ctDNA)], Circulating tumor cells (CTCs), Tumor-educated platelets (TEPs), Extracellular vesicles (EVs). Particularly exosomes, as a subclass of EVs, are interesting because of their tumor derived nature and their stability in plasma [5]. Many cell types secret exosomes as membrane vesicles 40-150nm in diameter. They can be found in plasma, serum, saliva, urine, amniotic fluid and malignant ascites samples. Recently, there are evidences supporting that these vesicles act as messengers and the tumor cells communicate with distant tissues by exosomes. The exosomes are able to change the function and the physiology of target tissues and they have specific proteins, lipids and nucleic acids that could serve their purposes. The secreted exosomes have pleiotropic effects related with tumor progression, angiogenesis, immunomodulation, horizontal transfer, drug resistance [6]. They behave as a genetic cargo; especially their miRNA content participates in genesis of premetastatic niche [7]. It is proposed that the miRNA content of exosomes may be influenced by *EGFR* mutations and they could be used as NSCLC cases [8]. So, we wish to investigate, exosomal *EGFR* pathway related 4 miRNAs (miR-30b, miR-30c, miR-221-3p, miR-22-3p and miR-1288 as control) in advanced stage NSCLC cases who are tested for *EGFR* mutations via liquid biopsy.

MATERIALS AND METHODS

There are 4 *EGFR* pathway related miRNA targets are selected for the investigation: miR-30b, miR-30c, miR-221-3p, mir-22-3p. As internal controls miR-1228 and SNORD48 (house keeping gene) are used.

Study Group

The study group is consisted of NCSCL cases who are investigated for *EGFR* mutations by liquid and solid biopsy, and followed in "Department of Pulmonary Medicine, Ege University Hospital; Genetic Daignosis Center, Tepecik Training and Research Hospital, Health Sciences University".

Sample Collection and RNA Isolation

The blood samples of the cases are derived by phlebotomy and their plasmas are separated in 24 hours. The plasma samples are stored in -80ºC until exosome isolation. In a stepwise manner exosome isolation, miRNA isolation, cDNA synthesis are done by commercial kits according to the protocols of producer (Norgen, Canada).

Real-Time PCR (Q-PCR);

The cDNA samples are diluted at 80 folds. The "LightCycler® 480 SYBR Green I Master" (Roche Molecular Systems) is used for PCR reaction with specific primers for the target miRNAs and the control genes. Δ/Δ Ct method is used for normalization of miRNA Ct values and relative quantitation.

RESULTS

The control miR1288 is expressed in all of the samples except one; SNORD48 is failed in seven cases. Therefore, miR1288 seems to be a good control for exosomal miRNA studies. Two of the targeted miRNAs (miR-30b, miR-221-3p) produce weak PCR curves but due to inadequate amount of isolated miRNA, they are discarded from the study. However, if the initial miRNA is increased, probably we could obtain proper PCR curves for them and they will be potential biomarkers. The rest of the miRNAs (miR-30c, miR-22-3p) produced PCR curves and their mean Ct values are 38.4 for miR-30c and 30.8 for miR-22-3p. As a conclusion, the exosomal miR-30c, miR-22-3p are successfully derived from plasma of NSCLC cases, they seems to be potential biomarkers for these patients, and our efforts are ongoing to identify their correlation with *EGFR* mutations and clinical findings.

ACKNOWLEDGEMENTS

None.

CONFLICT OF INTEREST

Authors declare that there is no conflict of interest for the presented study.

REFERENCES

1. Sabaila A, Fauconnier A, Huchon C. Chimiothérapie intrapéritonéale pressurisée en aérosol (CIPPA): Une nouvelle voie d'administration dans les carcinoses péritonéales d'origine ovarienne. Gynecol Obstet Fertil. 2015; 43(1):66–7.
2. Prognostic factors affecting survival in cases with lung cancer [A lung cancer mapping project in Turkey (LCMPT)]. European Respiratory Journal. 2013. p. P2920.
3. Lee CK, Brown C, Gralla RJ, Hirsh V, Thongprasert S, Tsai C-M, et al. Impact of EGFR Inhibitor in Non–Small Cell Lung Cancer on Progression-Free and Overall Survival: A Meta-Analysis. JNCI J Natl Cancer Inst. 2013; 105(9):595–605.
4. Onozato R, Kosaka T, Kuwano H, Sekido Y, Yatabe Y, Mitsudomi T. Activation of MET by gene amplification or by splice mutations deleting the juxtamembrane domain in primary resected lung cancers. J Thorac Oncol. 2009; 4(1):5–11.
5. Reclusa P, Sirera R, Araujo A, Giallombardo M, Valentino A, Sorber L, et al. Exosomes genetic cargo in lung cancer: A truly Pandora's box. Translational Lung Cancer Research. 2016.
6. Taverna S, Giallombardo M, Gil-Bazo I, Carreca AP, Castiglia M, Chacártegui J, et al. Exosomes isolation and characterization in serum is feasible in non-small cell lung cancer patients: Critical analysis of evidence and potential role in clinical practice. Oncotarget. 2016; 7(19):28748–60.
7. Nuzhat Z, Kinhal V, Sharma S, Rice GE, Joshi V, Salomon C. Tumour-derived exosomes as a signature of pancreatic cancer - liquid biopsies as indicators of tumour progression. Oncotarget. 2017; 8(10):17279-17291.
8. Rolfo C, Chacartegui J, Giallombardo M, Alessandro R, Peeters M. 71P Exosomes isolated in plasma of non-small cell lung cancer patients contain microRNA related to the EGFR pathway: Proof of concept. J Thorac Oncol. 2016; 11(4):S85.

OP-02

INVESTIGATION OF SURFACE ADHESION ABILITIES OF MCF-7 CELLS ON 3D PRINTED PCL AND PLA SCAFFOLD MODELS

R.B.Husemoglu[1], B.Nalbant[2], O.Gonul Geyik[3], T.Unek[4], Z.Yuce[3], H.Havitcioglu[5]

[1]Dokuz Eylul University, Institute Of Health Science, Department Of Biomechanic, Izmir, Turkey

[2]Dokuz Eylul University, Institute Of Health Science, Department Of Molecular Medicine, Izmir, Turkey

[3]Dokuz Eylul University, Faculty of Medicine, Department of Medical Biology and Genetics, Izmir, Turkey

[4]Dokuz Eylul University, Faculty Of Medicine, Surgery Medicine, Department Of General Surgery, Izmir, Turkey

[5]Dokuz Eylul University, Faculty Of Medicine, Surgery Medicine, Department Of Orthopedics and Traumatology, Izmir, Turkey

OBJECTIVES: Tissue scaffolds are usually rigid structures made of polymeric materials.Biocompatibility and biodegradability are important properties for scaffold materials to possess, ensuring they support for cell growth and are extremely useful in in vitro 3D cell cultures.2D in vitro studies do not provide the desired success in in vivo applications.Tissue scaffolds are 3Dcell culture systems that eliminate this problem with breast cancer cell culture.The main objective of this study was to produce biocompatible and suitable porosity scaffolds from PLA and PCL materials, which enables MCF-7breast cancer cells to proliferate in 3D

MATERIAL&METHODS: A custom 3Dprinter and 1.75 mm PCL and PLA filaments were used for the production of tissue scaffolds.Tissue scaffolds are produced with two different filling rates (20% and 40%).The design and production parameters of the scaffolds are defined and optimized by SolidWorks and Slic3r softwares to set the correct printing procedure.Biomechanical tests for mechanical characterization of all scaffolds were performed.MCF-7 breast cancer cell line was used to evaluate tissue scaffolds for 3Dcell culture.The ability of the cells to adhere to the scaffold surface was determined by crystal violet fixation and staining method used to detect viable cells

RESULTS: 3Dcell culture with PCL and PLA tissue scaffolds is useful to improve cancer cell culture applications and enhance cell proliferation.3D tissue scaffolds have shown that MCF-7 cells are more compatible with surface adhesion than 2Dcultures

CONCLUSIONS: The data obtained show that porous PLA and PCL tissue scaffolds are supportive for the 3Dculture and proliferation of MCF-7 breast cancer cells by providing a micro-environment in vivo mimic

INTRODUCTION

Two-dimensional *in vitro* cell culture is an low and easy method to observe the underlying mechanism of cell behavior [1]design and fabrication parameters need to be optimized to set up the correct printing procedure; a procedure in which the characteristics of the printing materials selected for use can also influence the process. This work focuses on optimizing the printing process of the open-source 3D extruder machine RepRap, which is used to manufacture poly(ε-caprolactone. In this way, we have the opportunity to study cell migration, differentiation, growth and mechanics in biochemical and biomechanical micro-environments. The results obtained here are important for understanding *in vivo* procedures. Although commonly used 2D cell cultures have often yielded useful results for the cell mechanism, studies have proven not to reflect the *in vivo* response. For

example, some quality of cancer cells cannot be appropriately modeled in 2D cell culture [2]. 2D cell cultures cannot reflect the differentiation and characteristics of cancer cells *in vivo* [3]resistance to conventional therapies, and a tendency to post-treatment recurrence. Increasing knowledge about CSCs' phenotype and functions is needed to investigate new therapeutic strategies against the CSC population. Here, poly(ϵ-caprolactone. Because the cells are located *in vivo* in the three-dimensional extracellular matrix that contains fibrosis proteins and molecules. Therefore, it is important to mimic the *in vivo* environment. Thus, scaffolds with 3D cell culture systems began to be used. These structures provide more reliable results. There are many 3D cell scaffolds. One of the most widely used materials is biopolymer. Its porous structure allows cells to interact with each other better in terms such as their natural morphology and *in vivo* environment [4]. 3D polymeric cell scaffolds are an increasingly innovative method for reconstructing tumor microenvironment in culture medium [5]but the role of the bone mineral hydroxyapatite (HA .

Our aim is to determine the optimal three-dimensional cell scaffold characteristics to ensure adhesion and proliferation of the breast cancer cell line MCF-7. For this purpose, we produced cell scaffolds in a 3D printer using polylactic acid (PLA) and polycaprolactone (PCL) filaments.

PLA is a thermoplastic aliphatic polyester suitable for biomedical and cell culture applications due to its biocompatibility, high strength and biodegradable properties [1], [4]but their research is limited by the impossibility to cultivate them in a monolayer culture. Scaffolds are three-dimensional (3D. PLA has been found to be beneficial because of the porous scaffold structure that enriches the cell microenvironment and also increasing the viability and proliferation of breast cancer cells. [4].

PCL is a biocompatible, biodegradable polymer such as PLA, without toxic dye. It differs from PLA with its mechanical and physical properties and slower degradation rate. Due to its low melting point, it is frequently preferred in cell culture applications and tissue engineering. [1]design and fabrication parameters need to be optimized to set up the correct printing procedure; a procedure in which the characteristics of the printing materials selected for use can also influence the process. This work focuses on optimizing the printing process of the open-source 3D extruder machine RepRap, which is used to manufacture poly(ε-caprolactone Here we present an *in vitro* investigation of adhesion levels of human breast cancer MCF-7 cell line cultures on PLA and PCL scaffolds with different densities.

MATERIALS AND METHODS

Design And Manufacturing of Scaffolds

Scaffolds were prepared with the PLA and PCL filaments using a custom made fused deposition modeling (FDM) printer. Scaffolds were fabricated according to the FDM method in a single extruder 3D printer, which uses hot end extruder for printing PLA and PCL filaments. This printer has a mechanical precision of 100-100-200 µm in the X-Y-Z axis. 0.3 mm nozzle and 1.75 mm filaments were used for the production of tissue scaffolds. Tissue scaffolds are produced with two different filling rates (20% and 40%). The nozzle temperature for PLA was set to 230˚C and for PCL to 80˚C.

The design and production parameters of the scaffolds are defined and optimized by SolidWorks and Slic3r software to set the correct printing procedure. Scaffolds template (Ø = 4 mm, thickness = 2.5 mm) were designed using SolidWorks 2017 software and subsequently filled and sliced using and Slic3r 1.2.9 software to obtain cylindrical STL models. Briefly, clump generator software was used to create squared pores into a 3D object in a "stl"file format. The printing head was computer-controlled in three axes (X, Y, Z) while extruding the PLA/PCL filament using the Slic3r software.

The melted PLA was then extruded through a 0.3 mm diameter stainless-steel nozzle on to a printing plate heated at 40˚C. Porous scaffolds were printed layer-by-layer in the form of squares surrounded by a dense PLA perimeter. We determined the optimal speed of 15 mm/s for the filling speed and 25 mm/s for the gap speed. The travel speed of extruder was set to be 100 mm/s. We fabricated scaffolds with two different pore sizes (%20-%40).

After printing, the scaffolds were carefully removed from the printing bed. Prior to biological evaluations, printed scaffolds were sterilized by ethylene oxide (EtO).

Mechanical Characterization

To investigate the possible influence of pore dimensions on mechanical properties of the printed PLA/PCL structure, a uniaxial compression test was performed on scaffolds. Five scaffolds were tested for each pore size (%20-%40) for each group. Scaffolds were tested by universal compression test machine (Shimadzu Autograph AG-IS 5kN). Scaffolds were compressed at a speed of 10 mm/min until 1 mm thickness. Maximal strength (F max) was then recorded simultaneously using the Trapezium software.

Cell Culture and Staining

MCF-7 breast adenocarcinoma cells were used in order to assess the optimum scaffold type and filling rate. MCF-7 cells were cultured in complete RPMI-1640 (10% FBS, 2 mM L-Gln, 1% 10,000 U/mL Penicillin/Streptomycin)(Gibco/Thermo Fisher, MA, USA) and incubated in humidified chamber with 5% CO_2 at 37˚C. After PLA and PCL scaffolds with 20% and 40% filling rates were printed, scaffold tablets were placed in 96 well plates under sterile conditions. 150,000 cells were seeded on each sterilized scaffold tablets in 50 µL complete growth medium and cultured overnight. Following the incubation period, media were removed from the wells, rinsed with PBS (Gibco/Thermo Fisher, MA, USA) and adhered cells on scaffolds were detected by crystal violet staining. Images were obtained using Olympus CKX41 microscope mounted with UIS2 camera. Cell counts were determined using ImageJ. Graphs were plotted using GraphPad Prism 7.

RESULTS

Mechanical Characterization of Scaffolds

The mean maximum tensile strengths for groups PCL%20, PCL%40, PLA%20, and PLA%40 were 66.00, 178.87, 211.46, and 653.01 N, respectively. When PLA and PCL scaffolds were compared, it was found that PLA had better strength than PCL scaffolds (Figure 1).

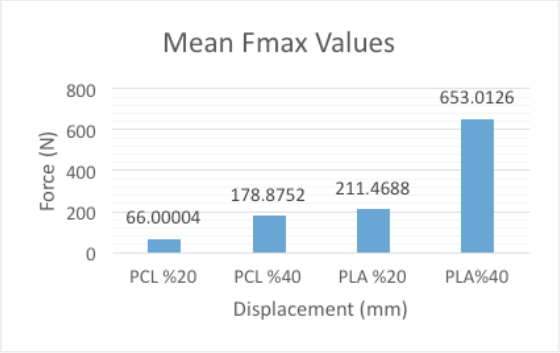

Figure 1: The mean values of maximum compressive strength of PLA and PCL scaffolds in all the groups.

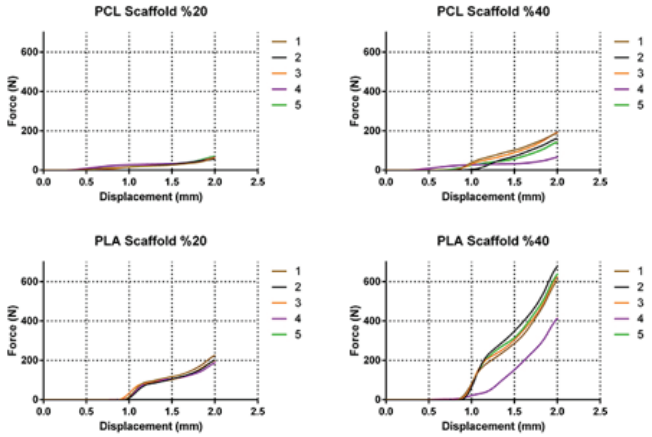

Figure 2: Curves resulting from the equations for the force-displacement ratio. Force-displacement curves for all groups (n=20) with a displacement rate of 10 mm/min.

Cell Culture and Staining

Five different regions and two different layers were captured for each scaffold tablet. Images of all regions of the lower and upper layers of scaffolds were taken with inverted microscope. PLA material showed higher number of stained cells than PCL material (Fig.3)

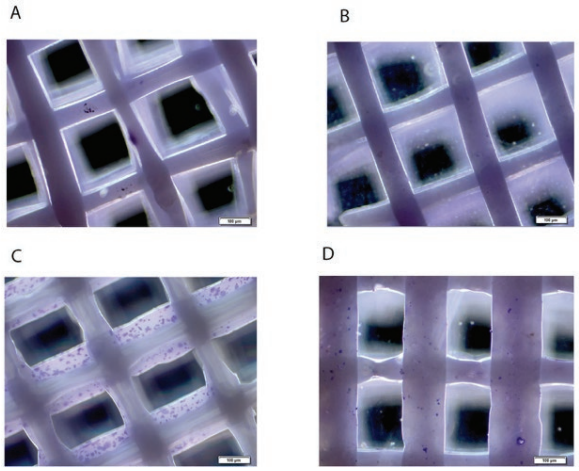

Figure 3 : Images of crystal violet stained MCF-7 cells on **A)** PLA 20% lower layer **B)** PLA %20 upper layer **C)** PCL 20% lower layer **D)** PCL %20 upper layer.

Cell count analysis by ImageJ showed that higher filling rate enabled more cells to adhere on (Fig.4A) and also showed that the number of cells adhered on the PLA scaffold is higher than the PCL scaffold (Fig.4B).

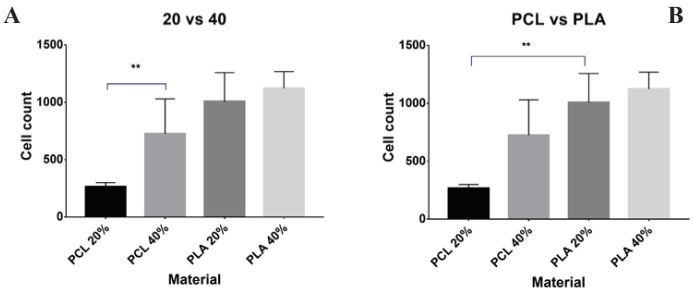

Figure 4: Cell numbers determined using ImageJ for PCL and PLA. **A)** A significant difference was found between PCL 20% and PCL 40%. **B)** A significant difference was found between PCL 20% and PLA 20%. (n=5, Bars: SD)

CONCLUSION

In conclusion, the data obtained showed that porous PLA and PCL tissue scaffolds can be supportive fort he 3D culture and for adhesion of MCF-7 breast cancer cells by providing a micro-enviroment in vivo mimic. PLA is a more preferable polymer when compared to PCL and more prous (40% filling rate) surface is better in terms of adhesion than porous surface (20% filling rate).

Progess on testing of different bio-compatible polymers in vitro would be great contribution in this field.

REFERENCES

1. M. Rabionet, E. Polonio, A. J. Guerra, J. Martin, T. Puig, and J. Ciurana, "Design of a scaffold parameter selection system with additive manufacturing for a biomedical cell culture," *Materials (Basel).*, vol. 11, no. 8, Aug. 2018.
2. K. Duval *et al.*, "Modeling physiological events in 2D vs. 3D cell culture," *Physiology*, vol. 32, no. 4. American Physiological Society, pp. 266–277, 14-Jun-2017.
3. S. Palomeras *et al.*, "Breast Cancer Stem Cell Culture and Enrichment Using Poly(ϵ-Caprolactone) Scaffolds," *Molecules*, vol. 21, no. 4, Apr. 2016.
4. E. Polonio-Alcalá, M. Rabionet, A. J. Guerra, M. Yeste, J. Ciurana, and T. Puig, "Screening of additive manufactured scaffolds designs for triple negative breast cancer 3D cell culture and stem-like expansion," *Int. J. Mol. Sci.*, vol. 19, no. 10, Oct. 2018.
5. S. P. Pathi, C. Kowalczewski, R. Tadipatri, and C. Fischbach, "A novel 3-D mineralized tumor model to study breast cancer bone metastasis," *PLoS One*, vol. 5, no. 1, Jan. 2010.

OP-03

ANTITUMOR EFFICACY OF QUERCETIN AND RESVERATROL IN PANC-1 PANCREATIC CANCER CELL LINE

Berzan Ekmen [1], Mehmet Gürdal [2], Elif Karadadaş [2], Bulent Ozpolat [3], Gulinnaz Ercan [2]

[1]Dokuz Eylul University, Molecular Medicine, Izmir

[2]Ege University, Medical Biochemistry, Izmir

[3]The University Of Texas MD Anderson Cancer Center, Experimental Therapeutics, Houston

INTRODUCTION: By the advance of recent anti-cancer approaches, the natural phenolic compounds like Quercetin and Resveratrol are offered as adjuvant therapies to potentiate and/or to reduce the side effects of the chemotherapeutics. Recent studies on various cancer types showed that Quercetin and Resveratrol may reduce Eukaryotic elongation factor 2 kinase (eEF2K) expression. In this study, the effect of the given polyphenols, Quercetin and Resveratrol, were evaluated in Pancreatic Cancer (PaCa) using PANC-1 cell line in vitro.

MATERIAL&METHODS: The IC50 values of Quercetin and Resveratrol in PANC-1 cells were determined by cytotoxicity tests. To evaluate the effect of the phenolic compunds on cellular migration, wound-healing assays were performed. To further elucidate the anti-cancer effects, colony forming (CFU) assays were used. Real-Time PCR was used to determine the changes in gene expression levels of eEF2K by the given compounds.

The determined IC50 values of Quercetin and Resveratrol in PaCa cells by cytotoxicity tests were 7.75 µM and 48.75 µM, respectively ($p<0,001$) at 72 hours. Quercetin and Resveratrol applied at the given doses decreased the colony forming ability and cellular migration of PANC-1 cancer cells. Eukaryotic Elongation Factor 2 Kinase (eEF2K) gene expression was decreased with Quercetin ($p<0.05$) but increased with Resveratrol treatment ($p<0.05$).

RESULTS: Based on our results, Quercetin showed an overall stronger effect with lower IC50 doses in PaCa treatment in vitro. Therefore, it might be recommended alone or in combination with chemotherapeutics in further research for development of new anti-cancer approaches.

Keywords: Quercetin; Resveratrol; Pancreatic Cancer; Panc-1; eEF2K; eukaryotic elongation factor-2 kinase

INTRODUCTION

Pancreatic cancer (PaCa) is one of the most common causes of cancer-related deaths, worldwide [1]. Natural compounds (NC) are attractive chemical agents for most investigations on cancer prevention/therapy [2]. Phenolic compounds (PHC) are a member of these NC. Various animal experiments have been used to investigate and reveal their beneficial effects on health [3], [4] where these health benefits of PHC are not only specific to cancer but also effective with their antioxidant and antitumorigenic effects against chronic degenerative diseases [5]. Quercetin and Resveratrol are members of NC where Quercetin has been shown to modulate signaling pathways and gene expressions with various anti-inflammatory, anti-oxidant and anti-cancer effects in cellular studies and animal models [6], [7]. For the past two decades, resveratrol has also received a lot of attention with its anti-cancer, anti-oxidant, anti-diabetic and chemopreventive effects, further supported by its benefits to the cardiovascular system [8]. In recent years, eukaryotic elongation factor-2 kinase (eEF2K) is suggested as a potential therapeutic target in cancer [9]. eEF2K is a proliferation-dependent mitogen-activated enzyme which regulates protein synthesis by controlling the rate of peptide chain elongation through phosphorylation [10]. eEF2K was shown to be up-regulated in various cancer types and increased activity eEF2K has been reported in rapidly proliferating malignant cells by several studies [11]. In this study, we investigated the effect of Quercetin and resveratrol on PaCa cell line; we determined the half maximal inhibitory concentration (IC_{50}) via Cell Viability Assay and cell migration via Wound Healing Assay, while evaluating colony forming ability of cells with Colony Forming Assay and eEF2K gene expression via using Real Time PCR.

MATERIALS AND METHODS

Cell Culture & Cell Viability Assays

PANC-1 cells (gifted from MD Anderson Cancer Center Bulent Ozpolat's Lab.) were used in this study and cultured according to ATCC protocol. Cellular viability was evluated pwith WST-8 according to the manufacturer's instructions (Cayman Chemical WST-8 Cell Proliferation Assay Kit). All doses were tested in triplicates and the experiments were repeated at least three times. Statistical calculations were performed using the Graphpad Prism 5.

Wound Healing Assay

2×10^5 cells/well were plated in 6-well plates. Afterwards, a straight line was

drawn in the center of the wells. Cells were treated with Quercetin (0 and 15 µM) and Resveratrol (0 and 75 µM) for 0, 24, 48 h of incubations.

Colony Forming Assay

2×10^3 cells/well were plated in 6-well plates and incubated overnight. The cells were treated with Quercetin (0, 10 and 60 µM) and Resveratrol (0, 50 and 75 µM) for 15 days. After the incubation period, the cells were stained with 0,05% crystal violet and evaluated by Image J, 2017.

RNA Isolation & cDNA Synthesis

Panc-1 cells were treated either with Quercetin (0 and 7,75 µM) and resveratrol (0, 48
µM) for 24 h. RNA isolation was performed (QIAGEN RNeasy Mini Kit) according to the manufacturer's instruction. Total mRNA was synthesized by the Reverse Transkriptase-PCR method (the Bio-Rad iScriptTM cDNA Synthesis Kit) according to the manufacturer›s instructions.

Real Time PCR

Changes in the expression of eEF2K gene were analyzed by Real Time PCR method. B-Actin and TBP were used as housekeeping genes. Ct values were obtained from Real Time PCR (ROCHE; LC480). Data presented are representative of those obtained in at least three independent experiments performed in triplicates. All data were statistically evaluated using non-parametric Mann-Whitney U test (IBM SPSS Statistics Version 20 program; n=3 for all groups)

RESULTS

Cytotoxicity Effects of Quercetin and Resveratrol on PANC-1

After the treatment of Quercetin and Resveratrol for 24, 48 and 72 hours: IC_{50} values of Quercetin were calculated with Calcusyn 2.0 Programme and found as 30,17 µM, 15,1 µM and 7,75 µM (**fig. 1.)** respectively and Resveratrol was found as 121,4 µM, 7 µM, 48,75 µM (**fig. 1.)** respectively ($p<0,001$).

Cell Migration Assay

In 15 µM (IC_{50}) Quercetin and 75 µM (IC_{50}) Resveratrol-applied wells, the line drawn at the 0th hour was completely open where partial closure occurred at the 24 th hour. However, at the 48 th hour, the control line was completely closed, while the openings in the 15 µM Quercetin and 75 µM Resveratrolapplied wells were still present (**fig. 2.** and **fig. 3.)**

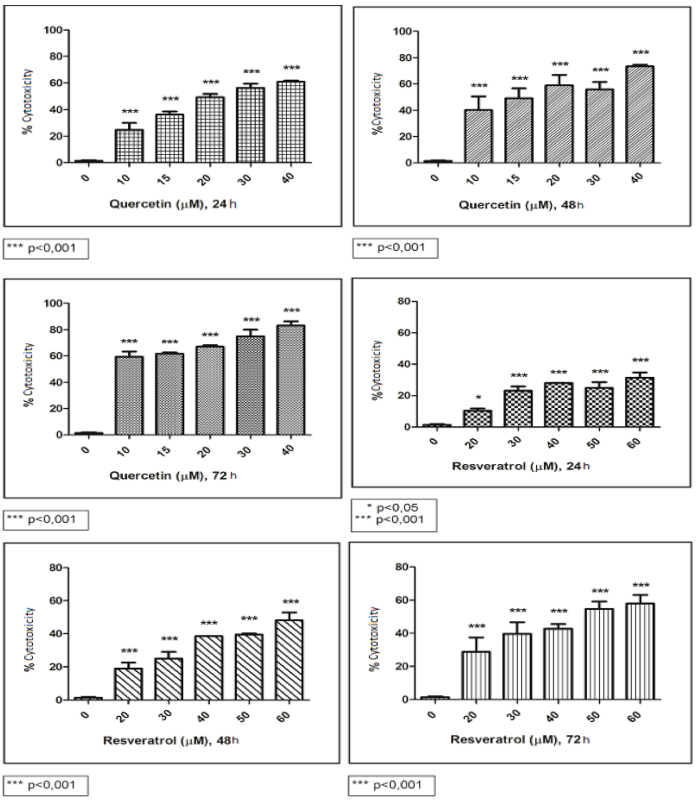

Figure 1. Dose depended Quercetin and Resveratrol % cytotoxicity for 24, 48, 72 h.

Colony Formation Assay

A normal proliferation was observed in the control group while the amount of colonies decreased to 49% in 10 µM Quercetin-applied well. There wasn't any colony in 60 µM Quercetin-applied well; therefore the colony count was 0% (**fig. 4.**). When the results were compared to the control group for Resveratrol, a normal proliferation was observed in
the control while the amount of the colonies decreased to 48% in 50 µM Resveratrol-applied well. In this study, 75 µM Resveratrol was the highest applied concentration where the colony percentage was 31% (**fig. 5.**).

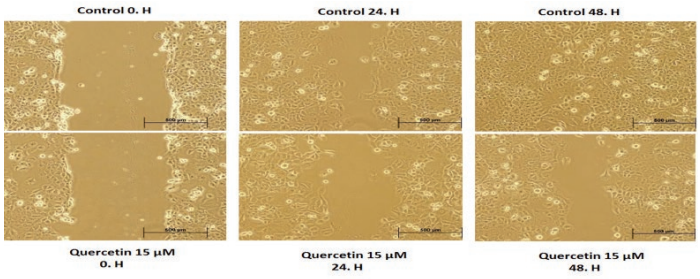

Figure 2 The results of cell migration assay of Quercetin at IC_{50} doses (15 µM) in comparison to the control groups at 0th, 24th and 48th h of incubations

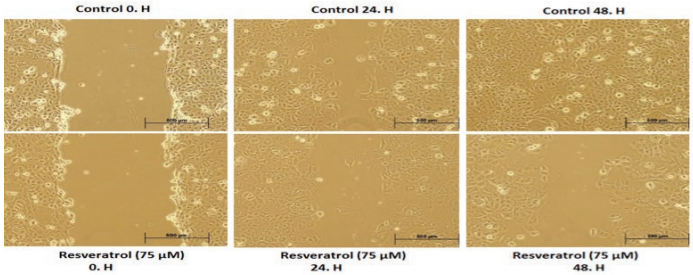

Figure 3 The results of cell migration assay of Resveratrol at IC_{50} doses (75 µM) in comparison to the control groups at 0th, 24th and 48th h of incubations

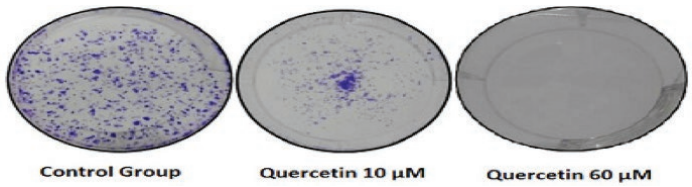

Figure 4 The amount of colonies after Quercetin application

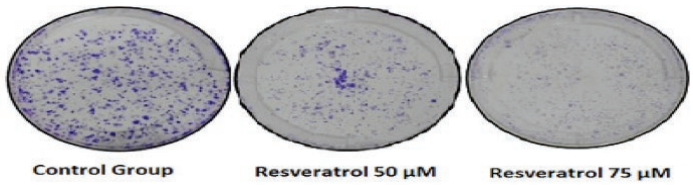

Figure 5 The amount of colonies after Resveratrol application

Gene Expression of eEF2K

There was a significant decrease ($p<0,05$) in eEF2K gene expression after 24 h incubation of PANC-1 cells with 7,75 µM Quercetin whereaas there was a significant increase ($p<0,05$) in eEF2K gene in cells treated with 48.75 µM Resveratrol (**fig.7**).

DISCUSSION

Based on IC_{50} doses, Quercetin was more effective with higher capacity at a lower concentration than Resveratrol on PANC-1 cells. The results of cell migration showed that Quercetin and Resveratrol probably suppressed cell proliferation and cell migration of PaCa cells at the given IC_{50} concentrations. There was still alive colonies at a high concentration of Resveratrol implying that IC_{50} concentration of Resveratrol was not as effective as Quercetin even at higher concentrations.

eEF2K expression was significantly decreased in PANC-1 cells at the given IC_{50} dose of Quercetin compared to its control group whereas eEF2K gene expression was significantly

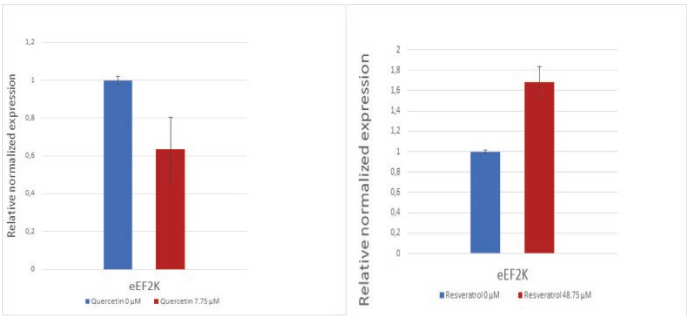

Figure 7 The effect of Quercetin and Resveratrol on eEF2K Gene Expression in PANC-1 Cells

increased in PANC-1 cells where Resveratrol was applied at the determined IC_{50} dose compared to the control group. According to this conflicting results on phenolic reagents, 24-hours incubation time is perhaps not sufficient for Resveratrol to show its effects on PANC-1 cells at the given IC_{50} doses. Therefore, the efficacy of Resveratrol with 48 and 72 h of incubations should be furher investigated.

Conflict of Interest

The authors declare that they have no competing interests.

Acknowledgements

This work is supported by scientific research foundation of Ege University, Faculty of Medicine (16-TIP-046).

REFERENCES

1. Jemal A, Siegel R, Ward E, Hao Y, Xu J, et al. Cancer Statistics. CA Cancer J Clin. 2009;59(4):1–25.
2. Amin ARMR, Kucuk O, Khuri FR, Shin DM. Perspectives for cancer prevention with natural compounds. J Clin Oncol. 2009;27(16):2712–25.
3. Srivastava S, Somasagara RR, Hegde M, Nishana M, Tadi SK, et al. Quercetin, a natural flavonoid interacts with DNA, arrests cell cycle and causes tumor regression by activating mitochondrial pathway of apoptosis. Nature 2016;6(March):1–13.
4. Hashemzaei M, Far AD, Yari A, Heravi RE, Tabrizian K, et al. Anticancer and apoptosis-inducing effects of quercetin in vitro and in vivo. Oncol Rep. 2017;38(2):819–28.
5. Pham-Huy LA, He H, Pham-Huy C. Free radicals, antioxidants in disease and health. Int J Biomed Sci 2008;4(2):89–96.
6. Wang W, Sun C, Mao L, Ma P, Liu F, et al. The biological activities, chemical stability, metabolism and delivery systems of quercetin: A review. Trends Food Sci Technol. 2016;56:21–38.
7. Nguyen TTT, Tran E, Nguyen TH, Do PT, Huynh TH, et al. The role of activated MEK-ERK pathway in quercetin-induced growth inhibition and apoptosis in A549 lung cancer cells. Carcinogenesis 2004;25(5):647–59.
8. Huminiecki L, Horbańczuk J. The functional genomic studies of resveratrol in respect to its anti-cancer effects. Biotechnol Adv. 2018;36(6):1699–708.
9. Tekedereli I, Alpay SN, Tavares CDJ, Cobanoglu ZE, Kaoud TS, et al. Targeted silencing of elongation factor 2 kinase suppresses growth and sensitizes tumors to doxorubicin in an orthotopic model of breast cancer. PLoS One. 2012;7(7).
10. Bagaglio DM, Hait WN. Role of calmodulin-dependent phosphorylation of elongation factor 2 in the proliferation of rat glial cells. Cell Growth Differ. 1994;5:1403–8.
11. Parmer TG, Ward MD, Yurkow EJ, Vyas VH, Kearney TJ, et al. Activity and regulation by growth factors of calmodulin dependent protein kinase III (elongation factor 2-kinase) in human breast cancer. Br J Cancer. 1999;79:59–64.

OP-04

ANTI-ANGIOGENIC EFFECT OF PROPOLIS IS CLOSELY RELATED TO THE SOLVATION METHOD AND BIOTRANSFORMATION PROCESS

Hikmet Memmedov[1], Burak Durmaz[1], Latife Merve Oktay[2], Nur Selvi Günel [2], Hatice Kalkan Yildırım[3] Eser Yıldırım Sözmen[1]

[1]Ege University Faculty of Medicine, Department of Medical Biochemistry, İzmir, Turkey

[2]Ege University, Faculty of Medicine, Department of Medical Biology, İzmir, Turkey

[3]Ege University Faculty of Engineering, Food Engineering, Department of Biotechnology, İzmir, Turkey

OBJECTIVES: The aim of this study was to investigate the effect of solvation methods and biotransformation process of propolis on the angiogenesis in colon cancer cell lines.

MATERIALS AND METHODS: Propolis sample was obtained from "Ceyan Arıclık" - Ankara (Ayas) company. Propolis samples were solved in three different solvents (water, ethanol and, PEG). Lactobacillus *plantarum* strains (L. *plantarum* ISLG-2, L. *plantarum* ATCC® 8014, L. *plantarum* Visbyvac) were used for biotransformation of propolis. The phenolic content of Propolis extracts was determined with LC-MS/MS. The effect of propolis on angiogenesis in HCT-116, HT-29 colon cancer cell lines and CCD-841-con normal epithelial cells were investigated by determining ERK1, ERK2, and VEGF levels.

RESULTS: Both transformed and non-transformed propolis samples did not show any significant effect on VEGF, ERK1 and ERK2 levels in CCD-841 normal colon cells. While Propolis solved in water has no effect on VEGF levels, it suppressed ERK1/ERK2 levels in HCT116 cells. Propolis dissolved in ethanol + transformed with L.*plantarum* ATCC® 8014 strain decreased VEGF, ERK1 and ERK2 levels in HT29 cell.

CONCLUSIONS: The transformed sample of propolis significantly reduced all three angiogenesis markers in HT-29 colon cell lines as compared to the control sample. We concluded that the solvation method and transformation process is highly important to get the significant effect of propolis on angiogenesis.

Keywords: Propolis, VEGF, ERK1, ERK2

INTRODUCTION

Propolis is a natural product produced by honey bees to protect the colony with their anti-bacterial, anti-viral and anti-fungal properties (1). Besides these common properties, propolis has pain relief, antihelmintic, liver protective and antihypertensive properties (2). It has been shown that propolis is effective both in cancer prevention and cancer treatment (3). However, it can cause various allergic reactions in approximately 10% of the population. There are more than 20 allergenic molecules in propolis, especially 1,1-dimethylallyl caffeic acid ester which is the main allergenic compound comprising 85% proportion of all allergens, and caffeic acid are the most important compounds (4,5). The biological transformation process of propolis aims to reduce the amount of allergen molecules in it by using various bacterial strains. It has been shown that cinnamoyl esterase enzymes in selected bacterial strains break the ester bonds of the allergen molecules in the propolis (6,7). We showed that some special strains of Lactobacillus *plantarum* (Patent No: TR2015 16914B, dated 2018/07/23) decreased the allergenic molecules especially DMEA and CAPE in propolis (7,8). Colorectal cancer is the third most common type of cancer worldwide (9) and is an important cause of mortality in patients. Vascular endothelial growth factor (VEGF) which is produced by epithelial cells, is known as a regulatory molecule for cell migration and neovascularization in cancer metastasis. It has been shown that suppression of VEGF might inhibit migration, Invasion and adhesion ability of different cancer cell lines (10,11). Although anti-cancer and cytotoxic effect of propolis has been shown in many studies, there is no study about the effect of propolis on VEGF in cancer. In this study we aimed to investigate the effect of solvation methods & biotransformation process of propolis on the anti-angiogenesis effect in colon cancer cell lines.

MATERIALS AND METHODS

Preparation of propolis extracts and biotechnological transformation process

Propolis samples were obtained from "Ceyan Arıcılık "- Ankara (Ayas) and stored at -20 ° C. Propolis samples were subjected to a series of preliminary physical processes (milling and sizing: 35 mesh) to prepare for the study. Three different bacterial strains (*Lactobacillus plantarum* İŞLG -2, *Lactobacillus plantarum* ATCC® 8014, *Lactobacillus plantarum* Visbyvac) were selected from the culture collection of Ege University Food Engineering for biotechnological transformation.

Propolis samples (w/v:1/1) were treated with different solutions (ethanol (10%), polyethylene glycol (40%) and water) and ultrasonication was applied at 40Hz (5, 10 and 15 min) for samples solvated in water. After extraction, filtration and centrifugation process, propolis samples were incubated with L.*plantarum* strains in different inoculum rates (1.5%, 2.5%, 3.5%) for 24-72 hours/30°C. At the end of the process, the mixture was filtered and liquid extracts were stored at +4°C prior to analysis.

Determination of phenolic content of propolis extracts

Quantitative analysis was performed on a Waters® ACQUITY XEVO ™ TQD tandem quadruple UPLC-MS / MS system and multiple reaction monitoring (MRM) in electrospray ionization (ESI) (mode Sular, Milford). (MA). This UPLC-MS / MS system was controlled by MassLynx™ 4.1 software. 1 mg / ml stock solution of each polyphenol in methanol was used for calculation.

Cell culture studies

HCT-116 and HT-29 human colon cancer cell lines were grown on McCoy's 5A medium containing 2mM L-glutamine, 10% fetal bovine serum (FBS), 100 units / ml penicillin and 100 g / ml streptomycin, and 5% CO_2 at 37°C. CCD-841 CoN healthy colon epithelial cell line was grown in MEM medium containing 2mM L-glutamine, 10% fetal bovine serum (FBS), 100 units / ml penicillin and 100 µg/ml streptomycin, and 5% CO_2 at 37°C. Propolis samples were added to HCT 116 and HT-29 colon cancer and CCD-841 CoN normal colon epithelial cell culture at the dose and duration determined in the cytotoxicity study. At the end of the pre-study period (24 hours), cells were harvested with PBS and stored at -80°C. On working day, samples were freeze-thawed 3 times and then centrifuged at 2500xg for 15 minutes. Each sample was run 3 times. ERK-1, ERK-2 and VEGF levels were determined with commercially available ELISA kit.

RESULTS

The LC-MS/MS results of the samples showed that amounts of phenolic contents changed with different solvents due to the solubility differences of phenolic compounds. 60 samples in total (6 different solvents, biotransformation with 3 different *L. plantarum* strains in different concentrations) were evaluated (data were presented in another publication) and the 12 samples which have the lowest concentration of allergen molecules (DMAE caffeic acid and CAPE) were chosen for this study. The amount of phenolic molecules in propolis samples added to cell culture were shown in Table.1.

The VEGF, ERK-1, and ERK-2 levels were presented in Figure-1, Figure-2, and Figure-3, respectively.

While all nontransformed propolis samples had no effect on VEGF levels in cancer cells, propolis dissolved in water (US 5 min) + transformed with L.*plantarum* ATCC® 8014 strain decreased VEGF levels (1673 vs 1488) in HCT116.

Generally, all nontransformed propolis samples suppressed ERK1 levels in HCT116 cells, transformed propolis samples had no effect on ERK1 and ERK2 levels in HCT116 cells. While Propolis dissolved in water had no effect on VEGF levels, it suppressed ERK1 (16.3 vs 12.2) and ERK2 (18.0 vs 15.7) levels in HCT116 cells.

Propolis dissolved in ethanol + transformed with L.*plantarum* ATCC® 8014 strain (2.5%) decreased VEGF (1865 vs 1600), ERK1 (19.5 vs 17.0) and ERK2 (16.2 vs 14.2) levels in HT29 cell line. On the other hand, the most effective in suppression of ERK2 levels in HT29 cell line was propolis sample dissolved in water (+US 5 min) and transformed with L.*plantarum* (16.2 vs 11.6).

Propolis dissolved in water led to depletion in ERK1 levels in CCD841.

Our data showed negative correlations between the ERK1 levels and quercetin (r=-0.387, p=0.042), ellagic acid (r=-0.341, p=0.07), myricetin (r=-0.409, p=0.031) levels in HCT116 cell line. Interestingly there was a negative correlation between the VEGF and ERK1 levels (R=-0.519, p=0.009) in HCT116 cells.

DISCUSSION

Our study reported the effect of propolis on VEGF, ERK1 and ERK2 levels in colon cancer cell line and the role of solvation methods and transformation process on its effect for the first time. Recent studies indicated that propolis has an anticancer effect with various mechanisms including induction of apoptosis, stopping the cell cycle, anti-proliferative effect, etc (12-17). And in a recent study has been observed that Chinese propolis suppressed VEGF-induced HUVEC migration (18),

In our study, propolis samples dissolved in different solvents showed different effects on VEGF, ERK1, and ERK2 due to the variability of its phenolic concentration. The effect of propolis may highly variable in the literature (12-17) because the content of propolis collected from different geographies is different from each other due to climate, flora, etc and the extracted amount phenolic molecule of propolis is vary depends on the solvent. So far, most of the studies on the biological activity of propolis used only the extract of propolis in ethanol. In this study, we tested 3 solvents and ultrasonic treatment and biotransformation processes. Most of them had no significant effect on CCD841 cells. Although different propolis samples dissolved in both water and ethanol decreased VEGF levels in the HT-29 cell line, transformed samples were more effective than control sample. The most effective sample on suppression of VEGF, ERK1 and ERK2 was the propolis sample dissolved in ethanol + transformed with L.*plantarum* ATCC® 8014 strain in HT 29 cell line. Wang et al similarly observed that propolis decreased ERK 1/2 level in Caco-2 colon cancer cell line and increased ERK 1/2 level in healthy colon cell line. They suggested that propolis fight colon cancer by preventing colon cancer proliferation and preserved healthy colon cells (19).

While all nontransformed propolis samples had no effect on VEGF levels in cancer cells, propolis dissolved in water (US 5min) + transformed with L.*plantarum* ATCC® 8014 strain decreased VEGF levels in HCT116. While Propolis dissolved in water had no effect on VEGF levels, it suppressed ERK1 and ERK2 levels in HCT116 cells.

Although we did not study the effect of propolis on HUVEC formation and neovascularization histologically, our data indicated that propolis might prevent cancer metastasis by inhibiting VEGF, ERK1, and ERK2. However, there was no clear correlation between the phenolic content and VEGF, ERK1, ERK2 levels in HT26 cell line, so the effect of any phenolic molecule which determined in this study on this inhibition remains unclear.

Since our data showed negative correlations between the ERK1 levels and quercetin, ellagic acid, myricetin, kaempferol levels in HCT116 cell line, the suppressive effect of propolis on ERK1 might be attributed to its content of quercetin, ellagic acid and myricetin. This conclusion was evidenced by the other studies showed inhibitory effects of myricetin in A549 cell, ellagic acid in endothelial cells, quercetin in HepG2 cells and kaempferol in oral cancer cells on ERK1 (20-22)

Ultimately, our results indicated that propolis might prevent tumor metastasis by inhibiting VEGF, ERK1/ERK2 signaling pathway. We conclude that the solution method and transformation processes are extremely important to obtain the significant effect of propolis on angiogenesis. The effect of propolis on other possible signal pathways during metastasis and anti-metastatic effect of propolis in vivo will be examined further.

Acknowledgement: This work was supported by Ege University Research Foundation (BAP-18TIP020).

REFERENCES

1. Kumova, U., Korkmaz, A., Avcı, B.C., Ceyran, G. (2002). Önemli bir arı ürünü: Propolis, Uludağ Bee Journal, (s.10-24).
2. Sforcina J.M., Bankovab V. (2011). Propolis: Is there a potential for the development of new drugs? Journal of Ethnopharmacology, 133, (s.253–260).
3. Lagouri V., Prasianaki D., Krysta F. (2014). Antıoxıdant Properties and Phenolıc Composıtıon of Greek Propolıs Extracts, International Journal of Food Properties, 17, (s.511–522).
4. Hausen, B.M., Wollenweber, E., Senff, H., Post, B. (1987). The sensitizing properties of 1,1-dimethylallyl caffeic acid ester. Propolis allergy (II), 17(3), (s.171-177).
5. 17. Basista-Sołtys K. Allergy to Propolis in Beekeepers-A Literature Review. Occup Med Health Aff 2013; 1-1.
6. Gardana C, Gardana C, Barbieri A, Simonetti P, Guglielmetti S. Biotransformation strategy to reduce allergens in propolis. Applied Environmental Microbiology 2012; 78(13), 4654–4658.
7. Yıldırım HK, Canbay E, Öztürk Ş, Aldemir O, Sözmen EY. Biotransformation of propolis phenols by L. plantarum as a strategy for reduction of allergens. *Food Science and Biotechnology* 2018; 27(6), 1727-1733.
8. Aldemir O, Yıldırım HK, Sozmen EY. Antıoxıdant and Antı-Inflammatory Effects of Bıotechnologıcally Transformed Propolıs. *Journal of Food Processing and Preservation* 2018; e13642. https://doi.org/10.1111/jfpp.13642.
9. Calva, A. M., Acevedo T. MT. (2009). Revisión y actualización general en cancer colorrectal. Revista de Radiología México. 1:99-115.
10. Liu Y, Qiao Y, Hu C, Liu L, Zhou L, Liu B, Chen H, Jiang X. VEGFR2 inhibition by RNA interference affects cell proliferation, migration, invasion, and response to radiation in Calu-1 cells. Clinical & translational oncology. 2016;18(2):212–9.
11. Zhang L, Wang JN, Tang JM, Kong X, Yang JY, Zheng F, Guo LY, Huang YZ, Zhang L, Tian L. VEGF is essential for the growth and migration of human hepatocellular carcinoma cells. Mol Biol Rep. 2012;39(5):5085–93.
12. De Mendonça ICG, Porto ICC de M, do Nascimento TG, de Souza NS, Oliveira JM dos S, Arruda RE. dos S. Brazilian red propolis: phytochemical screening, antioxidant activity and effect against cancer cells. *BMC Complementary and Alternative Medicine* 2015; 15(1),357.
13. Patel S. Emerging Adjuvant Therapy for Cancer: Propolis and its Constituents.

J Diet Suppl 2014; 0211,1–24.

14. Carvalho AA, Finger D, Machado CS, Schmidt EM, Costa PM, Alves APNN. In vivo antitumoural activity and composition of an oil extract of Brazilian propolis. *Food Chem* 2011; 126(3),1239–1245.
15. Kubina R, Kabała-Dzik A, Dziedzic A, Bielec B, Wojtyczka R, Bułdak R. The Ethanol Extract of Polish Propolis Exhibits Anti-Proliferative and/ or Pro-Apoptotic Effect on HCT 116 Colon Cancer and Me45 Malignant Melanoma Cells In Vitro Conditions. *Adv Clin Exp Med* 2015; 24,203–12.
16. Pratsinis, H., Kletsas, D., Melliou, E. ve Chinou, I. (2010). Antipro- liferative activity of Greek propolis. J Med Food, 13, (s. 286- 290).
17. Kleiton, S. B., María, S. B., Carlos, A. S., Ademilson, EES. ve Luiz, G. Tone. (2011). Antiproliferative effects of Tubi-bee propolis in glioblastoma cell lines. Genetics and Molecular Biology, 34, 2, (310-314).
18. Izuta H, Shimazawa M, Tsuruma M, Araki Y, Mishima S, Hara H. Bee products prevent VEGF-induced angiogenesis in human umbilical vein endothelial cells. BMC Complementary and Alternative Medicine 2009, **9**:45 http://www.biomedcentral.com/1472-6882/9/45
19. Wang K, Jin X, Chen Y, Song Z, Jiang X, Hu F, Conlon MA, Topping DL.Polyphenol-Rich Propolis Extracts Strengthen Intestinal Barrier Function by Activating AMPK and ERK Signaling. Nutrients. 2016 May 7;8(5). pii: E272. doi: 10.3390/nu8050272.
20. Rozentsvita A, Vinokura K, Samuel S, Lia Y, Gerdes AM, Carrillo-Sepulveda MA. Ellagic Acid Reduces High Glucose-Induced Vascular Oxidative Stress Through ERK1/2/ NOX4 Signaling Pathway Cell Physiol Biochem 2017;44:1174-1187
21. Shih YW, Wu PF, Lee YC, Shi MD, Chiang TA. Myricetin Suppresses Invasion and Migration of Human Lung Adenocarcinoma A549 Cells: Possible Mediation by Blocking the ERK Signaling Pathway. J. Agric. Food Chem. 2009, 57, 3490–3499
22. Ding Y, Chen X, Wang B, Yu B, Ge J, Shi X. Quercetin suppresses the chymotrypsin-like activity of proteasome via inhibition of MEK1/ERK1/2 signaling pathway in hepatocellular carcinoma HepG2 cells. Can J Physiol Pharmacol. 2018 May;96(5):521-526. doi: 10.1139/cjpp-2017-0655. Epub 2018 Feb 2.

Table.1.Phenolic molecules in propolis added into cell culture

Added propolis micro-gram/mL	E	E-L2	PEG	PEG-L2	W	W-L2	W-L3	W-US5	W-US 5-L2	W-US 10	W-US 10-L1	W-US 10-L3	W-US 15	W-US 15-L2
Ferulic acid ng/mL	469.6347	526.1142	112.7344	98.91087	1164.29	1224.923	377.6793	2080.627	877.8986	1659.72	914.9149	276.611	1831.569	861.7972
Caffeic acid ng/mL	75.08427	67.36631	14.23645	20.12847	155.2144	234.6706	59.90863	279.0329	104.0361	231.1382	129.1693	40.54656	278.8523	158.9499
Kampherol ng/mL	169.9414	94.7877	120.3957	135.6671	207.8231	309.3374	82.17358	537.2363	158.0608	394.9609	174.4913	53.09463	402.6304	180.5551
Miricetine ng/mL	61.33566	17.51912	125.1015	14.76679	72.85738	18.7759	14.82291	163.6773	68.56553	109.7614	65.88547	14.12656	130.0079	14.46816
Transsinnamic acid ng/mL	4494.501	0	1262.274	0	2163.108	2069.442	145.794	16378.28	522.711	6188.496	934.2	0	6525.036	431.841
Ellagic acid ng/mL	93.73335	13.38447	159.6034	107.8384	61.25499	256.2478	0	338.4439	72.54669	199.4902	11.19703	0	189.0351	89.50561
CAPE ng/mL	12.77845	4.69024	2.68164	0.890302	7.535246	4.913255	3.331631	23.60875	8.859541	10.26595	5.816531	3.562884	20.75713	8.093618
DMEA ng/mL	238.5111	0	0	0	115.5724	234.3245	0	696.1121	0	404.1919	37.61603	0	409.2152	2.053479
Naringenin ng/mL	62.70468	1.466997	1.237964	7.044474	13.72057	12.32105	271.4899	469.3796	263.9779	211.538	0	391.6689	129.3564	12.00818
Quercetine ng/mL	133.6889	109.6782	297.2649	215.6717	163.2451	285.2652	59.96005	396.222	152.2354	257.9135	145.3603	38.03067	309.8513	142.0489

E:Ethanol, PEG: Poly Ethylen Glycol, W:Water, US:Ultrasonic treatment-40Hz. 5- 5 minutes,10-10 minutes and 15-15 minutes. L1: L.*plantarum* ISL-2 strain, L2: L.*plantarum* ATCC® 8014 strain, L3: L.*plantarum* Visby vac strain.

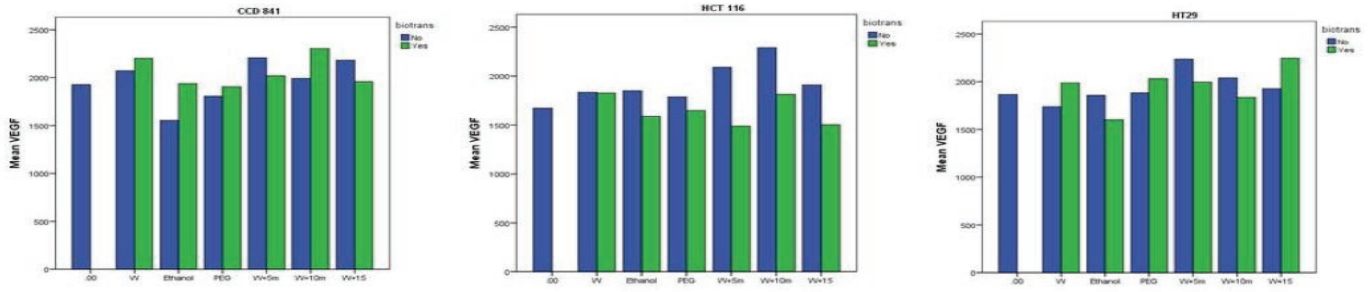

Figure. 1. Effect of propolis on VEGF levels in three cell lines

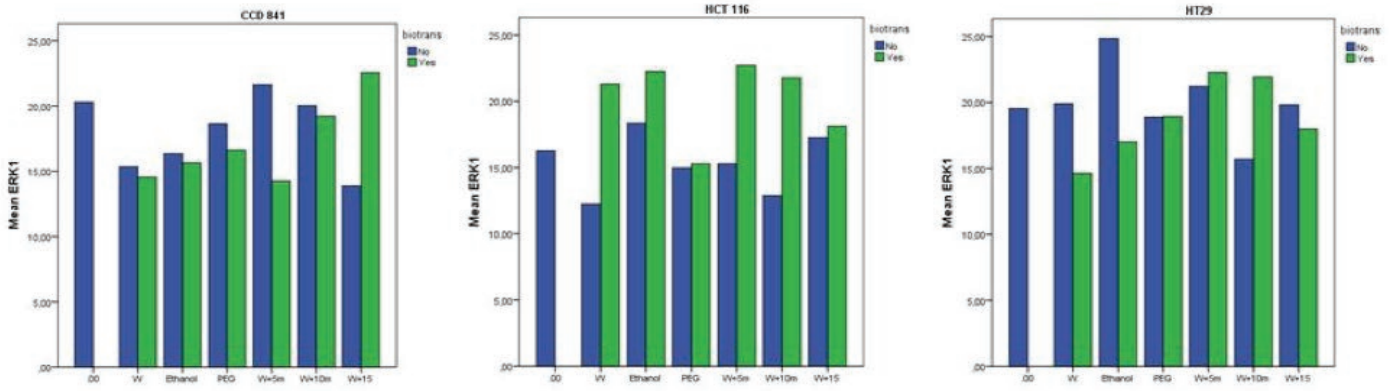

Figure. 2. Effect of propolis on ERK1 levels in three cell lines

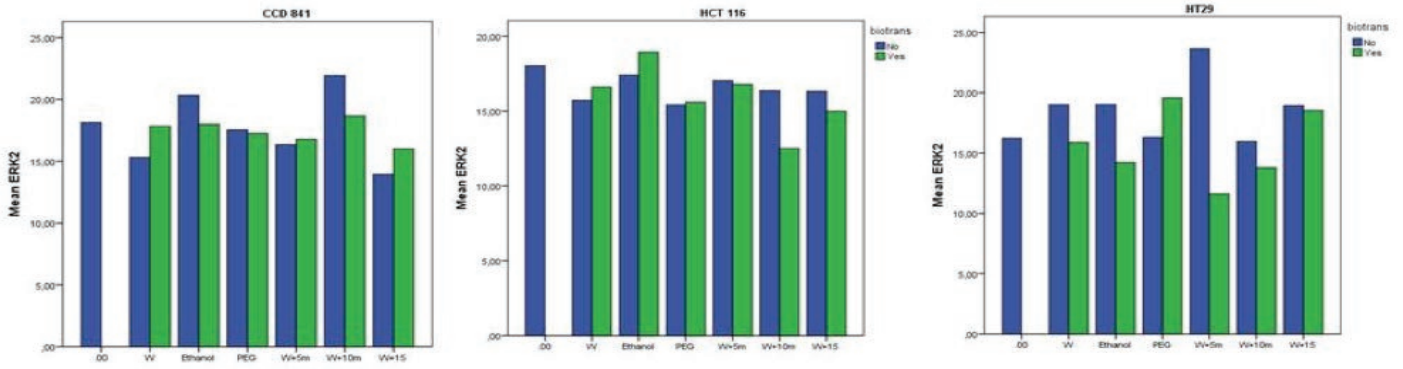

Figure. 3. Effect of propolis on ERK2 levels in three cell lines

OP-05

IDENTIFICATION OF MIR-145-1, MIR-21-2 AND MIR-92-1 EXPRESSION AND TARGET GENES IN COLON CANCER STAGE IIIA PATIENTS

Cigdem GUNGORMEZ[1], Dilek ACAR[2]

[1]Department of Medical Biology, Faculty of Medicine, Siirt University, Siirt, Turkey

[2]Department of Biology, Faculty of Arts and Sciences, Harran University, Sanliurfa, Turkey

Correspondence to: Department of Medical Biology, Faculty of Medicine, Siirt University, Siirt, Turkey

ABSTRACT

OBJECTIVES: Colorectal cancer is a complex disease which is caused by many factors and has genetic predisposition. In order to understand the molecular level of colorectal cancer, it is studied in detail and many factors such as miRNA, which cause cancer formation and which play a role in its development are identified. However, the molecular mechanisms affecting the regulation of the disease have not yet been fully elucidated. This deficiency necessitates the search for new markers that can predict the development and development of colon cancer and the mechanism of bioinformatics.

MATERIAL AND METHODS: This study, healthy and tumor tissues of 15 patients with colon cancer stage IIIA who underwent surgical removal were compared with the expression of miR-145-1 and miR-21-2 and miR-92-1 by qRT-PCR. The ability of these miRNAs to determine their target genes by bioinformatic analysis and their ability to be used for early detection was investigated.

RESULT: QRT-PCR tumor tissue compared to control tissue; expression levels of miR-145-1; 0.065 fold decreased; the tumor tissue of miR-21-2 relative to the control; 3.147-fold, miR-92-1 was found to increase 4.777-fold. As a result of FunRich enrichment biological pathway analysis of 21 genes determined by DIANA mirPath V3; these miRNAs have been found to have a significant effect on signaling pathways such as E-cadherin, mTOR and TGF-Beta receptor.

CONCLUSION: Thus, not only the determination of expression levels required for the determination of a suitable biomarker, but also the determination of the molecular targets of these microRNAs by bioinformatics analysis suggests that these microRNAs can be used for cancer diagnosis and prognosis.

Keywords: Bionformatic analysis, Colorectal cancer, Stage IIIA, miRNA, RT-PCR

INTRODUCTION

Colorectal cancer (CRC) is the most common gastrointestinal cancer that is a multifactorial disease caused by etiologic factors such as genetic factors, environmental exposures, diet and inflammatory conditions of the digestive system [1]. CRC constitutes an important health problem as it accounts for 10% of the worldwide cancer incidence [2,3]. Based on these results, it is clear that new and more effective strategies should be developed to allow early detection of this disease and that safer and more effective treatments can be developed to help reduce the global mortality rate associated with this disease. Considering all these situations, there is an increase in studies on CRC. The discovery of microRNAs, which are small RNA molecules, has led to different dimensions in the diagnosis and treatment of CRC (4). Currently, all of the studies on miRNA on cancers are based on the determination of different expression levels of miRNAs in cancer cells compared to normal cells [5,6].

Colon cancer in stage IIIA, the cancer has spread to up to 3 lymph nodes, from the innermost tissue of the colon to the middle wall of the colon. Therefore, it can be treated with chemotherapy after surgery [7]. Early diagnosis of colon cancer is very important for this stage [8].

The aim of this study is to determine the expression of miRNAs which have important effects in many biological processes such as regulation of gene expression at the transcriptional level. It is also aimed to understand the

mechanism of these miRNAs by identifying their target genes and pathways by performing bioinformatics analysis in order to better understand the cellular processes of these miRNAs.

MATERIAL AND METHODS

In this study, normal and tumor tissues were used obtained from the operation in 15 colorectal cancer patients who were classified as pathological from the general surgery department of Gaziantep Research and Application Hospital. It is aimed to determine the expression differences of miRNA-145-1, miRNA-21-2 and miRNA-92-1 between normal and tumor colorectal tissue obtained from patients using qRT-PCR.

RNA isolation and qRT-PCR analysis

Approximately 50 mg of tissue samples were homogenized in cold medium using 700 µL of QIAzol (Qiagen) reagent with Bertin Precell homogenizer (France). The miRNAeasy mini kit (Qiagen) was used to isolate total RNA containing miRNA from homogenates. The quantity and quality of the isolated RNAs were determined spectrophotometrically by NanoDrop 2000 Spectrometer (Implen). Measurements were made at 260 and 280 nm wavelengths. Samples with a concentration of miRNAs greater than 500 ng / µl and a ratio of 260/280 OD (optical density) of ~ 2 for RNA were included in the study. Total RNA was transcribed into cDNA using the miScript II RT (Qiagen) kit procedure. RT-PCR was performed on the Rotor-gene Q 5 PLEX HRM (Qiagen) at 37 °C for 60 minutes and then at 95 °C for 5 minutes. miRNA expression analysis was performed according to the reaction procedure using the miScript SYBR Green PCR kit (Qiagen) for RT-PCR reaction.

First, incubation for 15 minutes at 95 °C was performed to activate the DNA polymerase enzyme. Then the PCR protocol; Denaturation; (15 seconds at 94 °C) Hybridization; (30 seconds at 55 °C) Polymerization; (30 seconds at 70 °C). The reaction was repeated 40 times. RNAU6B was used as reference gen.

ΔCt values were calculated before the Ct values resulting from expression, then ΔΔCt and fold change were calculated using these values. ΔCt value calculation; ΔCtnormal was found by deducting the Ct value of the reference gene of normal tissue from the Ct value of normal tissue. Similarly, ΔCtumor was determined by subtracting the Ct value of the tumor gene's reference gene from the Ct value of the tumor tissue. Then, to calculate the ΔΔCt values tCt was performed by subtracting the ΔC tnormal value from the ΔCttumor. Fold change was calculated as $2^{-\Delta\Delta Ct}$.

Bioinformatic analysis and Statistical analysis

KEGG pathway analysis of target genes of miR-145-1 and miR-21-2 and miR-92-1 was performed with DIANA miRPath V3 Tarbase 7.0 software [9]. As a result of analysis, biological pathway analysis was carried out with 21 genes Funrich Gene Enrichment research tool. At the same time, Protein-Protein Interaction (PPI) analysis was performed with STRING software which shows the many connections of target genes to each other [10]. For all statistical analyses, p-values were two-tailed and differences were statistically significant at $p < 0.05$.

RESULT

Real-Time PCR (RT-PCR) was used to determine expression levels of miRNA-145-1, miRNA-21-2 and miRNA-92-1. Fold change was calculated over the Ct values obtained by qRT-PCR and miRNA expression levels in tumor tissue were compared with normal tissue expression levels. Clinicopathological information of the patients included in the study is shown in Table 1.

miRNA-145-1 was found to be down-regulated by decreased expression in tumor tissues (0.065 fold) than normal tissue ($p < 0.034$). When the expression profile of miRNA-21-2 was examined, it was found that the tumor tissue was expressed at increased compared to normal tissue (3.147) and was up-regulated. In addition, statistically significant difference was found between tumor tissue and normal tissue ($p = 0.045$). The expression profile of miRNA-92-1 was found to be up-regulated in the tumor tissue by expressing it higher than the normal tissue (4.777 fold). The ΔΔCt values of these miRNAs are shown in Figure 1.

Bioinformatics analysis

miR-145-1 and miR-21-2 and miR-92-1 were identified by colorectal cancer (hsa0521) KEGG analysis with DIANA miRPath V3. ($p<0.00048$). These genes: *BRAF, GSK3B, TGFBR1, SMAD2, APC, PIK3CB, BIRC5, AXIN1, APPL1, KRAS, MAPK9, JUN, CCND1, CTNNB1, MAPK8, MYC, MSH2, PIK3R1, TGFB2, MAPK1, TGFBR2*. Protein-Protein Interaction showing the interrelated interaction of the targeted 21 genes is shown in Figure 2. In PPI, the interaction of genes with another gene, gene activation, gene suppression shows many properties in relation to colors. FunRich Gene Enrichment with the biological pathway analysis of these genes; E-cadherin signaling event (47.62%), TGF Beta receptor signaling (57.14), mTOR signaling pathway (95.24%), such as cellular signaling affects many biological pathways (Figure 3).

DISCUSSION

Recent research has shown that the risk of death from CRC can be prevented by early screening and intervention [11]. Therefore, the discovery of biological markers at the molecular level is crucial for the early diagnosis of CRC [12]. By understanding the molecular basis of CRC, it is possible to develop diagnostic tests based on sensitive and specific molecular markers [12,13].

In a review by Zeinali et al., It was stated that miR-145 can be used as an important biomarker before metastasis in cancer studies and its molecular mechanisms will be possible by elucidating the target genes [14]. Thus, it supported the idea that miR-145 could be used as a biomarker before metastasis in colon cancer.

Pagliuca et al. showed that miRNA-145-1 may be a biomarker that acts as a tumor suppressor by inhibiting the activity of CRAS and BRAF genes in CRC [15]. In our study, miR-141-1 was found to be compatible with target genes determined by the decrease in expression level.

miRNA-21 has been shown to be a miRNA that acts oncogenic in almost all solid tumors and is highly expressed in tumor tissues compared to normal tissues [16-17]. According to studies, the expression of miRNA-21 targets several tumor suppressor genes leading to increased cell proliferation, decreased apoptosis, increased cell migration, invasion and metastasis [2,18,]. The data obtained in our study are in parallel with the results of other studies.

miRNA-92-1 is a miRNA that plays a key role in CRC. Studies have shown that miRNA-92 has a high level of expression in CRC [19]. Yamada et al. (2013) showed that the expression level of miRNA-92 varies according to the stage of cancer and that the expression of this miRNA is increased in tumors less than 40 mm [20] Since pre-stage IIIA metastasis tissues are used in our study and also by determining target genes of miRNA-92-1, it may contribute to the study of specific gene expression by contributing to the literature.

In this study, contributing to the scientific literature and revealing the roles of miRNAs in CRC treatment are among the expectations of this study.

Our results show that while miRNA-145-1 from expressed miRNAs is down-regulated in CRC tissues compared to control tissues, miRNA-21-2 and miRNA-92-1 are up-regulated relative to control groups. Differences in miRNA expression in all cancers, including CRC, do not result only from changes in miRNA biogenesis mechanisms. Epigenetic control also depends on reasons such as transcription factors or mutated protein controls. In this case, it is possible to say that miRNAs that may have tumor-suppressing or oncogenic effects will contribute to the onset, progression, and diffusion of CRC. In conclusion, it is thought that miRNAs will provide important benefits in the early diagnosis of cancer and in the development of treatment methods by determining the expression levels of miRNAs in cancerous tissues and evaluating the targeted mRNA.

Acknowlegment: In this study, we thank Ersin BORAZAN who provided surgical tissues.Ethical approval for the study was given by Harran University Ethics committee with the number 19.02.12. Our study was funded by Harran University Scientific Research Project (HUBAK) (grant no: 17093)

Conflict of interest: None of the authors declare any competing interests in the matters related to this paper.

REFERENCES

1. Burt RW, Disario JA, and Cannon-Albright L. Genetics of colon cancer: impact of inheritance on colon cancer risk. Annu Rev Med 1995; 46: 371-378.
2. Schetter AJ, Okayama H, and Harris CC. The Role of microRNAs in Colorectal Cancer. Cancer J., 2012; 18(3): 244–252.
3. Cancer Registry in Turkey. Turkey Cancer Institute Department of Public Health.http://kanser.gov.tr/daire-faaliyetleri/kanser-kayitciligi/ Erişim Tarihi: 02.08.2019.
4. Chen CY, Chen S-T, Fuh CS, Juan HF, Huang HC. Coregulation of transcription factors and microRNAs in human transcriptional regulatory network. BMC Bioinformatics. BioMed Central Ltd 2011; 12 p41.
5. Zhang B, Pan X, Cobb GP and Anderson TA. MicroRNAs as oncogenes and tumor suppressors. Dev. Biol. 2007; 302(1): 1–12.
6. Chen X, Ba Y, Ma L, Cai X, Yin Y, Wang K, et al. Characterization of microRNAs in serum: a novel class of biomarkers for diagnosis of cancer and other diseases. Cell Res., 2008; 18: 997–1006.
7. Ahmed A, Tahseen A, England E, Wolfe K, Simhachalam M, Homan T, Sitenga J, Walters RW, Silberstein PT (2019) Association Between Primary Payer Status and Survival in Patients With Stage III Colon Cancer: An National Cancer Database Analysis. Clin Colorectal Cancer. 2019 18(1): 1-7.
8. Cappell MS. The pathophysiology, clinical presentation, and diagnosis of colon cancer and adenomatous polyps. Med Clin N Am, 2005; 89: 1-42.
9. DIANA Website http://diana.imis.athena-innovation.gr/DianaTools/index.php?r=site/page&view=software (Last accessed September 2019)
10. STRING Website http://string91.embl.de/newstring_cgi/show_input_page.

pl?UserId=s9E0QV1YES8h&sessionId=bk2A4p19XbRm&input_page_type=multiple_identifiers (Last accessed September 2019)

11. Gattolliat CH, Uguen A, Pesson M, Trillet K, Brigitte S, Doucet L, et al. MicroRNA and targeted mRNA expression profiling analysis in human colorectal adenomas and adenocarcinomas. European Journal of Cancer 2015; 51: 409– 420.
12. Tsang AH. Current and future molecular diagnostics in colorectal cancer and colorectal adenoma. World Journal of Gastroenterology, 2014; 20(14): 3847-3857.
13. Garcea GA, Sharma RA, Dennıson A, Steward WP, Gescher A, Berry DP. Molecular biomarkers of colorectal carcinogenesis and their role in surveillance and early intervention. Eur J Cancer 2003; 39(8): 1041-52.
14. Zeinalia T, Mansooria B, Mohammadia A, Behzad Baradaran B. Regulatory mechanisms of miR-145 expression and the importance of its function in cancer metastasis Biomedicine & Pharmacotherapy 2019; 109: 195–207.
15. Pagliuca A, Valvo C, Fabrizi E, Di-Martino S, Biffoni M, Runci, D, et al. Analysis of the combined action of miRNA-143 and miRNA-145 on oncogenic pathways in colorectal cancer cells reveals a coordinate program of gene repression. Oncogene 2013; 32(40): 4806–4813.
16. Meng F, Henson R, Wehbe-Janek H, Ghoshal K, Jacob ST and Patel T. MicroRNA-21 regulates expression of the PTEN tumor suppressor gene in human hepatocellular cancer. Gastroenterology 2007; 133(2): 647-658.
17. Zhu W, XU B. MicroRNA-21 Identified as Predictor of Cancer Outcome: A Meta-Analysis. Plos One 2014; 9(8): 1033-1073.
18. Bahnassy AA, Salem SE, Sayed M, Khorshid O, Abdellateif MS, Youssef AS, Mohanad M, Hussein M, Zekri AN, Ali NM. MiRNAs as molecular biomarkers in stage II egyptian colorectal cancer patients. Exp Mol Pathol. 2018; 105(3): 260-271.
19. Chen E, Li Q, Wang H, Yang F, Min L, Yang J. MiR-92a promotes tumorigenesis of colorectal cancer, a transcriptomic and functional based study. Biomedicine & Pharmacotherapy 2018; 106: 1370–1377.
20. Yamada N, Yoshihito Nakagawa Y,Tsujimura N, Kumazaki M, Noguchi S, Mori T, Hirata I, Maruo K, and Akao Y. Role of intracellular and extracelular miRNA 92a in Colorectal Cancer Translational Oncology 2013; 6: 482–492.
Table 1. Clinical information of colon cancer stage IIIA patients included in the study

Table 1. Clinical information of colon cancer stage IIIA patients included in the study

Characteristics (n=15, control and tumor tissue)		Number
Gender	Male	6
	Female	9
Age (age range)		63(58-67)
Locations of Tumors	Colon	11
	Rectum	4
	T1	5
Pathologic T classification	T2	10
	T3	0
Pathologic N classification	N0	0
	N1	15
	N2	0
Metastatic classification	M0	15
	M1	0
AJCC Classification	Stage IIIA	15

Figure 1: miRNA expression fold change relative to health tissue.

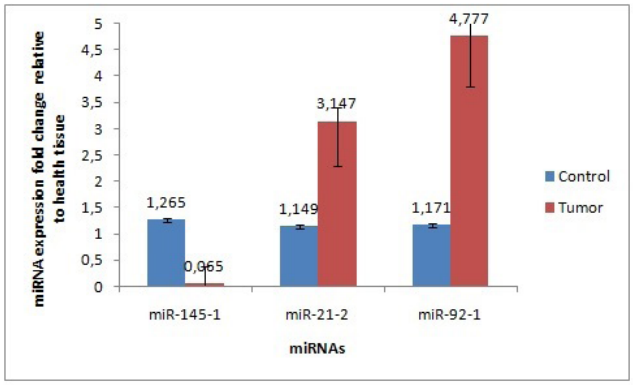

Figure 2: Protein-Protein Interaction of miRNA targets.

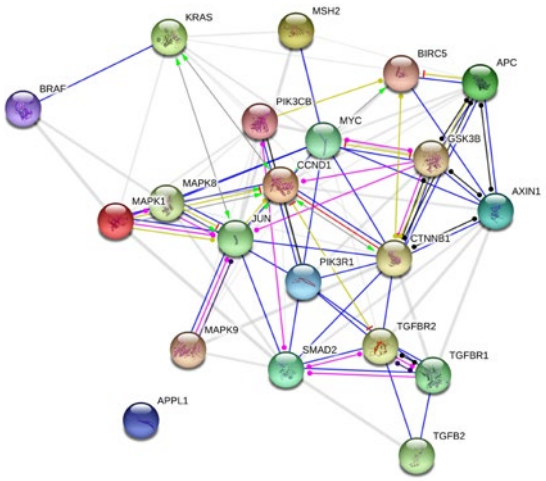

Figure 3: miRNA targets Biological pathway

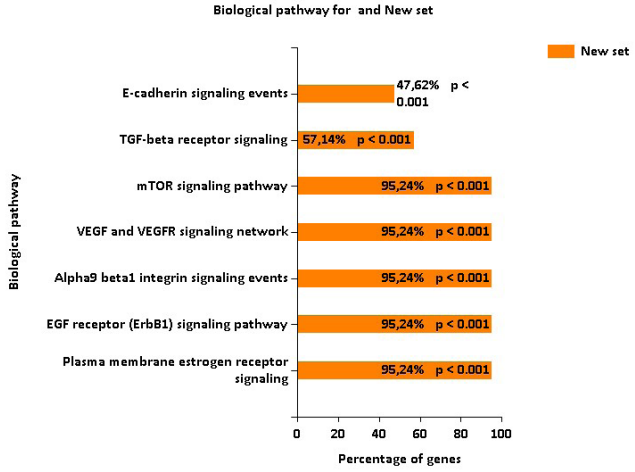

OP-06

THE EFFECT OF CORM-2 MOLECULE ON HYDROGEN PEROXIDE-INDUCED NEUROBLASTOMA CELLS

Deniz Catakli [1], Melania Ronfani [2], Cristina Lanni [2], Gonen Ozsarlak-Sozer [1]

[1] Ege University, Faculty of Pharmacy, Department of Pharmacology, Bornova, İzmir, Turkey

[2] Department of Drugs Sciences, Università degli Studi di Pavia, Viale Taramelli 12/14, 27100, Pavia, Italy.

OBJECTIVES: Oxidative stress caused by reactive oxygen species (ROS) inhibiting the effects of the body's antioxidant system is the main pathology of many diseases. Heme oxygenase (HO) in the cellular antioxidant system is oxidative sensor protein induced by ROS formation or carbon monoxide (CO) production. CORM-2 (tricarbonyldichlororuthenyum-II), Co releasing molecule induces the expression of heme oxygenase-1 (HO-1). The aim of the study is to determine the effect of CORM-2 on hydrogen peroxide (H2O2) induced neuroblastoma cells (SH-SY5Y) through HO-1 induction.

MATERIAL&METHODS: To determine the effective concentration of CORM-2, MTT analyze was performed. The cells were treated with 1 µM, 5 µM, 10 µM, 25 µM and 50 µM concentrations of CORM-2. At the end of the MTT analysis 20 µM and 50 µM concentrations were determined for Western Blot and Real-Time PCR experiments. The cells were pre-treated with the 20UM and 50 UM concentrations of CORM-2 for 3 hours, then they were induced with 300 µM H2O2 for 3 hours. The samples were prepared for Western Blot and Real-Time PCR experiments.

RESULTS: CORM-2 molecule significantly affected cell viability in SHSY-5Y cells in the dose range of 10 µM– 50 µM. The expression of HO-1 (0.42 ± 0.02 and 0.82 ± 0.13 control and 20 µM respectively, n = 3) was increased in SH-SY5Y cells which are pretreated with the 20 µM and 50 µM CORM-2 concentrations as a result of Western Blot experiments.

CONCLUSIONS: In the presence of oxidative stress, CORM-2 increased HO-1 expression. This may be significant in carcinogenesis and neurodegenerative disorders.

Keywords: CORM-2, HO-1 induction, Oxidative stress

INTRODUCTION

Oxidative stress is characterized by the imbalance between oxidants and antioxidants. Reactive oxygen species (ROS) are one of the oxygen metabolism products and they are categorized as cellular oxidants. In some pathological conditions which can be a result of oxidative stress, inflammation, xenobiotics, radiation, overexpression of ROS is seen. This overexpression can lead to oxidative DNA damage, gene mutation, and carcinogenesis, also it can cause lipid peroxidation which contributes the cell death [1]. In mammalian cells, cellular heme is catalyzed to free iron, biliverdin/bilirubin and carbon monoxide (CO) by the rate-limiting enzyme heme oxygenase -1 (HO-1). Although the main role of HO-1 is the heme catabolism, it also shows anti-oxidative and anti-inflammatory effects through biliverdin and CO metabolites [2]. It was characterized as a survival molecule for stress-related conditions and exhibits crucial role in cancer progression. The main mechanism of the HO-1 is still unclear. Although the augmented expression of HO-1 is protective in cellular stress conditions in many disease states including kidney injury and neurodegeneration, its role in carcinogenesis is controversial [1,3,4,5]. It is reported to play a cytoprotective role in tumor cells preventing apoptosis and autophagy and to promote cell proliferation and metastasis causing resistance to chemotherapy and radiation therapy [6]. On the other hand, depending on the excessive cellular iron production during HO-1 breakdown HO-1 can be beneficial in cancer therapy [1]. CO and CO releasing molecules (CORMs) have protective effects in inflammatory and vascular diseases as well as neurodegeneration [7]. More recently, there is accumulating evidence demonstrated CO and CORMs as therapeutic agents for cancer therapy [8,9]. The aim of the study was to determine the effect of CORM-2 on hydrogen peroxide (H_2O_2) induced neuroblastoma cells (SH-SY5Y) through HO-1 induction.

MATERIALS AND METHODS

Cell Culture

The human neuroblastoma cell line (SH-SY5Y) was cultured in 50% MEM/HAM'S F-12 medium containing 1% L-Glutamine, 10% FBS (fetal bovine serum), 1% penicillin/streptomycin, 1% non-essential amino acids and kept at 37 ^{o}C in a humidified 5% CO_2 incubator. To demonstrate the effect of CORM-2 in the H_2O_2-induced oxidative stress condition, cells were pre-treated with CORM-2 for 3 hours then 300µM of H_2O_2 was added and incubated 3 hours.

Cell viability assay

To investigate the viability of cells, MTT assays were performed. Cells were cultured in 96 well plates (1.5x10^4 cells/ well) for 24 hours. At the end of 24 hours, cells were pre-treated with different concentrations (1µM, 5µM, 10µM, 25µM and 50 µM) of 100ul of tricarbonyldichlororuthenium(II) dimer (CORM-2, Sigma) for 24 hours. 1mg/ml MTT solution was added to each well and waited for 4 hours then, 100 µl of lysing buffer (20% SDS, dimethylformamide, and distilled water) was added. The absorbance was measured at 570 nm by using microplate reader. The same protocol was performed for the human monocyte cell line (THP-1) to see the effect of CORM-2 on different cell types.

Western blot analysis

The expression of HO-1 and β-actin in cell homogenates was determined by the Western blot analysis. Briefly, for every three groups (control, 20µM, and 50µM), 3x10^6 cells were plated in a petri dish 60mm. Cells were pre-treated with CORM-2 for 3 hours and 300µM H_2O_2 added. At the end of the 3 hours, samples were collected, washed with PBS twice, centrifuged and lysed with RIPA buffer and protease inhibitor mixture. Lysates were centrifuged at 13,000 rpm for 5 min. The protein content was measured by using Bradford method. The samples of Western blotting were prepared with the mixing the cell lysate with the sample buffer (125 mM Tris−HCl pH 6, 8.4% SDS, 20% glycerol, 6% β-mercaptoethanol, 0.1% bromophenol) and the mixture was denatured at 95 °C for 5 minutes. Proteins (20 µg/ml) were loaded each lane and separated by electrophoresed on SDS-PAGE gels. The proteins were transferred to PVDF membrane (Amersham, Little Chalfont, UK). Membranes were incubated with 5% BSA for 1h. Then membranes were incubated with primary antibodies against β-actin (BD Biosciences) and HO-1 which were diluted with the 5% BSA (1:1000) during an overnight at 4 °C. After that, membranes were incubated with secondary antibodies (Sigma-Aldrich, USA) (anti-mouse for β-actin and anti-rabbit for HO-1) for 2 hours at 37°C. Lastly, bands were visualized by ECL detection system.

Real-Time PCR

The cells were plated in a Petri dish (60 mm) for analyzing mRNA expression of HO-1 gene. Total RNA was extracted by using RNeasy Plus Mini Kit (Qiagen, Valencia, CA, USA) following manufacturer's instructions. RNA quantification was measured by Quantus™ Fluorometer (Promega, Madison, WI). cDNA synthesis was performed with the QuantiTect reversion transcription kit (Qiagen, Valencia, CA).

GoTaq®G2 DNA-polymerase (Promega, Madison, WI) was used for the amplification of polymerase chain reaction (PCR). Real-time PCR was performed by QuantiTect Syber Green PCR kit and for gene expression analysis of GAPDH and HO-1, primers were provided by Qiagen. Quantification of the transcripts was performed by $2^{-\Delta\Delta CT}$method.

Statistical Analysis

The data were presented as mean ±SEM. For Western Blot analysis, a two-tailed Student t-test was used. MTT and Real-Time PCR analyses were determined by One-Way ANOVA followed by Dunnett's Multiple Comparison Test.

RESULTS

CORM-2 reduces the viability of SH-SY5Y cells

To determine the effective dose of CORM-2 on SH-SY5Y cells, MTT assay was performed. SH-SY5Y cells were treated with CORM-2 in concentrations ranging from 1µM to 50µM for 24h. The significant reduction of cell viability was observed with 10-50µM by MTT assay (Fig. 1.A). As shown in Figure 1.B, CORM-2 did not affect the viability of THP-1 cells which means it did not show the same effect with the SH-SY5Y cells.

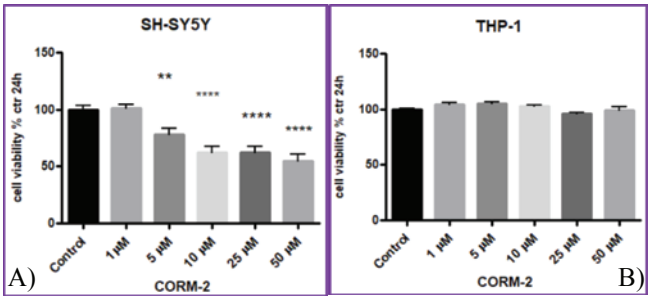

Fig .1 A) The effect of CORM-2 on SH-SY5Y cell viability in different concentrations. Values represent mean ± SEM, *control vs. 5*µM *CORM-2* ***p<0.0001, control vs. 10*µM *CORM-2* ***p<0.0001, control vs. 25*µM *CORM-2* ***p<0.0001, control vs. 50* MM *CORM-2* ***p<0.0001, Dunnett's Multiple Comparison Test, n =16.* B) The effect of CORM-2 on THP-1 cell viability in different concentrations. p>0.1, One-way ANOVA, *Dunnett's Multiple Comparison Test, n =16.*

CORM-2 induced HO-1 expression in SH-SY5Y cells

Western Blot analysis was performed to observe the expression of HO-1 in SH-SY5Y cells. The concentrations which were determined by MTT assay were used for the Western Blot analysis. As shown in Figure 2, 20μM and 50μM concentrations of CORM-2 increased the expression of HO-1 under H_2O_2 induced oxidative stress conditions (0.42 ± 0.02 and 0.82 ± 0.13 control and 20 μM respectively, n = 3).

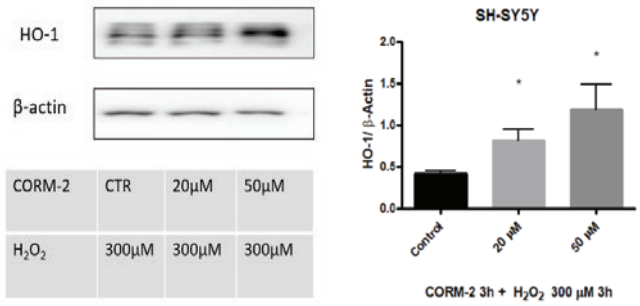

Fig. 2 The effects of CORM-2 on the expression of HO-1 in 300μM H_2O_2 induced SH-SY5Y cells. *Control vs. 20* μM *CORM-2 and control vs. 50* μM *CORM-2, p<0.1Student-t test, n=3.*

CORM-2 induced the mRNA expression of HO-1 in SH-SY5Y cells

The effect of CORM-2 on HO-1 expression in SH-SY5Y cells treated with the 300 μM H_2O_2 was investigated with Real-Time PCR. HO-1 levels were not significantly increased in SH-SY5Y cells.

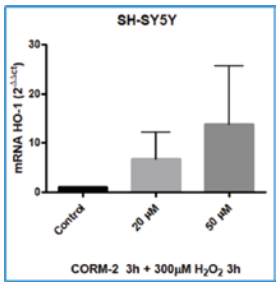

Fig. 3 The effects of CORM-2 on mRNA expression of HO-1 in 300μM H_2O_2 induced SH-SY5Y cells. *Control vs. 20* μM *CORM-2 and control vs. 50* μM *CORM-2, n.s. Student t-test, n=3.*

CONCLUSION

CORM-2 induced mRNA expression of HO-1 in SH-SY5Y cells, but significance was not seen between the groups. As a comparison, it induced the protein expression of HO-1 significantly (Fig.2). The reason may be the post-translational mechanism and also RNA turnover because protein synthesis is a long process and more resistant. RNA shows sensitivity with time, its structure may change by time. To get more accurate results RT-PCR could be repeated time-dependently.

Briefly, results of this study showed that CORM-2 has a concentration-dependent cytotoxic effect on SH-SY5Y cells. On the other hand, it induced HO-1 expression which is an important pathway in both carcinogenesis and neurodegenerative diseases. Further studies should be performed to enlighten the outcomes of this induction.

Acknowledgments

The authors would like to thank to Michele Catanzaro and Francesca Fagiani for their suggestions and technical supports.

Conflict of Interest

The authors declare no conflict of interest.

REFERENCES

1. Chiang SK, Chen SE, Chang LC. A dual role of heme oxygenase-1 in cancer cells. Int J Mol Sci. 2019;20(1):1–18.
2. Chau LY. Heme oxygenase-1: Emerging target of cancer therapy. J Biomed Sci. 2015;22(1):1–7.
3. Gozzelino R, Jeney V, Soares MP. Mechanisms of Cell Protection by Heme Oxygenase-1. Annu Rev Pharmacol Toxicol. 2010;50(1):323–54.
4. Nitti M, Piras S, Brondolo L, Marinari UM, Pronzato MA, Furfaro AL. Heme oxygenase 1 in the nervous system: Does it favor neuronal cell survival or induce neurodegeneration? Int J Mol Sci. 2018;19(8):1–20.
5. Bolisetty S, Zarjou A, Agarwal A. Heme Oxygenase 1 as a Therapeutic Target in Acute Kidney Injury. Am J Kidney Dis . Elsevier Inc; 2017;69(4):531–45.
6. Loboda A, Jozkowicz A, Dulak J. HO-1/CO system in tumor growth, angiogenesis and metabolism - Targeting HO-1 as an anti-tumor therapy. Vascul Pharmacol . Elsevier Inc.; 2015;74:11–22.
7. Motterlini R, Otterbein LE. The therapeutic potential of carbon monoxide. Nat Rev Drug Discov . Nature Publishing Group; 2010;9(9):728–43.
8. Kourti M, Jiang WG, Cai J. Aspects of Carbon Monoxide in Form of CO-Releasing Molecules Used in Cancer Treatment: More Light on the Way. Oxid Med Cell Longev. 2017;2017.
9. Motterlini R, Mann BE, Foresti R. Therapeutic applications of carbon monoxide-releasing molecules. Expert Opin Investig Drugs. 2005;14(11):1305–18.

OP-07

COMPARATIVE TOXICITY ASSESSMENT of CANCER-TARGETED POLYMERIC NANOPARTICLES: *IN VIVO C. ELEGANS* AND *IN VITRO* CELL CULTURE MODELS

Elif Yavuz-Dokgöz[1,*], Emircan Tengirşek[2], Meltem Güleç[3], Zeynep Püren Akgüner[4], Tuğba Erol[5], Serkan Emik[5], Abdullah Olgun[1], Ayça Bal-Öztürk[4,6,*]

[1]Department of Biochemistry, Faculty of Pharmacy, Istinye University, 34010 Istanbul, Turkey

[2]Faculty of Pharmacy, Istinye University, 34010 Istanbul, Turkey

[3]Department of Pharmacognosy, Faculty of Pharmacy, Istinye University, 34010 Istanbul, Turkey

[4]Department of Stem Cell and Tissue Engineering, Institute of Health Sciences, Istinye University, 34010 Istanbul, Turkey

[5]Department of Chemical Engineering, Faculty of Engineering, Istanbul University-Cerrahpasa, Istanbul 34320, Turkey

[6]Department of Analytical Chemistry, Faculty of Pharmacy, Istinye University, 34010 Istanbul, Turkey

Corresponding authors: *aycabal@gmail.com, *aozturk@istinye.edu.tr, *eyavuz@istinye.edu.tr

INTRODUCTION: We aimed to perform a comparative toxicity assessment of our previously developed CTPNs using *C. elegans* as *in vivo* model organism and cell culture (in HeLa and L929 cell lines) based MTT assay as an *in vitro* model. A comparative *in vitro* and *in vivo* toxicity assessment of our previously developed-hyperbranched poly(amino ester) based- cancer-targeted polymeric nanoparticles (CTPNs) was performed.

MATERIALS AND METHOD – N2 wild type *C. elegans* strain was grown under standard conditions. Synchronized worms were exposed to CTPNs from the beginning of L1 larval stage. Phenotypic evaluation was done under microscope. *In vivo* toxicity was assessed at 6th, 24th, 48th hours and during reproductive adult stage. *In vitro* toxicity was tested by MTT assay to CTPNs for 6, 24 and 48 hours.

RESULTS: No observational and statistically significant difference was found between CTPNs treated and control groups in *C. elegans* toxicity study and MTT assay.

CONCLUSION: The fact that CTPNs that we have developed did not show toxic effects in *in vivo* and *in vitro* models we have tested, is expected to support further preclinical research in the future.

Keywords: Cytotoxicity, MTT, *C. elegans*, cancer-targeted polymeric nanoparticles.

INTRODUCTION

Current developments in the field of targeted therapeutics has allowed selective and specific treatment of patients by targeted drug systems with decreased side/adverse effects and increased therapeutic potential. This becomes possible by specific uptake of the drug by non-healthy cells. There are many different ways to target a drug molecule in human body, but nanoparticles are one of the most popular options due to their advantages [1-3]. In our previous study, we reported the development of folic acid- conjugated hyperbranched nanoparticles (CTPNs) for cancer targeted drug delivery and pH-controlled drug release. The developed folic acid-conjugated nanoparticles have hyperbranched poly(aminoester) based polymeric core and poly(ethylene glycol)-*b*-poly(ε-caprolactone) diblock polymer arms. They show selective binding to the surface receptors of tumor cells through targeted ligands and are internalized into the cells by folate receptor-mediated endocytosis [4-5].

Caenorhabditis elegans (*C. elegans*), being an *in vivo* model organism, have been widely used in a number of biological studies, and gained increasing attention as a promising multicellular alternative for *in vivo* toxicity tests. Among the unique features of *C. elegans* that make it a proper model for toxicity assays are its fully sequenced genome that is closer to human genome [6-7], its easy maintenance with low cost, relatively short life span, transparent body and suitability for high throughput screening studies. Its developmental process and behavior can be easily monitored under a microscope. The nematode reaches the adult stage by passing through four larval stages (L1, L2, L3 and L4) after hatching. It is

easily cultured on petri dishes or in axenic liquid medium using *Escherichia coli* (*E. coli*) OP50 strain as a food source. Therefore several toxicity tests using *C. elegans* can be performed in different conditions including water [8], and soil [9]. Toxicity of nanoparticles were also tested on *C. elegans* [7, 10-12]. *C. elegans* provides researchers the chance to bridge the gap between *in vitro* and *in vivo* approaches. However there are no studies using *C. elegans* for CTPNs' toxicity to our knowledge. In this study, we performed a comparative toxicity assessment of our previously developed- hyperbranched poly(amino ester) based- cancer-targeted polymeric nanoparticles (CTPNs) in both *C. elegans* and cell culture (HeLa and L929 cell lines for MTT assay).

MATERIALS AND METHODS

Materials: HeLa cells and L929 cells were kindly provided by Istinye University Molecular Cancer Research Center and Department of Genetics and Bioengineering at Yeditepe University, respectively. *C. elegans* (Wild type, Bristol strain N2) and *E.coli* OP50 strain were obtained from the Caenorhabditis Genetics Center (CGC), Minnesota University (Minnesota, ABD).

MTT assay: MTT is a colorimetric enzyme activity based assay, which is widely used for the detection of living cells. This method is based on the conversion of MTT (3, (4,5-dimethylthiazol-2-yl)-2,5-diphenyl tetrazolium bromide) to colored formazan derivatives (red-purple) by viable cells. MTT assays were performed with same concentration of CTPNs in HeLa and L929 cell lines. Exposure times of CTPNs for toxicity assays were 6h, 24h and 48h. Roswell Park Memorial Institute (RPMI) 1640 medium, 10% Fetal Bovine Serum (FBS) and 1% penicillin-streptomycin were used for culturing HeLa cells. L929 cells were cultured in Dulbecco's Modified Eagle's Medium (DMEM), 10% Fetal Bovine Serum (FBS) and 1% penicillin-streptomycin. The cultured cells were seeded in 96-well plates with $5x10^3$ cells/well. Cells were incubated overnight at 37°C in 5% CO_2. CTPNs were diluted in the culture media and then added to the wells (final conc. 0.5 mg/mL). After incubation at 37°C, 5% CO_2, and 90% humidity for 6, 24 and 48 h, the medium was removed and washed with PBS three times. Subsequently, 200 µL of culture media and 20 µL of MTT solution (2µg/mL, diluted with PBS) were added to each well and cells were subjected to a further incubation of 4 h at 37°C in 5% CO_2 to allow formation of formazan crystals. Then, the unreduced MTT and medium was removed, and the cells were washed three times with PBS. 200 µL of DMSO was added to each well to dissolve the purple MTT formazan crystals and the plate was incubated at 37°C for 30 min. The absorbance of formazan products was measured at 570 nm using a microplate reader (Spektrostar Nano S/N 601-1047 BMG Labtech, Offenberg, Germany).

The cytotoxicity of the nanoparticle formulations was calculated using the following equation [3]:

Cell viability (%) = $(OD_{570}(sample)/OD_{570}(control))x\ 100$

***C. elegans* toxicity assays:** Wild type *C. elegans* N2 strain was used and fed with *E. coli* OP50. All worms were maintained on nematode growth medium [(NGM: NaCl (Carlo Erba) 3 g/L; bacteriological peptone (Multicell) 2.5 g/L; bacteriological grade agar (Multicell) 17 g/L; 1 M potassium phosphate (Sigma) 25 mL; 1 M $CaCl_2$ $2H_2O$ (Merck) 1 mL; 1 M $MgSO_4.7H_2O$ (Merck) 1 mL; 5 mg/mL cholesterol (Sigma-Aldrich) 1 mL; (100µg/mL penicillin-streptomycin (Multicell, WISENT INC.) 10 mL per dish to avoid contamination)] plates at 22±2°C.

Worms were maintained using standard procedures. After autoclaving at 121°*C for 15 minutes,* NGM was cooled to 55°C down. Penicillin-streptomycin was added. The homogeneous mixture was transferred to the petri dishes to fill 2/3 of the 60 mm petri dishes. Heat killed OP50 was supplied as a food source. Bacteria at OD 0.4 were killed by treating at 65°C for 10 minutes. CTPNs were added in *E. coli* mixture.

The protocol used to obtain synchronized worms is based on the fact that worms are sensitive to bleach (hypochlorite) while the eggshell protects embryos from it. Firstly, dishes with eggs were washed with distilled water. The liquid was transferred into a 15 mL tube and the desired amount of bleach: 5N NaOH (1:2) mixture was added on it. It was vortexed once per 2 minutes for 10 minutes. After that, it was centrifuged at 1300 xg for 30 seconds and the supernatant was decanted without disturbing the worm pellet. The pellet was washed three times and transferred to new petri dish. Synchronized worms were allowed to grow to L1 stage and followed until they became adults. Exposures were initiated at the L1 stage [13].

Worms at L1 larval stage (n=10) were transferred to each well in four replicates for survival and reproduction analyses. For general maintenance, worms were transferred into the petri dish seeded with 200 µL OP50 using a worm pick.

The nematode toxicity assay was carried out on the NGM plates. *E.coli* mixtures with CTPNs (at a final concentration of 0.5 mg/mL) were used in experimental group. The exposure periods for the survival and reproduction assays were 6h, 24h and 48h. In the control group, there was no CTPNs in *E.coli* mixture (Table1). After exposure, nematodes were observed under the microscope. The toxicity was evaluated by counting the number of surviving worms. All groups were studied in petri dishes with four replicates. In order to obtain quantitative results at the 6th, 24th and 48th hours from the larval stage, the animals were counted on a stereomicroscope and their images were captured with high resolution scanner (Epson Perfection, V800 Photo). Larvae viability was monitored on a fluorescent microscope (Zeiss Axiocam ICc5). Reproduction was evaluated by observing new progeny under stereomicroscope (Zeiss Stemi 508).

Statistics: Calculations were performed using Prism software package, ANOVA with Tukey post test. A value of $p<0.05$ was considered statistically significant.

RESULTS

In vivo* toxicity analysis of CTPNs in *C. elegans

CTPNs were found to be non-toxic at the studied concentrations (final conc. 0.5 mg/mL) in worms. Worms were %100 viable at 6th, 24th and 48th hours of treatment. In the control groups there was 1 dead worm at 24th and 48th hours. Their larval development and egg laying were normal compared to controls (Table 2).

***In vitro* toxicity analysis of CTPNs in L929 and HeLa cell lines**

In MTT assays, 100.3% cell viability was detected in the L929 cell line at the end of the 6th hour. The viability decreased to 88.7% and 89.7% at the end of 24th and 48th hour, respectively. In the HeLa cell line the cell viability detected 101.8% at 6th hour, 85% at 24th hour and 82.2% at 48th hour (Figure 1).

DISCUSSION

Targeted theraneustics are very important in reducing side/adverse effects and increasing effectiveness of medications. Targeted nanoparticle type therapeutics, if optimized, also have the advantage of slow and sustained release of drugs into target cells.

There is a very significant increase in the variety and number of nanomedicines developed. Therefore their safety needs to be assured. During the development process of nanomedicines, their safety have to be tested at very early stages of preclinical phase in order to make a rational decision to continue or not. Preclinical phase covers *in vitro* and *in vivo* studies. *C. elegans*, an invertebrate model organism that does not require ethical approval to study, is a very convenient *in vivo* model for preclinical phase of drug development. Another preclinical model is MTT assay that is used to test the safety of candidate drugs in cells.

In this study, we tested the safety of CTPNs in both *C. elegans* and cell lines including L929 and HeLa cells. We observed no toxic effects of CTPNs in these *in vivo* and *in vitro* systems. These findings are encouraging to continue our studies in vertebrate model organisms before starting clinical studies.

Acknowledgment:

This study does not require ethical approval.

It was supported by Turkish Scientific and Technical Research Council (TUBITAK) (Grant No: 117Z732).

REFERENCES:

1. Rosenholm JM, Sahlgren C, Lindén M. Towards Multifunctional, Targeted Drug Delivery Systems Using Mesoporous Silica Nanoparticles–Opportunities & Challenges. Nanoscale. 2010; 2(10): 1870–1883.
2. Yokoyama M. Drug Targeting with Nano-Sized Carrier Systems. J. Artif. Organs. 2005; 8(2): 77–84.
3. Hu JJ, Liu MD, Gao F, Chen Y, Peng SY et al. Photo-controlled liquid metal nanoparticle-enzyme for starvation/photothermal therapy of tumor by win-win cooperation. Biomaterials. 2019: 217:119303.
4. Bal Öztürk A. In vitro targeting of synthesized folic acid-conjugated poli(amino ester) based-hyperbranched polymeric nanoparticles. Brightlands Rolduc Polymer Conference: Kerkrade, Netherhands, 2019; Abstract #156.
5. Bal Öztürk A. In vitro Release Behaviour of Folic Acid Functionalized Hyperbranched Nanoparticular Systems, NANOTR-15 Conference: Antalya, Turkiye, 2019.
6. The C. elegans Sequencing Consortium. Genome sequence of the nematode C.elegans: a platform for investigating biology. Science. 1998; 282: 2012–2018.
7. Roh JY, Park YK, Park K, Choi J. Ecotoxicological investigation of CeO2 and TiO2 nanoparticles on the soil nematode Caenorhabditis elegans using gene expression, growth, fertility and mortality as endpoints. Environ. Toxicol. Pharmacol. 2010; 29:167–172.
8. Van Kessel WH, Brocades Zaalberg RW, Seinen W. Testing environmental pollutants on soil organisms: a simple assay to investigate the toxicity of environmental pollutants on soil organisms using CdCl2 and nematodes. Ecotoxicology and Environmental Safety. 1989; 18:181–190.
9. Donkin SG, Dusenbery DB. A soil toxicity test using the nematode Caenorhabditis elegans and an effective method of recovery. Archives of Environmental Contamination and Toxicology. 1993; 25:145–151.
10. Gonzalez-Moragas L, Roig A, Laromaine A. C. elegans as a tool for *in vivo* nanoparticle assessment. Advances in Colloid and interface Science. 2015; 219: 10-26.
11. Meyer JN, Lord CA, Yang XY, Turner EA, Badireddy AR, Marinakos SM et al. Intracellular uptake and associated toxicity of silver nanoparticles in *Caenorhabditis elegans*. Aquatic Toxicology. 2010; 100(2):140-150.
12. Wang H, Wick RL, Xing B. Toxicity of nanoparticulate and bulk ZnO, Al2O3 and TiO2 to the nematode *Caenorhabditis elegans*. Environmental Pollution. 2009;157(4):1171-1177.
13. Meyer JN, Boyd WA, Azzam GA, Haugen AC, Freedman JH, Van Houten B. Decline of nucleotide excision repair capacity in aging *Caenorhabditis*

elegans. Genome Biol. 2007;8(5):R70.

Table 1. *C. elegans* toxicity assays

Groups	Treatment	Number of worms x replicate number
Experimental	200µL *E.coli* in LB with CTPNs (0.5mg/mL final conc.)	10 x 4
Control	200 µL *E.coli* in LB	10 x 4

Figure 1. *In vitro* toxicity of CTPNs in L929 and HeLa cell lines

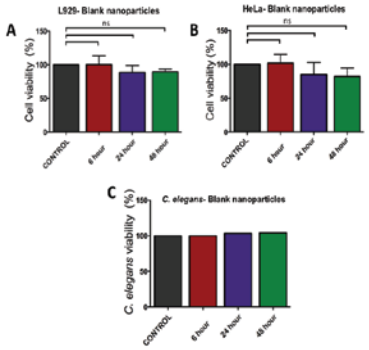

Table 2. *In vivo* toxicity of CTPNs in *C. elegans*

		Groups	
		Control	**CTPNs treatment**
Treatment time (hour)	**24**	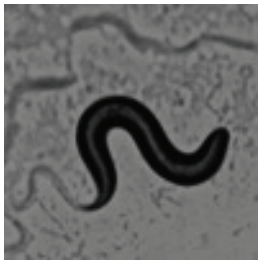	
	48	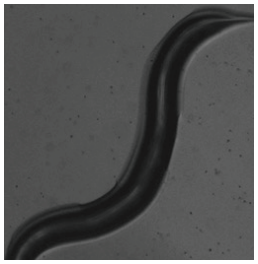	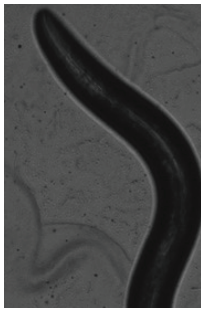
Reproductive period			

OP-08

AN ASSESSMENT OF BIOCHEMICAL AND STRUCTURAL RESPONSE OF RADIOACTIVE IODINE THERAPY IN PAPILLARY THYROID CANCER

Emine Acar[1,2], Özhan Özdoğan[3]

[1] İzmir Kâtip Celebi University, Ataturk Training and Research Hospital, Department of Nuclear Medicine, Izmir, Turkey

[2] Dokuz Eylul University, Institute of Health Sciences, Department of Translational Oncology, Izmir, Turkey

[3] Dokuz Eylul University, Faculty of Medicine, Department of Nuclear Medicine, Izmir, Turkey

OBJECTIVES: The aim of this study is to evaluate the biochemical and structural response of Iodine-131 (I-131) radioactive iodine (RAI) therapy that enters the thyroid cell through sodium iodide symporter in patients with papillary thyroid cancer.

MATERIAL&METHODS: The patient who had undergone total thyroidectomy with the diagnosis of papillary thyroid cancer between July2007–December2015 then received 100 mCi I-131 RAI therapy, have no metastasis and in low-moderate risk group were included in the study. The pathological findings were obtained by medical records. Pre-treatment off serum thyroglobulin (Tg) and anti-thyroglobulin (ATG) values were measured. The whole body scintigraphy images were examined in terms of postoperative residual tissue. Off Tg, ATG values were obtained in post-treatment month-9. The treatment response was then evaluated in scanning images.

RESULTS: Overall 456 patients were included in the study. The mean age was 46±12 (372 F, 84 M) years. While the pre-treatment Tg and ATG mean values were 8.8±21, 23.7±158 ng/ml, post-therapy measurements were 1.3±15, 5.0±37 ng/ml ($p<0.001$; $p<0.001$, respectively). Residual disease was observed in 445 (97.6%) patients in post-ablation images and in 67 (14.7%) patients in 9th month scanning images ($p<0.001$). There was no significant difference among pre-and post-treatment Tg, ATG values and lympho-vascular invasion, extra-thyroid spread, surgical margin positivity, central lymph node metastasis, risk group and post-treatment residual disease.

CONCLUSIONS: Our results have demonstrated that I-131 therapy succeeded to achieve better biochemical and structural response in patients with papillary thyroid cancer. However, we have determined that pathological features and surgery did not affect biochemical parameters in the low-moderate risk group patients.

Keywords: RAI, thyroid cancer, thyroglobulin, anti-thyroglobulin

INTRODUCTION

Thyroid cancer is the most common malignancy of the endocrine system and the incidence of the disease has significantly increased in recent years [1, 2]. Thyroid cancer treatment consists of surgery, followed by radioactive iodine (RAI) treatment and thyroid hormone replacement.

RAI ablation treatment targets to demolish the residual tissue, furthermore allows the clinicians to use serum thyroglobulin (Tg) values as a tumor marker by resetting Tg values. It also eliminates residual tissue and reduces the likelihood of local recurrence and metastasis. Metastatic areas that cannot be detected before treatment can be shown via post-ablation imaging. In case of residual micro or macroscopic disease ‘’adjuvant RAI therapy is administered, for distant metastasis treatment ‘’RAI treatment” is preferred [3, 4].

The aim of this study to evaluate the biochemical and structural response to iodine (I) -131 radioactive iodine (RAI) therapy entering the thyroid cell via sodium iodide symporter in patients with papillary thyroid cancer.

MATERIALS AND METHODS

The hospital records regarding the patients who underwent total thyroidectomy for papillary thyroid carcinoma between July 2007 and December 2015 were retrospectively analyzed. Then, those who were treated with 100 milicurie (mCi) I-131 RAI with low to moderate risk and have no metastasis were included in the study. The pathology results of the patients (lymphovascular invasion, extra-thyroid spread, surgical margin positivity, central lymph node metastasis) were obtained from patient files. The L-thyroxin replacement was discontinued 4 weeks before the treatment. Thyroid stimulating hormone (TSH), Tg, and anti-thyroglobulin (ATG) values were obtained on the morning of treatment. Then, whole-body scintigraphy was performed on the 8th day after treatment and the existence of residual tissue was investigated.

At the 9th post-treatment period, L-thyroxine replacement was terminated and off-Tg and ATG values were obtained, followed by low-dose I-131 full-body screening to evaluate the success of treatment.

In statistical analysis, parametric and nonparametric tests were used according to the distribution of data in binary comparisons. A p-value of <0.05 was considered significant.

RESULTS

Overall 456 (372 F, 84 M) patients were included in the study. The mean age was 46±12 years. Vessel invasion was observed in 61 (13%) patients while extra-thyroidal invasion was in 20 (4.4%) patients. There was surgical margin positivity in 7 (1.5%) patients. Two patients (0.4%) had central lymph node metastasis, and none had lateral lymph node metastasis.

Multifocal tumors and microcarcinoma were observed in 262 (57.5%), 158 (34.6%) patients, respectively. According to American Thyroid Association (ATA) guidelines, 377 (82.7%) patients were at low risk and 79 (17.3%) patients were in moderate-risk groups. The patients' characteristics and pre and post-ablation TNM staging results were presented in Table 1.

While the mean Tg and ATG measurements were 8.8±21, 23.7±158 ng/ml before the treatment, respectively; the same values were calculated as 1.3±15, 5.0±37 ng/ml after the treatment ($p<0.001$; $p<0.001$, respectively).

The local residue was observed in 445 (97.6%) patients in post-ablation images and 67 (14.7%) patients in the 9th month screening images ($p <0.001$). Complete biochemical response in 369 (81%) patients, indeterminate response in 17 (4%), biochemical incomplete response in 3 (1%), and structural incomplete response in 67 (14%) were observed.

Suspected focal activity involvement was observed in 33 (7.2%) patients in terms of lymph node metastasis.

There was no significant difference between pre- and post-treatment Tg, ATG values and lymphovascular invasion, extra-thyroid spread, surgical margin positivity, central lymph node metastasis, risk groups and the presence of post-treatment residual disease (Table 2).

DISCUSSION

Our results indicate that I-131 ion channel treatment is a favorable method in papillary thyroid cancer patients. While the complete response was observed in the majority of patients, the structural incomplete response was observed in approximately 12% of the patients and this proportion is compatible with the literature [5, 6]. It is known that patients with incomplete response have more progression [7, 8].

Pre-ablation stimulated Tg value also indicates surgical success in the literature, the mean Tg value was reported as 48 ng/ml before RAI treatment in a study conducted with the low- and medium-risk group patients, however, our study demonstrated a lower value [9]. We interpret this outcome in favor of the surgical success arising from being a high-volume center. On the other hand, the aforementioned study reported suspicious lymph node metastasis in the 3% of the patients, whereas this rate was 7.2% in our study.

Although several studies apply various doses of treatment in the low and moderate-risk groups in the literature, we included patients who received the same dose of RAI to obtain a homogenous group [10]. In our study, no statistically significant difference was found between pathological features and ablation success.

CONCLUSION

Our results have demonstrated that I-131 therapy succeeded to achieve better biochemical and structural responses in patients with papillary thyroid cancer. However, we have determined that pathological features and surgery did not affect biochemical parameters in the low-moderate risk group patients.

Keywords: RAI, thyroid cancer, thyroglobulin, anti-thyroglobulin

ACKNOWLEDGEMENTS

Declared none.

CONFLICT OF INTEREST

The authors declared no conflicts of interest with respect to the authorship and/or publication of this article.

FUNDING

The authors received no financial support for the research and/or authorship of this article.

Table 1: Patients characteristics

Parameter	Value
Number of Patients	456
Age, median	46±12 (14-79)
Gender	
Female	372 (81.6%)
Male	84 (18.4%)
Blood vessel invasion	
Positive	61 (13.4%)
Negative	395 (86.6)
Extrathyroidal invasion	
Positive	20 (4.4%)
Negative	436 (95.6%)
Surgical margin positivity	
Positive	7 (1.5%)
Negative	449 (98.5%)
Santral lymph node metastasis	
Positive	2 (0.4%)
Negative	454 (99.6%)
Multifocalite	
Positive	262 (57.5%)
Negative	194 (42.5%)
Microcarsinoma	
Positive	158 (34.6%)
Negative	298 (65.4%)

REFERENCES

1. Li N, Du XL, Reitzel LR, Xu L, Sturgis EM. Impact of enhanced detection on the increase in thyroid cancer incidence in the United States: review of incidence trends by socioeconomic status within the surveillance, epidemiology, and end results registry, 1980-2008. Thyroid 2013;23(1):103-10.
2. Harari A, Singh RK. Increased rates of advanced thyroid cancer in California. J Surg Res 2016;201(1):244-52.
3. Samaan NA, Schultz PN, Hickey RC, Goepfert H, Haynie TP, Johnston DA, et al. The results of various modalities of treatment of well differentiated thyroid carcinomas: a retrospective review of 1599 patients. J Clin Endocrinol Metab 1992;75(3):714-20.
4. Sawka AM, Brierley JD, Tsang RW, Thabane L, Rotstein L, Gafni A, et al. An updated systematic review and commentary examining the effectiveness of radioactive iodine remnant ablation in well-differentiated thyroid cancer. Endocrinol Metab Clin North Am 2008;37(2):457-80, x.
5. Avram AM, Rosculet N, Esfandiari NH, Gauger PG, Miller BS, Cohen M, et al. Differentiated Thyroid Cancer Outcomes After Surgery and Activity-Adjusted 131I Theragnostics. Clin Nucl Med 2019;44(1):11-20.
6. Jimenez Londono GA, Garcia Vicente AM, Sastre Marcos J, Pena Pardo FJ, Amo-Salas M, Moreno Caballero M, et al. Low-Dose Radioiodine Ablation in Patients with Low-Risk Differentiated Thyroid Cancer. Eur Thyroid J 2018;7(4):218-24.
7. Malandrino P, Tumino D, Russo M, Marescalco S, Fulco RA, Frasca F. Surveillance of patients with differentiated thyroid cancer and indeterminate response: a longitudinal study on basal thyroglobulin trend. J Endocrinol Invest 2019.
8. Vaisman F, Tala H, Grewal R, Tuttle RM. In differentiated thyroid cancer, an incomplete structural response to therapy is associated with significantly worse clinical outcomes than only an incomplete thyroglobulin response. Thyroid 2011;21(12):1317-22.
9. Dessoki N, Nasr I, Badawy A, Ali I. Value of the Postablative Thyroglobulin Measurements for Assessment of Disease-Free Status in Patients with Differentiated Thyroid Cancer. Indian J Nucl Med 2019;34(2):118-24.
10. Qu Y, Huang R, Li L. Low- and high-dose radioiodine therapy for low-/intermediate-risk differentiated thyroid cancer: a preliminary clinical trial. Ann Nucl Med 2017;31(1):71-83.

Table 2: Comparison of pathological features and biochemical parameters

	Pre-ablation				Post-ablation			
	Tg (ng/ml)	P value	ATG (ng/ml)	P value	Tg (ng/ml)	P value	ATG (ng/ml)	P value
Blood vessel invasion Positive Negative	 11.1±19.7 8.4±21.1	0.345	 5.1±18.4 26.4±169	0.326	 2.6±15.7 1.0±14.6	0.432	 1.3±4.7 5.5±39.3	0.407
Extrathyroidal invasion Positive Negative	 6.2±6.9 8.9±21.3	0.574	 204±694 15.3±58.3	0.237	 0.5±1.1 1.3±15	0.812	 46.4±158 3.1±15	0.236
Surgical margin positivity Positive Negative	 8.9±5.9 8.8±21.1	0.983	 1.2±1.8 23.9±159	0.706	 0.9±1.2 1.3±14.8	0.946	 2.3±5.9 5.0±14.8	0.848
Santral lymph node metastasis Positive Negative	 2.1±1.1 8.8±20.9	0.650	 0±0 23.7±158.1	0.832	 6.1±0 1.2±14.7	0.639	 0±0 5±36.7	0.847
Multifocality Positive Negative	 9.9±23.7 7.3±16.2	0.190	 21.5±88.8 26.4±219.1	0.742	 1.4±17.9 1.0±8.9	0.748	 6.6±46.2 2.8±16.7	0.279
Microcarsinoma Positive Negative	 11.2±29.2 7.6±14.6	0.146	 29.2±113 20.6±177	0.580	 2.1±23.0 0.8±7.2	0.366	 9.3±58.7 2.6±14.8	0.159

OP-09

DIFFERENT FEATURES OF LIVER AND NON-LIVER CANCER STEM CELLS IN HCC CELL LINE, HUH-7

Emine Kandemiş[1,3], İmge Kunter[1,4], Neşe Atabey[1,2], Esra Erdal[1,2]

[1]Department of Medical Biology and Genetics, Faculty of Medicine, Dokuz Eylül University, 35340-Izmir, Turkey

[2]Izmir Biomedicine and Genome Center (IBG-Izmir), 35430 Izmir, Turkey

[3]Department of Molecular Biology and Genetics, Faculty of Engineering and Natural Sciences, Bahçeşehir University, Beşiktas, 34353 Istanbul, Turkey (Current Adress)

[4]Faculty of Pharmacy, Eastern Mediterranean University, Northern Cyprus via Mersin 10, 99628 Famagusta, Turkey (Current Adress)

OBJECTIVES: Hepatocellular carcinoma (HCC) has remarkably high rate of mortality due to its heterogeneity. It has been increasingly recognized that liver cancer stem cells (LCSCs) are responsible for the carcinogenesis, recurrence, metastasis and chemoresistance of HCC while non-LCSCs behave as proliferating tumor cells. Hepatocyte growth factor (HGF) plays a critical role in cancer growth, invasion, and metastasis and activation of HGF/c-Met signaling pathway leads to a significantly worse prognosis in HCC. The aim of this study is to analyze the differences of biological features of LCSCs and non-LCSCs in HCC.

MATERIALS AND METHODS: HCC cell line, HuH-7 was used in the study to isolate LCSCs (EpCAM+/CD133+) and non-LCSCs (EpCAM-/CD133-) by magnetic separation. Their EpCAM and CD133 expression levels were further analysed by flow cytometer. Then spheroid formation capacities of LCSCs and non-LCSCs are compared to define in vitro tumorogenesis. Finally, motility and invasion abilities of both subgroups are analysed under HGF induction.

Results: The EpCAM+/CD133+ and EpCAM-/CD133- cells formed different number and size of spheroids representing different tumorogenesis capacities in vitro. HGF induction caused significant increase in the number of migrating cells in both LCSC and non-LCSC groups. Moreover, increase in the number of invading cells in non-LCSC group with HGF treatment was extremely high compared to the ones in LCSCs.

CONCLUSIONS: Non-LCSCs were found to be more susceptible to HGF induction than LCSCs in terms of invasion capacity. Thus, inhibition of HGF signalling provides a promising treatment strategy via targeting non- LCSCs in HCC.

Keywords: HCC, HGF/c-Met, liver cancer stem cells, non-liver cancer stem cells

INTRODUCTION

Hepatocellular carcinoma (HCC) is the fifth most common cancer type in the world [1]. HCC is thought to be hierarchically organized with growth driven by small sub-population of undifferentiated cancer stem cells (CSCs) or termed tumor-initiating cells (TICs) [2]. In HCC, accumulating evidence has demonstrated the existence of particular subsets of cancer cells with stem cell properties (self-renewal and differentiation) expressing several cell surface markers such as CD133, EpCAM, CD90, CD44, CD24 and CD13 [3]. These subsets of liver cancer stem cells (LCSCs) are likely to cause high heterogeneity in tumor as well as resistance to chemotherapy and radiotherapy [4]. EpCAM, an epithelial cell adhesion molecule previously identified as a marker for stem/progenitor cells of adult liver and it was shown that proliferating EpCAM-positive progenitor cells in the inflamed liver give rise to HCC [5, 6]. CD133 (also known as PROM1) is a pentaspan transmembrane glycoprotein primarily has widely been believed to be a potential marker of cancer stem cells, including HCC [7]. Importantly, CD133 can interact with p85 to activate PI3K/AKT/mTOR-signaling pathways in cancer stem cells, and this activation consequently provokes cancer stem cells to promote tumorigenic capacity [8]. Expressions of EpCAM and CD133 are positively related to poor prognosis in HCC patients [9,10].

Hepatocyte growth factor/scatter factor (HGF/SF), which is secreted in tumor microenvironment generally by mesenchymal cells and cancer associated fibroblasts (CAF) acts on the growth, migration and morphogenesis of cell types and plays a key role in the invasion and metastasis of HCC. Recently, it was shown that CAF-derived HGF and IL6 enhanced the stemness properties of $CD24^+$ cells via activating STAT3 phosphorylation [11]. Notably, the effect of HGF on the motility and invasion of LCSCs and non-CSCs remain largely unknown. The aim of this study is to analyze the differences of biological features of LCSCs and non-LCSCs in HCC.

MATERIALS AND METHODS

The human HCC cell line HuH-7 was supported with Dulbecco's Modified Eagle Medium (DMEM) containing 10% FBS (Fetal Bovine Serum) and antibiotics (100mg/L penicillin and 100mg/L streptomycin). Cells were incubated in a humidified incubator under 5% CO_2 at 37°C. In order to isolate EpCAM+/CD133+ and EpCAM-/CD133- subgroups, HuH-7 cells were stained with EpCAM-FITC (Miltenyi Biotech) and CD133-APC (Miltenyi Biotech) antibodies, and sorted by using magnetic separation [12]. Then percentage of EpCAM and CD133 in cells was further analyzed by flow cytometer. After HGF induction c-Met phosphorylation levels of EpCAM+/CD133+ and EpCAM-/CD133- cells were analyzed via western blot in basal conditions. In-vitro motility and invasion assays were performed as described previously [13]. For invasion assay, collagen type I coated inserts were used. Briefly, EpCAM+/CD133+ and EpCAM-/CD133- cells were placed upper chambers. Lower wells of the inserts contained 2% FBS with/without HGF (40 ng/ml). After 24 hours incubation at 37°C, the medium was removed, cells were fixed and stained with Diff Quick (Siemens Healthcare Diagnostics). For spheroid assay, 1000 cells mixed in matrigel (2.5 mg/ml) were inoculated to 48 well plate which were previously coated with poly-HEMA to prevent cell adhesion and incubated for 12 days. Fresh media was added every 4 days. Cells/spheroids were photographed 4th, 8th and 12th days . Statistical analysis was performed using the GraphPad Prism.

RESULTS

EpCAM+/CD133+ LCSCs and EpCAM-/CD133- non-LCSCs in HuH-7

EpCAM+/CD133+ and EpCAM-/CD133- subgroups were enriched from parental HuH-7 without any induced conditions. Upon after all enrichment experiments, EpCAM+/CD133+ and EpCAM-/CD133- were detected as in purity range between of 83-71% (Figure 1).

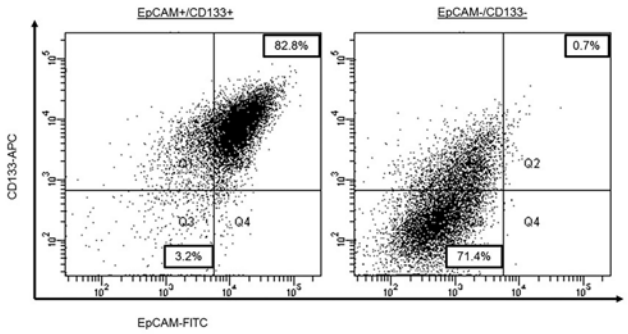

Figure 1: A representative flow cytometry analysis showing the purity of EpCAM+/CD133+ and EpCAM-/CD133- subgroups after enrichment from HuH-7.

In order to understand in vitro tumorogenesis capacity of each subgroup of cells, spheroid formation assays were done for 12 days. Spheroid sizes were different between EpCAM-/CD133- and EpCAM+/CD133+ subgroups (Figure 2a). Moreover, the number of spheroid formed by EpCAM+/CD133+ cells was higher than that of EpCAM-/CD133- subgroup (Figure 2b). *(*p<0.05, **p<0.001, ***p<0.0001).*

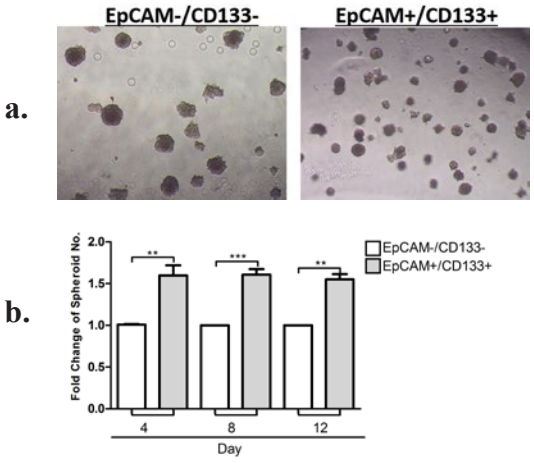

Figure 2: In vitro tumorogenesis for LCSCs and non-LCSCs. a. Spheroids formed by EpCAM-/CD133- and EpCAM+/CD133+ subgroups, b. The number of spheroids for EpCAM-/CD133- and EpCAM+/CD133+ subgroups. All experiments were performed in at least triplicates.

Effect of HGF induction on the motility and invasion capacities of LCSCs and non-LCSCs

We first showed the activation of c-MET signaling after HGF induction in both EpCAM-/CD133- and EpCAM+/CD133+ subgroups in basal conditions (Figure 3). After HGF induction for 1 hr, phosphorylated form of c-Met was increased compared to non-induced condition.

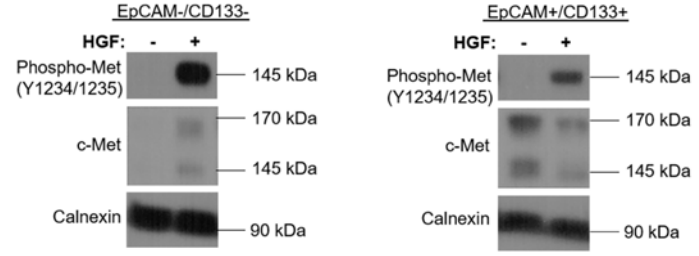

Figure 3: c-Met phosphorylation levels of EpCAM-/CD133- and EpCAM+/CD133+ in basal condition.

In order to understand the effect of HGF on the motility and invasion capacities of LCSCs and non-LCSCs, we used this induction condition and showed that under HGF induction, motility of EpCAM-/CD133- and EpCAM+/CD133+ have both increased approximately 4 and 2.5 fold, respectively (Figure 4a). Additionally, HGF induction caused remarkable increase in the invasion of EpCAM-/CD133- subgroups nearly 20 fold with respect to basal conditions. However, invasion of EpCAM+/CD133+ were increased nearly 2 fold with respect to basal conditions (Figure 4b). *(*p<0.05, **p<0.001, ***p<0.0001).*

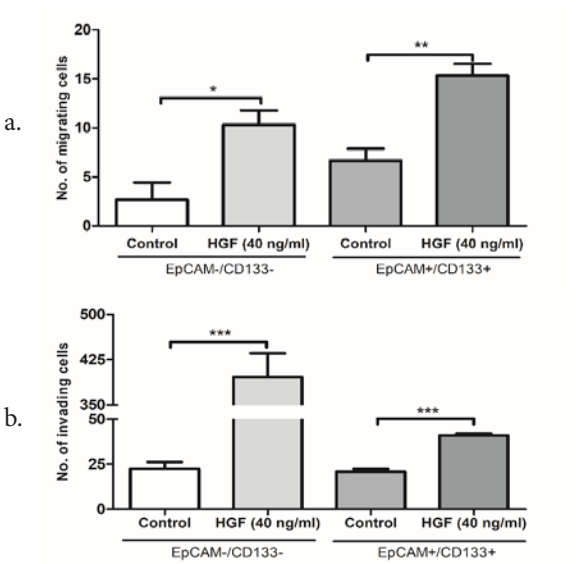

Figure 4: a. Motility of EpCAM-/CD133- and EpCAM+/CD133+ after HGF induction, b. Invasion of EpCAM-/CD133- and EpCAM+/CD133+ after HGF induction. All experiments were performed in at least triplicates.

DISCUSSION

HCC is believed to originate from LCSCs [14]. In particular, LCSCs are responsible for the initiation, relapse, metastasis and chemoresistance in HCC [15]. The fate of CSCs is largely determined by the cells and secreted factors, which are present in the tumor microenvironment. In the CSCs niche, non-CSCs play a considerable role in facilitating a microenvironment. Recent studies demonstrated that, mixing LCSCs with non-LCSCs could significantly increase proliferation and tumorogenesis capability of LCSCs in HCC. Cytokines and growth factors perform a significant role in mediating the crosstalk between LCSCs and non-LCSCs [16]. HGF is expressed ubiquitously in HCC microenvironment and particularly promotes tumorigenesis [17, 18]. In accordance with the literature, our results showed that EpCAM+/CD133+ cells had a higher number spheroid than EpCAM-/CD133- cells and subgroups had different spheroid size. In this study, we demonstrated that, HGF was more effective on EpCAM-/CD133- subgroups than EpCAM+/CD133+ and EpCAM-/CD133- cells were found to be more invasive than EpCAM+/CD133+ cells under HGF induction. Consequently cell surface markers detected in LCSCs may be good targets for immunotherapy and inhibition of HGF signalling provides a promising treatment strategy via targeting EpCAM-/CD133- in HCC.

ACKNOWLEDGEMENTS

This project was funded by grants to Prof. Dr. Esra ERDAL from Turkish Scientific and Technological Research Council (TÜBİTAK, project no: 112T173). Conceived and designed the experiments: EK, İK, NA, EE. Performed the experiments: EK, İK. Analyzed the data: EK, İK, NA, EE. Wrote the paper: EK, EE.

CONFLICT OF INTEREST

The authors have declared that no competing interests exist.

REFERENCES

1. Torre LA, Bray F, Siegel RL, Ferlay J, Lortet-Tieulent J, et al. Global cancer statistics, 2012. CA Cancer J Clin 2015; 65(2):87-108.
2. Shackleton M, Quintana E, Fearon ER, Morrison SJ. Heterogeneity in cancer: cancer stem cells versus clonal evolution. Cell. 2009 Sep 4;138(5):822-9.
3. Marquardt JU, Andersen JB, Thorgeirsson SS. Functional and genetic deconstruction of the cellular origin in liver cancer. Nat Rev Cancer 2015; 15(11): 653-67.
4. Yamada T, Abei M, Danjoh I, Shirota R,Yamashita T,et al. Identification of a

unique hepatocellular carcinoma line, Li-7, with CD13(+) cancer stem cells hierarchy and population change upon its differentiation during culture and effects of sorafenib. BMC Cancer 2015;15:260.
5. Terris B, Cavard C, Perret C. EpCAM, a new marker for cancer stem cells in hepatocellular carcinoma. J Hepatol 2010; 52(2):280-1.
6. Matsumoto T, Takai A, Eso Y, Kinoshita K, Manabe T, et al. Proliferating EpCAM-Positive Ductal Cells in the Inflamed Liver Give Rise to Hepatocellular Carcinoma. Cancer Res. 2017; 77(22): 6131-6143.
7. Ma S, Chan KW, Hu L, Lee TK, Wo JY, et al. Identification and characterization of tumorigenic liver cancer stem/progenitor cells. Gastroenterology 2007;132(7):2542–56.
8. Xia P, Xu XY. PI3K/Akt/mTOR signaling pathway in cancer stem cells: from basic research to clinical application. Am J Cancer Res. 2015; 5(5):1602–9.
9. Yamashita T, Forgues M, Wang W, Kim JW, Ye Q, et al. EpCAM and alpha-fetoprotein expression defines novel prognostic subtypes of hepatocellular carcinoma. Cancer Res 2008; 68(5):1451-61.
10. Lan X, Wu YZ, Wang Y, Wu FR, Zang CB, et al. CD133 silencing inhibits stemness properties and enhances chemoradiosensitivity in CD133-positive liver cancer stem cells. Int J Mol Med 2013; 31(2):315-24.
11. Li Y, Wang R, Xiong S, Wang X, Zhao Z, et al. Cancer-associated fibroblasts promote the stemness of CD24+ liver cells via paracrine signaling. J Mol Med (Berl) 2019; 97(2): 243-255.
12. Delman M, Avcı ST, Akçok İ, Kanbur T, Erdal E, et al. Antiproliferative activity of (R)-4'-methylklavuzon on hepatocellular carcinoma cells and EpCAM+/CD133+ cancer stem cells via SIRT1 and Exportin-1 (CRM1) inhibition. Eur J Med Chem 2019; 180: 224-237.
13. Atabey N, Gao Y, Yao ZJ, Breckenridge D, Soon L, et al. Potent blockade of hepatocyte growth factor-stimulated cell motility, matrix invasion and branching morphogenesis by antagonists of Grb2 Src homology 2 domain interactions. JBiol Chem 2001;276(17):14308-14
14. Yamashita T, Wang XW. Cancer stem cells in the development of liver cancer. J Clin Invest 2013; 123: 1911–1918.
15. Li N, Zhu Y. Targeting liver cancer stem cells for the treatment of hepatocellular carcinoma. Ther Adv Gastroenterol 2019; 12: 1–22.
16. Luo Y, Yang Z, Su L, Shan J, Xu H, et al. Non-CSCs nourish CSCs through interleukin-17E-mediated activation of NF-κB and JAK/STAT3 signaling in human hepatocellular carcinoma. Cancer Lett. 2016; 375(2): 390-399.
17. Mizuno S, Nakamura T. Improvement of sepsis by hepatocyte growth factor, an anti-inflammatory regulator: emerging insights and therapeutic potential. Gastroenterol Res Pract, 2012: 909350.
18. Firtina Karagonlar Z, Koc D, Iscan E, Erdal E, Atabey N. Elevated hepatocyte growth factor expression as an autocrine c-Met activation mechanism in acquired resistance to sorafenib in hepatocellular carcinoma cells. Cancer Sci 2016; 107(4): 407–416.

OP-10

MICROSCALE CANCER MODELS FOR TUMOR BIOLOGY

Gizem Calibasi-Kocal
Dokuz Eylul University, Institute of Oncology, Department of Translational Oncology, Izmir, Turkey.

The importance of microfluidics has already been revealed regarding the study of tumor biology. Mostly, its ability to study fundamental mechanisms associated with invasion, proliferation, metastasis, angiogenesis and microenvironment have been shown. These microfluidics-based models of cancer are designed to include both cancer cells and neighbour cells such as endothelial cells, immune cells. Microfluidic platforms have different progress in mimicking organs based on the spread of cancer cells to distant organs or predict the toxicity and pharmacokinetics of oncologic agents. Accurate recapitulation of the full metastatic processes or metabolism of an oncologic agent, different organ-on-a-chip' platforms can be combined to create more advance 'human-on-a-chip' platforms. These platforms have accepted as useful models for the prediction of the efficacy and toxicity of chemotherapeutic agents and improving animal models for the aim of preclinical use. Above all, primary tumor cells isolated from patients can be cultured on microfluidic culture based systems and tested for different agents with high specificity. In future, more complex and physiologically relevant 'human-on-a-chip' platforms will be developed to focus on the mechanistic features of tumor biology, and these systems will be candidate to test individualized cancer therapies before traditional *in vivo* models.

INTRODUCTION

Microfluidic platforms have different improvements to mimick the tumor microenvironment for understanding the spread of cancer cells or predict the toxicity of chemotherapeutic agents. Alterations in the physical conditions of the tumor microenvironment, which are driven by increased proliferation and angiogenesis, may cause phenotypic switches [1]. Especially increased fluid flow in the tumor microenvironment, affect the key factors of cancer, such as progression, immune-escaping and metastasis [2]. Traditional common in vitro models lack to mimic physical cues of tumor microenvironment. At this point, using of microfluidic culture techniques help researchers to control physical cues such as fluid flow exposure [3].

Ovarian cancer is the 5th common cancer in women and the deadliest gynecological cancer. On the diagnosis process, nearly 75% women were detected with locally or metastatic advanced cancer. Limited information about the origin and biology of ovarian cancer is the result of the lack of specific ovary cancer markers, and drug resistance in advanced cases [4]. Like the other cancers, ovarian cancer tend to spread by lymphatic/hematogenic dissemination via vasculature, but also transcoelomic dissemination, in which cancer cells spread from primary tumor bulk to peritoneal cavity (a spread mode which is also used by colon and gastric cancers), is very common way to metastasize [5]. In literature, the effects of flow-based dynamic forces due to the increased interstitial flows were shown as molecular and biological features of tumor metastases. The effects of physical dynamic flows on the ovarian cancer cell phenotype are still unknown [6]. Here, a dynamic microfluidic 3-dimensional cancer culture platform was used for the understanding of the alterations on ovarian cancer cells with the effect of flow mediated mechanical stimuli.

MATERIAL AND METHODS

3-dimensional microfluidic dynamic cell culture

Ovarian adenocarcinoma ONCO-DG-1 (ACC 507) and omental metastasis of ovarian adenocarcinoma EFO-27 (ACC 191) cells were provided from DSMZ-German Collection of Microorganisms and Cell Culture. Cell lines were maintained in RPMI 1640 medium (Biochrom AG, Berlin, Germany) supplemented with 10% (v/v) fetal bovine serum (Biological Industries, Germany), 100 U/ml penicillin/streptomycin (Biochrom AG, Berlin, Germany), 2 mM L-glutamine (Biochrom AG, Berlin, Germany) and 1% (v/v) non-essential amino acid (Biochrom AG, Berlin Germany) in a humidified incubator at 37°C with 5% CO_2. After tyripsinization, cells were counted and resuspended in 1 ml resuspension medium (without serum). Then resuspended cells and Matrigel (BD Biosciences) were mixed in 1:1 ratio (final concentration of Matrigel 10-12 mg/ml). Cells in Matrigel/resuspension medium mixture were seeded on the channels ($1x10^5$ cells/channel). For dynamic culture polymethyl methacrylate based microfluidic chips with 2 channels were used (Figure 1). Continuous flow based dynamic microenvironment was maintained by using specific air permeable tubing and syringe pumps. For continuous medium flow, 4 ul/minute flow rate was used. Cells morohology was monitored by microscopy (Carl Zeiss, Axio Vert, Germany).

Immunofluorescence for metastatic phenotype

To evaluate the epithelial and mesenchymal phenotype of ovarian cancer cells, cells were stained with E-cadherin, N-cadherin and vimentin. After the fixation, cells were incubated with appropriate primary and secondary antibodies for E-cadherin (Primary: Abcam, Cambridge, MA, USA; Secondary: Alexa Fluor- 488, Life Technologies, Carlsbad, CA, USA), N-cadherin (Primary: Abcam, Cambridge, MA, USA; Seconday: Alexa Fluor- 568, Life Technologies, Carlsbad, CA, USA) and vimentin (Primary: Novus Biological, Littleton, CO, USA; Secondary: Alexa Fluor- 647, Jackson ImmunoResearch Lab, West Grove, PA, USA). After the staining, cells were visualized under fluorescence microscope (Carl Zeiss, Axio Vert, Germany) and fluorescence intensity of images was analyzed with ImageJ software (NIH, Bethesda, MD, USA).

Chemotherapeutic application

Ovarian cancer cells were plated on channels of microfluidic chips on the day before treatment with cisplatin (Sigma, USA). Cells were continuously exposed to different doses (0, 10, 20 μM) of cisplatin and incubated for 24 hours in a humidified incubator at 37 °C with 5% CO_2. After the incubation, WST-1 reagent was used to measure the effects of cisplatin.

Cell viability analysis

Relative cell viability and proliferation were measured by using colorimetric assay WST-1 (Roche Applied Sciences, Mannheim, Germany). WST-1 reagent was prepared as per the manufacturers instructions. Briefly, culture medium supplemented with 10 μl of the reconstituted reagent was added to each channel. After 2 hours incubation at 37°C in a CO_2 incubator, the absorbance of each channel was measured by using a microplate reader at 450 nm.

RESULTS

Here, a dynamic microfluidic 3-dimensional cancer cell culture platform was used to mimic dynamic microenvironment of ovarian cancer (Figure 1A). For dynamic culture, ovary adenocarcinoma cells (EFO-27 and ONCO-DG-1) in Matrigel/ resuspended media mixture were seeded on two channels of microfluidic chips. Dynamic and static culture conditions were compared for the differences of cancer cell phenotype, such as morphology, proliferation, epithelial-mesenchymal transition, drug response and viability.

The proliferation of ovarian cancer cells was increasing under continuous fluid flow. It was confirmed that by both monitoring the cells under microscope and counting cells (Figure 1B-F). The increased proliferation of cells was correlated with the increase of fluid flow rate.

Immunocytochemical analysis to evaluate the phenotype of ovarian cancer cells, showed that fluid flow caused a reduction in E-cadherin and an increase in N-cadherin and vimentin expressions (Figure 2). This results show that fluid flow induces mesenchymal phenotype on ovarian cancer cells.

Cisplatin, a common used chemotherapeutic for the ovarian cancer, was applied to test the drug response under dynamic conditions. It was seen that viability results were also changed under dynamic conditions (Figure 3). Flow also affects the distribution and response of drugs, so this kind of changes on drug response can be seen.

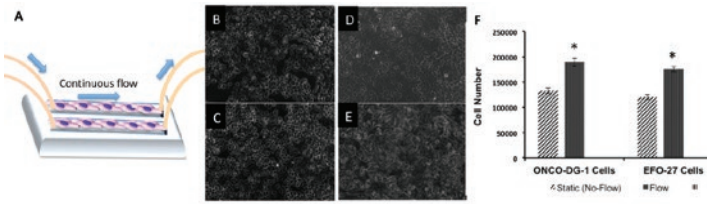

Figure 1. A) Dynamic microfluidic 3-dimensional cancer cell culture platform. B) Brightfield microscopic image of ONCO-DG-1 cells under static culture condition. C) Brightfield microscopic image of ONCO-DG-1 cells under dynamic culture condition. D) Brightfield microscopic image of EFO-27 cells under static culture condition. E) Brightfield microscopic image of EFO-27 cells under dynamic culture condition. F) Alterations on cell number of ONCO-DG-1 and EFO-27 ovarian cancer cells under dynamic and static culture conditions. Star (*) indicates statistically significance $p < 0.05$.

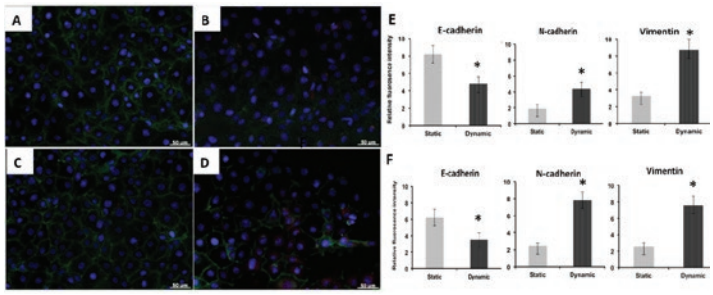

Figure 2. A) Immunofluorescence staining on ONCO-DG-1 cells for E-cadherin (green), N-cadherin (red) and vimentin (cyan) under static conditions. B) Immunofluorescence staining on ONCO-DG-1 cells for E-cadherin, N-cadherin and vimentin under dynamic conditions. C) Immunofluorescence staining on EFO-27 cells for E-cadherin, N-cadherin and vimentin under static conditions. D) Immunofluorescence staining on EFO-27 cells for E-cadherin, N-cadherin and vimentin under dynamic conditions. E) Quantification of fluorescence intensities from the images of ONCO-DG-1 cells. F) Quantification of fluorescence intensities from the images of EFO-27 cells. Star (*) indicates statistically significance $p < 0.05$.

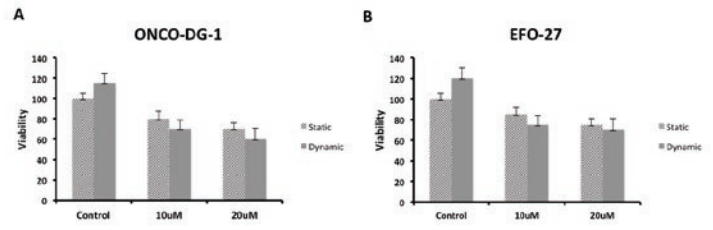

Figure 3. Viability results after 24 hours cisplatin application. A) Viability results of ONCO-DG-1 cells. B) Viability results of EFO-27 cells.

CONCLUSION

These results showed that ovarian cancer cells present different phenotype under fluid flow based dynamic tumor microenvironment. To understand and evaluate the effects of fluid flow dynamics by using microfluidic dynamic culture models is a key to study the mechanisms underlying metastasis and chemotherapeutic screenings. It may even lead to new diagnostics and therapeutic approaches. Different organ-on-a-chip' platforms can be also create for accurate recapitulation of the full metastatic processes or response related metabolism of a chemotherapeutic agent. These platforms have accepted as useful models for the prediction of the efficacy and toxicity of chemotherapeutic agents and improving animal models for the aim of preclinical use.

Conflict of Interest

The author declares no conflict of interests.

REFERENCES

1. XU H, Liu X, Le W. Recent advances in microfluidic models for cancer metastasis research. TrAC Trends in Analytical Chemistry 2018;105:1-6.
2. Moore N, Doty D, Zielstorff M, Kariv I, Moy LY, et al. A multiplexed microfluidic system for evaluation of dynamics of immune-tumor interactions. Lab Chip 2018;18(13):1844-1858.
3. Shang M, Soon RH, Lim CT, Khoo BL, Han J. Microfluidic modelling of the tumor microenvironment for anti-cancer drug development. Lab Chip 2019;19(3):369-386.
4. Jacob F, Nixdorf S, Hacker NF, Heinzelmann-Schwarz VA. Reliable in vitro studies require appropriate ovarian cancer cell lines. J Ovarian Res 2014;7:60.
5. Masiello T, Dhall A, Hemachandra LPM, Tokranova N, Melendez JA, Castracane J. A Dynamic Culture Method to Produce Ovarian Cancer Spheroids under Physiologically-Relevant Shear Stress. Cells 2018;7(12):E277.
6. Rizvi I, Gurkan UA, Tasoglu S, Alagic N, Celli JP, et al. Flow induces epithelial-mesenchymal transition, cellular heterogeneity and biomarker modulation in 3D ovarian cancer nodules. Proc Natl Acad Sci U S A 2013;110(22):E1974-83.
7. Sontheimer-Phelps A, Hassell BA, Ingber DE. Modelling cancer in microfluidic human organs-on-chips. Nat Rev Cancer 2019;19(2):65-81.

OP-11

THE EFFECTS OF SINAPIC ACID ON TRP CHANNELS EXPRESSION IN LNCAP PROSTATE CANCER CELL LINE

Fatma Seçer Çelik[1], Hatice Kübra Yıldız[1], Safaa Altveş[1], Canan Eroğlu Güneş[1], Hasibe Vural[1], Ercan Kurar[1]

[1]Department of Medical Biology, Meram Faculty of Medicine, Necmettin Erbakan University, Konya, Turkey

OBJECTIVES: The aim of study was to evaluate effects of SA on TRP channel expression in LNCaP human prostate cancer cells.

TRP family of ion channel expression changes were observed in different cancers including breast, brain, prostate, ovary and colon. Prostate cancer is one of the leading threats to men's health in the world. There are still limited therapeutic options for metastatic prostate cancer. Sinapic acid (SA) is a naturally occurring phenolic compound that can be found in free form. SA is also found in various fruits, vegetables, cereals, oilseeds and some spices.

MATERIALS AND METHODS: The effect of SA on cell viability was determined using XTT assay. After SA treatment, total RNAs were isolated and cDNAs were synthesized. Expressions of ion channels genes including TRPM2, TRPM7, TRPM8 and TRPV2 were evaluated by qPCR.

RESULTS: The IC_{50} dose of SA in LNCaP cell line was found to be 1000 µM for 72 hour. SA treatment increased the expression of TRPV2. However, expressions of TRPM2 and TRPM8 were significant decreased the in LNCaP cells. An insignificant increase was observed for TRPM7 mRNA expression.

CONCLUSIONS: Changes in the expression of TRP ion family may have an effect on cell viability, cell invasion, migration and apoptosis. The decreased expression of TRPM2 and TRPM8 may induce apoptotic cell death by reducing Ca^{+2} input. Elevated TRPM7 and TRPV2 expressions were found to be statistically insignificant.

Keyword: Sinapic acid, Prostate cancer, Calcium channels

INTRODUCTION

Sinapic acid (SA) (3,5-dimethoxy-4-hydroxy cinnamic acid) is a member of the phenylpropanoid family. Sinapic acid has been shown to have various effects

against metabolic disorders, hypertension, cardiovascular disorders and ischemia damage [1]. Anti-cancer effect of sinapic acid against prostate and colon cancer has been reported in studies [2-3]. Although prostate cancer (PC) is the second most frequent cancer in men worldwide [4], PC treatment options are limited. The oncogenic process is closely associated with many molecular changes in expression of Ca^{+2} ion channel genes are seen in various cancers [5]. In mammalian, transient receptor potential (TRP) have important physiological role in response to sensory stimuli. TRP family of ion channels divide into six subfamilies [6]. Most of TRP permeable to Ca^{+2} except TRPM4 and TRPM5 which are subfamily of transient receptor potential melastatin (TRPM), thus the activation of TRP lead to increase of Ca^{+2} and activate the Ca^{+2} related pathways. It is known that Ca^{+2} is the second messenger contributed in numerous biological signal pathways as secretion, gene transcription, and cell death [7]. In this study, aim was to assess the use of SA as a potential treatment for prostate cancer by investigating its role in calcium channels in LNCaP cells.

MATERIALS AND METHODS

Cell Culture

LNCaP (Androgen Dependent Phenotype, ATCC® CRL1740™) prostate cancer cell line was obtained from ATCC. These cells were cultured in completed RPMI-1640 medium.

Cytotoxicity assay

IC_{50} dose of SA were determined by using XTT assay in LNCaP cells. SA was dissolved in ethanol. The cells were treated with different SA doses of 0-2500 µM for 24, 48 and 72 hours. This assay was conducted according to the manufacturer's instructions.

RNA isolation, cDNA synthesis and qPCR analysis

Total RNA isolation, cDNA synthesis and qPCR analyzes were performed with using TRIzol Reagent (Invitrogen, USA), Transcriptor first strand cDNA synthesis kit (BIO-RAD) and iScript™ reverse transcription Supermix (BIO-RAD) according to the manufacturer's instructions, respectively. The primer sequences of target and reference genes were designed using IDT PrimerQuest program (Table 1.).

Table 1. Primers sequences used for qPCR analysis.

Gene	Primer sequence	PCR product size (bp)
TRPM2	F:5-TCGGACCCAACCACACGCTGTA-3 R:5-CGTCATTCTGGTCCTGGAAGTG-3	339
TRPM7	5-CTTATGAAGAGGCAGGTCATGG-3 5-CATCTTGTCTGAAGGACTG-3	214
TRPM8	F:5-TGAACTCTTCTCCAACCACTTC-3 R:5-CGTGAGGAGGGCATCATTATAG-3	85
TRPV2	F:5-GACCCTTGACATCTCCATCTG-3 R:5-CATCTTCTTGGCCTCCATCTAA-3	127
ACTB	F:5-TGGCTGGGGTGTTGAAGGTCT-3 R:5-AGCACGGCATCGTCACCAACT-3	179

Statistical analysis

The qPCR analysis was conducted with the ΔΔCT method. The comparisons of the control and dose groups have been performed with "RT² Profiles™ PCR Array Data Analysis" ($p<0.05$ is statistically significant).

RESULTS

Cytotoxic effect of SA in LNCaP cells

The IC_{50} dose of SA in LNCaP cells was determined as 1000 µM for 72 h, which was also reported by Eroğlu et al. 2018 [2] (Fig. 1).

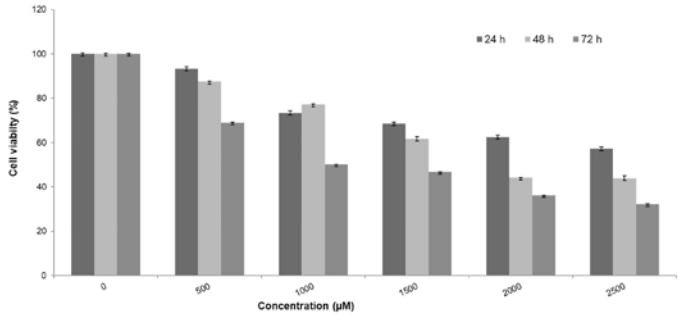

Fig.1. Effect of SA on the viability in the LNCaP cells. The cells were treated with SA and at different concentrations and time intervals and anti-proliferative effect was assessed by XTT assay. IC_{50} dose of SA in LNCaP cell line was found to be 1000 µM for 72 h. Data are the average results of three independent experiments.

Gene expression analysis with qPCR

According to qPCR analyzes results, it was observed that SA in LNCaP cells caused a significant decrease in the expression of *TRPM2 and TRPM8* genes, and no significant increase in the expression of *TRPM7* and *TRPV2* genes (Fig.2, $p<0.05$).

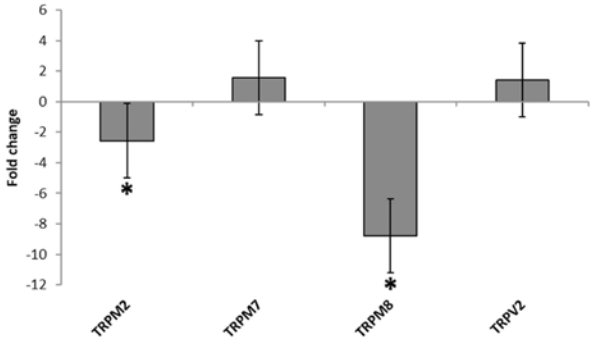

Fig.2. The changes in expression of genes relative to the control group after SA treatment in LNCaP cells. *indicates statistically important ($p<0.05$) difference.

DISCUSSION

It has been reported in previous studies that SA, which is a natural derivative of cinnamic acid and antioxidant properties, is anti-cancer effect for colon and prostate cancer [2-3]. The previous studies suggested that TRPM2 and TRPM8 genes have an effect on cell viability and proliferation while the TRPM7 and TRPV2 genes are effective in cell migration rather than cell viability.

In a study, it was observed that the proliferation of prostate cancer cells was inhibited but normal prostate cells were not affected, when TRPM2 was targeted with siRNA [8]. Also, TRPM8 is a Ca^{+2} channel, which is characteristic in prostate cell epithelium. Asuthkar et al., (2015) showed that TRPM8 expression was significantly decreased with anti-androgen treatments in PC [9]. In this study, TRPM2 and TRPM8 mRNA expression significantly decreased in LNCaP cells treated with SA.

Chen et al., reported that TRPM7 was expression increased PC cells compared to benign prostate hyperplasia cells [10]. In the other a study, TRPV2 level was found to be higher in patients with metastatic cancer compared to primary solid tumors [11]. In this study, SA caused an insignificant increase in TRPM7 and TRPV2 in LNCaP cells.

In this study, changes in expression of TRPM2, TRPM7, TRPM8 and TRPV2 genes were investigated in SA treated LNCaP cells. Decreased expression of TRPM2 and TRPM8 genes, which are associated with cell viability, has been thought to induce apoptosis by reducing Ca^{2+} entry into cells. According to Fuessel et al. [12], TRPM8 may be considered as a marker for prostate cancer, and in this study, SA significantly reduced expression of TRPM8. On the other hands, there is a statistically insignificant increase in expression of TRPM7 and TRPV2 genes. However, further research is needed to investigate effects of SA on TRP channels in LNCaP cells prostate cancer cells.

Acknowledgements

None.

Conflict of Interest

None.

REFERENCES

1. Silambarasan T, Manivannan J, Raja B, Chatterjee S. Prevention of cardiac dysfunction, kidney fbrosis and lipid metabolic alterations in l-NAME hypertensive rats by sinapic acid–Role of HMG-CoA reductase. Eur J Pharmacol 2016; 777:113–123.
2. Eroğlu C, Avcı E, Vural H, Kurar E. Anticancer mechanism of sinapic acid in PC-3 and LNCaP human prostate cancer cell lines. Gene 2018; 671: 127-134.
3. Balaji C, Muthukumaran J, Nalini N. Chemopreventive effect of sinapic acid on 1, 2-dimethylhydrazine-induced experimental rat colon carcinogenesis. Hum Exp Toxicol 2014; 33(12):1253–1268.
4. Rawla, P. Epidemiology of Prostate Cancer. World J Clin Oncol 2019; 10(2):63-89.
5. Monteith GR, Davis FM, Roberts-Thomson SJ. Calcium channels and pumps in cancer: changes and consequences. J Biol Chem 2012; 287:31666–31673.
6. Wong KK, Banham AH, Yaacob NS, Nur Husna SM. The oncogenic roles of TRPM ion channels in cancer. J Cel Physiol 2019; 234 (9):14556-14573.

7. Hasan R, Zhang X. Ca2+ regulation of TRP ion channels. Int J Mol Sci 2018; 19(4): 1256.
8. Zeng X, Sikka SC, Huang L, Sun C, Xu C, Jia D, et. al. Novel role for the transient receptor potential channel TRPM2 in prostate cancer cell proliferation. Prostate Cancer Prostatic Dis 2010; 13(2):195-201.
9. Asuthkar S, Velpula KK, Elustondo PA, Demirkhanyan L, Zakharian E. TRPM8 channel as a novel molecular target in androgen-regulated prostate cancer cells. Oncotarget 2015; 6(19):17221-17236.
10. Chen L, Cao R, Wang G, Yuan L, Qian G, Guo Z, et. al. Downregulation of TRPM7 suppressed migration and invasion by regulating epithelial–mesenchymal transition in prostate cancer cells. Medical Oncology 2017; 34(7):127.
11. Monet M, Lehen'kyi VY, Gackiere F, Firlej V, Vandenberghe M, Roudbaraki M, et. al. Role of cationic channel TRPV2 in promoting prostate cancer migration and progression to androgen resistance. Cancer Res 2010; 70(3):1225-1235.
12. Fuessel S, Sickert D, Meye A, Klenk U, Schmidt U, Schmitz M, et al. Multiple tumor marker analyses (PSA, hK2, PSCA, trp-p8) in primary prostate cancers using quantitative RT-PCR. Int J Oncol 2003; 23:221–228.

OP-12

DEVELOPMENT OF PACLITAXEL-PAMAM G5 CONJUGATE TO OVERCOME MULTIDRUG RESISTANCE OF OVARIAN CANCER CELL LINE MDAH 2774

Meltem Kocamanoğlu[1], Bakiye Göker Bağca[2], Cumhur Gündüz[2], Zihni Onur Uygun[1], Emel Öykü Çetin Uyanıkgil[3], Ferhan Girgin Sağın[1], Yasemin Akçay[1]
[1]Ege University, Department of Medical Biochemistry, İzmir, Turkey
[2]Ege University, Department of Medical Biology, İzmir, Turkey
[3]Ege University, Department of Pharmaceutic Technology, İzmir, Turkey

OBJECTIVES: Ovarian cancer is a common form of cancer types among women. Effectiveness of chemotherapeutics for treatment cancer decreases with the multidrug resistance that is occured by cancer cells. Different research groups develop various strategies to overcome multidrug resistance. We aimed to achieve a Paclitaxel-PAMAM G5 conjugate to overcome multidrug resistance and evaluate its effectiveness in Paclitaxel resistant ovarian cancer cell line MDAH 2774.
MATERIALS AND METHODS: We exposed the IC50 of Paclitaxel to MDAH 2774 cell line to obtain Paclitaxel resistant cell line during 8 passage and measured MDR1 gene expression level to demonstrate the progression of resistance to Paclitaxel. We conjugated the Paclitaxel and PAMAM G5 for effective drug release and characterized it with FTIR analysis and studied in vitro release kinetics, performed cytotoxicity analysis to cell lines with and without resistance and compared the effects of Paclitaxel and Paclitaxel-PAMAM G5 conjugate.
RESULTS: According to MDR1 gene expression profile we achieved the Paclitaxel resistant MDAH 2774 cell line. In vitro release kinetics of Paclitaxel-PAMAM G5 conjugate showed that the release of Paclitaxel is slow and it is necessary to optimize the release characteristic of the conjugate. The data from cytotoxicity analysis showed that the Paclitaxel alone has high efficacy compare with conjugate
CONCLUSIONS: Paclitaxel-PAMAM G5 conjugate promises preferred drug release characteristic since biocompatible properties of PAMAM G5. The data from our study shows that the in vitro release characteristic of this conjugate needs to be improved with further studies.
Keywords: Ovarian cancer, MDR1, Paclitaxel, PAMAM G5

INTRODUCTION

Ovarian cancer is the most lethal type of gynecologic cancers and is the second most common cancer related female patient (1). Only 25% of patients in the late stage have a 5-year survival (2)the predictive value of symptoms remains very low. The aim of this paper is to obtain the views of general practitioners (GPs, (3). Genetic factors, age, the use of postmenopausal hormone therapy, infertility and nulliparity are involved in the development of ovarian cancer as risk factors (4)cells of origin, molecular compositions, clinical features and treatments. Ovarian cancer is a global problem, is typically diagnosed at a late stage and has no effective screening strategy. Standard treatments for newly diagnosed cancer consist of cytoreductive surgery and platinum-based chemotherapy. In recurrent cancer, chemotherapy, anti-angiogenic agents and poly(ADP-ribose. Obesity, depression, smoking etc. are other risk factors for ovarian cancer.
Taxanes are widely used in ovarian cancer chemotherapy. Oral bioavailability of taxanes is less than 10%, its solubility in water is less than 0.01 mg/ml, it is a group of drugs in which MDR develops, it can be applied by only invasively, its biological half-life is short, the permeability of tissues to taxanes is low (5), (6). In order to reduce these negative properties of taxanes, it is being conjugated with drug delivery systems and its use in treatment is being investigated.
PAMAM dendrimers, which are formed by covalent modification and binding of drug particles to their terminal ends, are effective systems for drug release (7). The use of PAMAM dendrimers as pharmaceutical adjuvants has not yet been realized, but these dendrimers have the potential to prove that they may have an important potential as a nanotransmitter (8). For these reasons, we aimed to evaluate the cytotoxic effects of ovarian cancer cells by developing Paclitaxel-PAMAM G5 conjugate.

MATERIAL AND METHODS

Materials MDAH 2774 cell line was from laboratory of Prof. Dr. Cumhur Gündüz, Ege University Department of Medical Biology. All chemicals were purchased from Sigma-Aldrich.
We exposed the MDAH 2774 cell line with IC50 value of Paclitaxel during 8 passage for development of Paclitaxel resistant MDAH 2774 cells. Cell culture conditions were contained %5CO_2, %9air, temperature was 37°C, culture media contained %1 penicillin-streptomiscin, %1 L-glutamine, %10fetal bovine serum in DMEM-high glucose. We measured MDR1 gene expression to see whether resistance was occured. MDR1 gene expression levels were measured with quantitative polymerase chain reaction (qPCR). We conjugated Paclitaxel and PAMAM G5 as described previously (9)and then the remaining dendrimer terminal amines were sequentially modified with fluorescein isothiocyanate as an imaging agent and folic acid as a targeting ligand. The multifunctional dendrimers formed (G5.NHAc-FI-FA. We used Nicolet™ iS50 Spectrometer (FTIR) to characterizing Paclitaxel-PAMAM G5 conjugate. *In vitro* release kinetics analyses were carried out with HPLC measurements, pH: 7,4, 37°C temperature were conditions of *in vitro* release media that consisted of 20 µL Paclitaxel-PAMAM G5/1 mL phosphate buffer saline in a molecular weight cut off 10000 dialysis bag. At the end of every 1 hour we took 3 ml of in vitro release media and added 3 ml of fresh media. Unreleased Paclitaxel amount was measured by HPLC as described previously (9)and then the remaining dendrimer terminal amines were sequentially modified with fluorescein isothiocyanate as an imaging agent and folic acid as a targeting ligand. The multifunctional dendrimers formed (G5. NHAc-FI-FA. Cell viability assay MTT was performed after cells were treated with Paclitaxel-PAMAM G5 conjugate for 3 hours following 48 hours incubation of cells with and without resistance in the 96 well ($1X10^4$ cells per well) plate. The plates were read at 570 nm. The means and standart deviation fort he triplicate well were recorded.
Statistical Analysis One way analysis of variance was used to evaluate the statistical significance of efficiency of Paclitaxel-PAMAM G5 conjugate on cell cultures.

RESULTS

The data of transmittance values from FTIR showed that Paclitaxel-PAMAM G5 conjugate had non-spesific binding (Figure 1).

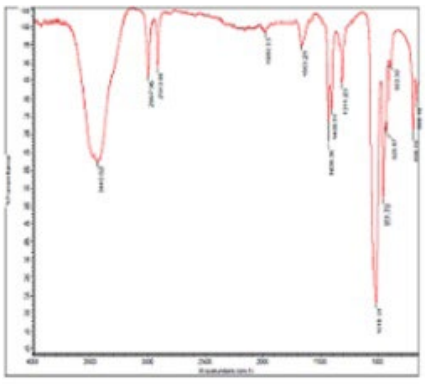

a

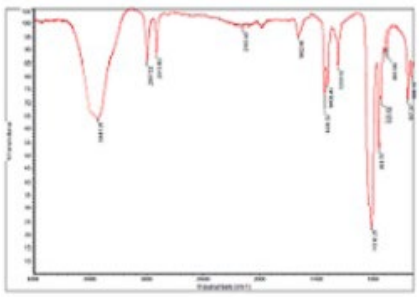

b

Figure 1: a FTIR results of reaction products. b FTIR results obtained by Paclitaxel binding to reaction products

Released cumulative Paclitaxel amount from Paclitaxel-PAMAM G5 conjugate was under the %50 of total Paclitaxel content of the conjugate for the first 10 days (Figure 2).

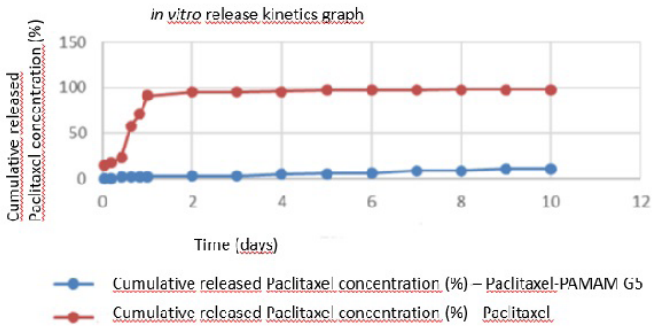

Figure 2: in vitro release kinetics of Paclitaxel

MDR1 gene expression level of MDAH 2774 cells was increased after exposing the cells during 8 weeks of IC_{50} amount of Paclitaxel. The results showed that MDR1 resistance was $6/10^6$ fold increased at Paclitaxel-exposed cells compared with MDAH 2774 cells (Figure 3).

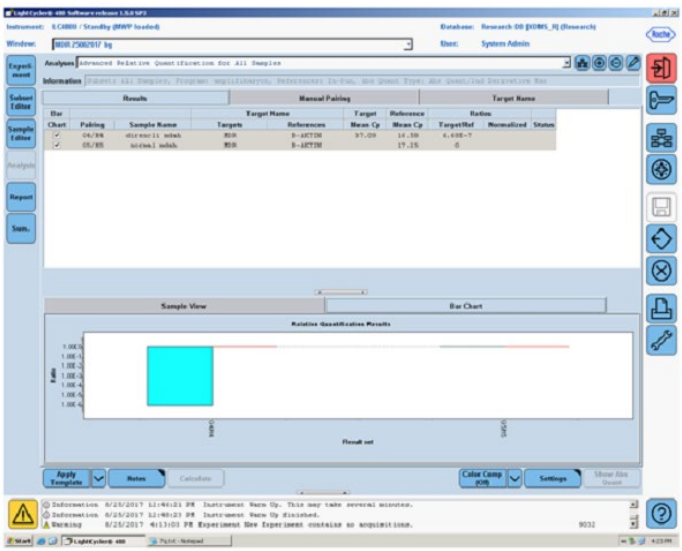

Figure 3: MDAH 2774 MDR-1 gene expression markers in resistant and non-resistant cell lines

IC50 doses were determined for PAMAM G5, Paclitaxel and conjugate (Table 1).

	MDAH 2774 Cell Line			MDAH 2774 Paclitaxel_Resistant Cell Line		
	Paclitaxel	Paclitaxel-PAMAM G5	PAMAM	Paclitaxel	Paclitaxel-PAMAM G5	PAMAM
24. h IC_{50}	5.632 µM	1.99 µM	16.93 µM	5.276 µM	5.038 µM	3.33 µM
48. h IC_{50}	1.15 nM	29.82 nM	34.68 µM	0.78 nM	41.91 nM	23.53 µM
72. h IC_{50}	0.39 nM	21.45 nM	24.70 µM	0.01 nM	36.62 nM	10.82 µM

Table 1: IC_{50} concentrations of Paclitaxel, PAMAM G5, conjugate at MDAH 2774 and MDAH 2774 Paclitaxel resistant cell lines

DISCUSSION

Ovarian cancer is the most lethal type among gynecological cancers and is the second most common cancer-related female patient death (1). Treatment of ovarian cancer is usually chemotherapy with platinum and taxane following surgery (10). Conjugation studies of taxanes with drug delivery systems have major importance not only in terms of overcoming physicochemical barriers, but also in improving drug efficiency performance (11)docetaxel and cabazitaxel. In this study, we aimed to increase the effectiveness of Paclitaxel conjugated with PAMAM G5.

Signal increases on the FTIR graph indicate that Paclitaxel binds non-specifically to the PAMAM G5. Treatment of the conjugate with cell culture yielded low drug activity. Reduction in drug yield might be due to slow drug release. Therefore, drug release kinetics should be optimized.

In our study, no significant toxicity occurred due to PAMAM. Majoros et al. found no significant cytotoxic effect due to dendrimer in their cytotoxicity analysis by flow cytometry also (12). In this research, viability test results showed that IC_{50} concentration of Paclitaxel-PAMAM G5 was higher than the IC_{50} dose of free Paclitaxel for the 24th, 48th and 72th hours. A study showed that the lethal effect of the Paclitaxel-PAMAM G5 at 200 nM concentration was equivalent to the lethal effect of free Paclitaxel at 800 nM concentration (13). According to our hypothesis Paclitaxel-PAMAM G5 should be more effective than free Paclitaxel, in further studies this phenomena needs to be clarified. It has been reported that the formation of hydroxyl linkage rather than folic acid binding has a better effect on active targeting in terms of cytotoxicity (14).

Acknowledgements

This study was supported by a grant supplied Ege University Scientific Research Projects Coordination Fund (Project 16-TIP-007).

REFERENCES

1. Jemal A, Siegel R, Xu J, Ward E. Cancer statistics, 2010. CA Cancer J Clin [Internet]. 2010;60(5):277–300. Available from: http://www.ncbi.nlm.nih.gov/pubmed/20610543
2. Gajjar K, Ogden G, Mujahid MI, Razvi K. Symptoms and Risk Factors of Ovarian Cancer: A Survey in Primary Care. ISRN Obstet Gynecol. 2012;2012:1–6.
3. Ferlay J, Soerjomataram I, Dikshit R, Eser S, Mathers C, Rebelo M, et al. Cancer incidence and mortality worldwide: Sources, methods and major patterns in GLOBOCAN 2012. Int J Cancer. 2015;136(5):E359–86.
4. Matulonis UA, Sood AK, Fallowfield L, Howitt BE, Sehouli J, Karlan BY. Ovarian cancer. Nat Rev Dis Prim. 2016;2:16061.
5. Baker J, Ajani J, Scotté F, Winther D, Martin M, Aapro MS, et al. Docetaxel-related side effects and their management. Eur J Oncol Nurs. 2009;13(1):49–59.
6. Biganzoli L, Licitra S, Moretti E, Pestrin M, Zafarana E, Di Leo A. Taxanes in the elderly: Can we gain as much and be less toxic? Vol. 70, Critical Reviews in Oncology/Hematology. 2009. p. 262–71.
7. Kaminskas LM, McLeod VM, Porter CJH, Boyd BJ. Association of chemotherapeutic drugs with dendrimer nanocarriers: An assessment of the merits of covalent conjugation compared to noncovalent encapsulation. Vol. 9, Molecular Pharmaceutics. 2012. p. 355–73.
8. Otto DP, de Villiers MM. Poly(amidoamine) Dendrimers as a Pharmaceutical Excipient. Are We There yet? Vol. 107, Journal of Pharmaceutical Sciences. 2018. p. 75–83.
9. Shi X, Zhang, Guo, Wang, Cao, Shen. Multifunctional dendrimer/combretastatin A4 inclusion complexes enable in vitro targeted cancer therapy. Int J Nanomedicine. 2011;
10. Liu Z, Tabakman S, Welsher K, Dai H. Carbon nanotubes in biology and medicine: In vitro and in vivo detection, imaging and drug delivery. Nano Res. 2009;2(2):85–120.
11. Kumar P, Raza K, Kaushik L, Malik R, Arora S, Katare OP. Role of Colloidal

Drug Delivery Carriers in Taxane-mediated Chemotherapy: A Review. Curr Pharm Des. 2016;22(33):5127–43.
12. Majoros IJ, Myc A, Thomas T, Mehta CB, Baker JR. PAMAM dendrimer-based multifunctional conjugate for cancer therapy: Synthesis, characterization, and functionality. Biomacromolecules. 2006;
13. Parsian M, Mutlu P, Yalcin S, Tezcaner A, Gunduz U. Half generations magnetic PAMAM dendrimers as an effective system for targeted gemcitabine delivery. Int J Pharm. 2016;515(1–2):104–13.
14. Lv T, Yu T, Fang Y, Zhang S, Jiang M, Zhang H, et al. Role of generation on folic acid-modified poly(amidoamine) dendrimers for targeted delivery of baicalin to cancer cells. Mater Sci Eng C. 2017;

OP-13

ANTIBODY ENGINEERING APPROACHES ON VERNIER ZONE RESIDUES TO DEVELOP BIOBETTER ANTIBODY THERAPEUTICS FOR CANCER TREATMENT

Merve Arslan[1,2], Gulcin Cakan-Akdogan[1,3], Sibel Kalyoncu[1]
[1]Izmir Biomedicine and Genome Center, Izmir, Turkey
[2]Izmir International Biomedicine and Genome Institute, Dokuz Eylul University, Izmir, Turkey
[3]Faculty of Medicine, Dokuz Eylul University, Izmir, Turkey

Binding affinity, biological efficacy, solubility, stability and aggregation are among the important factors that affect antibody developability. Biophysical and biochemical challenges can occur during early development phase due to the protein's large complex profile and these can cause faster antibody clearance, reduced antigen binding affinity/specificity, higher immunogenicity and toxicity. It is important to improve some of these characteristics for original and biobetter antibody development. Rational design is one of the commonly used antibody engineering techniques which aims to engineer problematic regions of protein structures to minimize these challenges. In our project, we aim to implement rational design approaches on Vernier zone residues of a single chain variable fragment (scFv) to derive biobetter anti-Vascular Endothelial Growth Factor (VEGF) antibodies for cancer treatment. Vernier zone residues locate in framework regions and underlie the complementary determining regions (CDRs) of antibodies and potentially affect conformations of CDRs. Vernier zone residues are mostly considered for humanization approaches but our preliminary results show that Vernier zone residues can also be used to improve key biochemical/biophysical properties of antibodies. We mutated Y49 on variable light chain to several amino acids to see the effect of this Vernier zone position on antibody characteristics. And, we found that one of our mutants, Y49N, showed higher affinity and similar biological efficacy (anti-angiogenic activity *in vivo*) compared to WT. This study shows the importance of Vernier zone residues for antibody engineering.
Keywords: Antibody; Antibody fragments; Single chain variable fragment (scFv); Antibody engineering; Vascular Endothelial Growth Factor (VEGF); Biobetter; Vernier zone residues; Zebrafish angiogenesis model

INTRODUCTION

There are more than 80 approved antibodies for therapeutic use [1]. Although most of these antibodies are in full-length format, antibody fragments have been emerging as next-generation biopharmaceuticals [2]. Antibody fragments are smaller but they keep essential antigen binding functionality and can have better biophysical properties [3]. Compared to full-length antibodies, there are many advantages of antibody fragments for therapeutic use: (i) lower immunogenicity due to lack of constant regions (ii) higher tumor penetration, (iii) cheaper and larger scale production with microbial systems (iv) availability of various *in vitro* screening technologies to improve several characteristics [4]. The most common antibody fragment formats are Fab, single chain variable fragment (scFv) and nanobody which are currently gaining more attention for therapeutic use [2].

Most approved antibodies are used for treatment of cancer and autoimmune diseases. There are three main therapeutic mechanisms of antibodies in cancer treatment: (i) direct killing of tumor cell by binding to overexpressed cell surface markers, (ii) immune-mediated tumor cell killing by activation of immune system against cancer cells, (iii) ablation of tumor cell growth by factor inhibition [5]. For the last mechanism, Vascular Endothelial Growth Factor A (VEGF) inhibition is one of the most successful cancer treatment strategies [6]. VEGF is an essential cytokine/factor for angiogenesis and vasculogenesis. Although VEGF was first described as an important growth factor for vascular endothelial cells, it was shown that VEGF and its receptors are also expressed on various non-endothelial cells including tumor cells [7]. It is known that VEGF has essential roles for tumor development and enlargement [8]. New and improved anti-VEGF therapeutics are needed for more effective cancer treatment [9], thus we aim to develop a biobetter, next-generation anti-VEGF scFv.

Vernier zone residues of antibodies underlie antigen binding complementary determining regions (CDRs) and potentially affect conformations of CDRs [10]. Although Vernier zone residues are mostly engineered for humanization approaches [11], we hypothesize that Vernier zone residues affect both antigen binding and biophysical properties. This study aims to implement rational design approaches on Vernier zone residues of an anti-VEGF scFv to derive biobetter antibodies for cancer treatments. Here, we engineered one of Vernier zone residues, Y49 on variable light chain, and found out that Y49 is very important for both affinity and biophysical characteristics. Although Y49 does not directly interact with VEGF, Y49N mutation surprisingly increased binding affinity almost 3-fold. Biological efficacy of WT and Y49N mutant are similar based on anti-angiogenic activity in zebrafish experiments while some biophysical characteristics such as stability and aggregation deteriorated depending on mutation. This is a good example of a trade-off between antibody characteristics. This study shows the importance of Y49 in antibody engineering and potential of Vernier zone residues to develop biobetter drugs.

MATERIAL AND METHODS

Expression and purification: A pET17-b expression plasmid encoding anti-VEGF scFv (design based on bevacizumab) was used (GenScript). Mutant variants were generated by QuikChange Lightning Site-Directed Mutagenesis Kit (Agilent). Plasmids were transformed into competent *E.coli* strain BL21 (DE3) pLysS using heat-shock. The transformed cells were plated and ten colonies were picked and inoculated into Luria-Bertani (LB) broth. The cultures were grown overnight at 37°C, 200 rpm. Inoculum was transferred into auto-induction media and allowed to grow at 18°C, 200 rpm for 48 h[12]. Cultures were centrifuged to remove cell pellets. Protein containing supernatant was incubated with HisPur Ni-NTA resin for 2 h at 4°C shaking vigorously. Mixture was loaded into 10 ml vacuum column and purified by affinity chromatography. Purified protein was buffer-exchanged into PBS (pH 7.4) through membrane filtration. Purity was analyzed on 12% SDS-PAGE and concentration was determined by NanoDrop (at 280 nm).

Enzyme-linked immunosorbent assay (ELISA): 96-well plates were coated with VEGF (1.5 ng/ml) at 4°C for overnight. Wells were blocked with 10% (w/v) skimmed milk in PBS at room temperature for 6-8 h. Varying concentrations of protein samples (0-1000 nM) were added into wells in triplicates. The plate was incubated at 4°C for overnight. Primary (mouse anti-FLAG-M2 IgG) and secondary antibody (anti-mouse IgG HRP conjugated) with dilution of 1:5000 or 1:10000 was each incubated at room temperature for 1 hour. 1-Step Ultra TMB substrate was added and reactions were quenched with 2 M H_2SO_4. Readings were taken by Thermo Varioskan flash plate reader at 450 nm. Apparent binding affinity (dissociation constant, K_d) was calculated based on Hill equation fit.

Thermal denaturation: Protein Thermal Shift kit (ThermoFisher) was used. 8x-16x dye was mixed with 0.1-1 mg/ml protein. ABI 7500 Fast RT-PCR was used to obtain thermal shift data (25-99°C with 0.05% ramp rate). Thermal melting point (T_m) was calculated based on Hill equation fit.

Equilibrium denaturation: Protein-Guanidinium Chloride (GdmCl) mixtures containing final protein concentration of 75 µg/mL and GdmCl concentrations ranging from 0 to 5 M were incubated at 10°C for overnight. Intrinsic fluorescence (Ex. 280 nm) was measured by Thermo Varioskan flash plate reader from 300 to 400 nm. Fluorescence ratio (345 nm/ 325 nm) was used to plot unfolding curve and chemical melting point (C_m) was calculated based on Hill equation fit.

Aggregation kinetics: Protein aliquots (20 µM) were incubated at 60°C in a thermal cycler with heated lid. At various time points, a single aliquot was centrifuged at 17,000x g for 10 minutes at 4°C and protein concentration of soluble fraction was measured using NanoDrop. Assuming the loss of protein to be aggregate fraction, the data was fitted to a single exponential function: $y = a \cdot (1\text{-}\exp(-b \cdot x))$ where a is final amplitude, b is apparent aggregation rate constant (k_{app}) and x is time.

Zebrafish experiments: All procedures were approved by IBG-HADYEK ethical committee. fli1a:EGFP transgenic line was used for visualization of zebrafish vasculature[13]. 40 ng (22.5 nL of 1.8 mg/ml) protein or equal volume of PBS control was microinjected into yolk sac of 2 dpf embryos under anesthesia, n≥ 10 embryos per condition. At 3 dpf, embryos were mounted in agarose and imaged live with confocal microscope (LSM 880), 20X objective. SIV area and branch lengths were measured using ImageJ and student's t-test was applied to calculate significance.

RESULTS

Vernier zone residue Y49 was rationally mutated to three different amino acids (Y49N, Y49K, Y49D) in order to improve characteristics of designed WT scFv. After expression and purification of those variants, only Y49D mutant could not be obtained (**Figure 1A**). Protein yield of Y49N increased 2-fold and that of Y49K

stayed same compared to WT (**Table 1**). It was surprisingly found that Y49N mutant showed about 3-fold higher affinity for VEGF compared to WT (**Figure 1B, Table 1**). While Y49N has a K_d value of 87.7 nM which is in therapeutic range, Y49K mutant has similar K_d values with that of WT (**Table 1**).

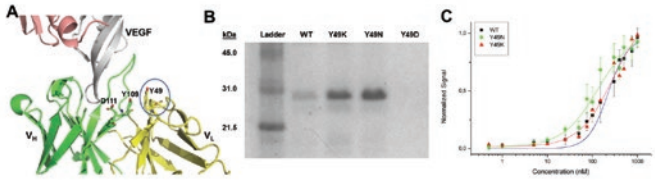

Figure 1. scFv variants used. (A) Bevacizumab (PDB ID: 1BJ1)-VEGF interaction with position of Y49 circled, (A) SDS-PAGE analysis, and (B) ELISA results of scFv variants.

Table 1. Biochemical and biophysical characterization of WT, Y49N, Y49K, Y49D.

	Yield (mg/L culture)	T_m (°C)	C_m (M)	k_{app} (s^{-1})	K_d (nM)
WT	0.830	55.8	2.86	0.0011	222.6
Y49N	1.620	44.0	4.54	0.0049	87.7
Y49K	0.916	51.6	N/A	0.0028	264.7
Y49D	0.001	N/A	N/A	N/A	N/A

Although binding affinity of Y49N increased significantly, some of its biophysical characteristics were not as good as WT (**Figure 2**). Thermal melting point (T_m) of WT was the highest (55.8 °C) compared to Y49N and Y49K mutants (**Table 1, Figure 2A**). On the other hand, Y49N was more stable upon chemical denaturation with a C_m value of 4.54 M (**Table 1, Figure 2B**). We also analyzed aggregation kinetics of all three variants and WT was found to be more resistant to aggregation with a k_{app} value of 0.0011 s^{-1} (**Table 1, Figure 2C**).

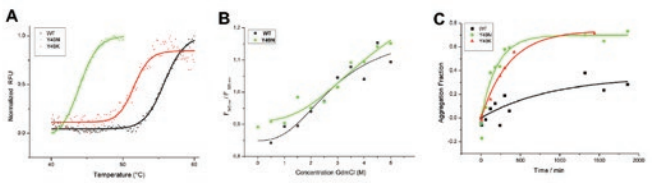

Figure 2. Biophysical characterization of WT, Y49N and Y49K. (A) Thermal denaturation, (B) Chemical denaturation, (C) Aggregation kinetics.

Biological efficacies of the most promising mutant, Y49N, and WT were tested on a zebrafish angiogenesis model. Transgenic fli1a:EGFP zebrafish allows fluorescent visualization of blood vessels[13]. Angiogenesis of Subintestinal Veins (SIVs) in zebrafish embryos have been used to evaluate anti-angiogenic treatments[14]. WT and Y49N antibodies and control (PBS) were injected into yolk sac of 2 dpf embryos and SIV angiogenesis was evaluated by total area and vessel branch length measurements (**Figure 3E-G**). While SIVs of PBS injected embryos were formed normally with good length of dorsal branches that lined orderly, SIVs of WT and Y49N were underdeveloped with disordered dorsal branches. The SIV area decreased very significantly upon WT and Y49N antibody injection compared to control (**Figure 3C**). The dorsal branches that form between 2dpf-3dpf were shorter in both WT and Y49N injected embryos (**Figure 3D**). No significant difference was observed between WT and Y49N injections.

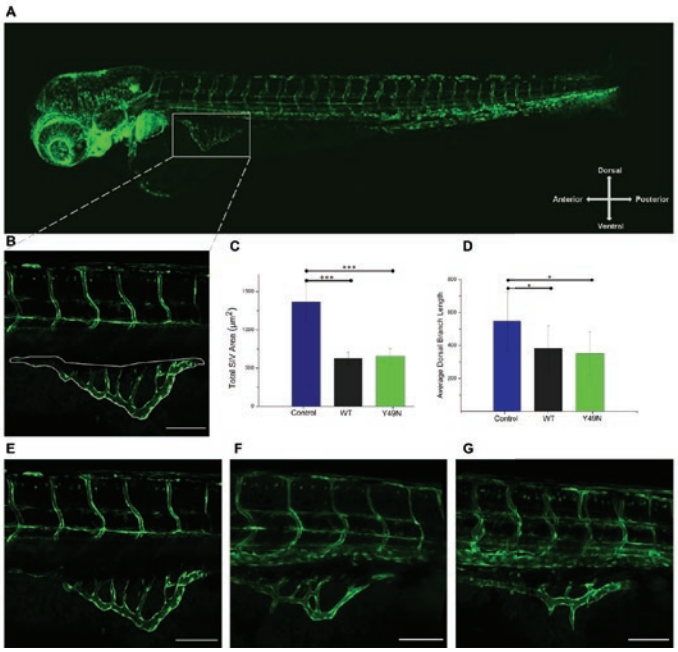

Figure 3. Anti-angiogenic activity of WT and Y49N variant in zebrafish embryos: (**A**) Representative image of 3 days post fertilization (dpf) Tg(flia:EGFP) embryo showing the embryonic vasculature. The SIV region is selected (boxed area) for measurements (**B**) Representative image of SIV region. SIV was selected by segmented line tool in ImageJ (white lines) and measured. Quantification of the (**C**) SIV areas and (**D**) average dorsal branch lengths of PBS, WT and Y49N injected embryos. Representative fluorescent images of (**E**) PBS control and embryos treated with (**F**) WT and (**G**) Y49N. *P<0.05, ***P<0.001. Scale bar is 100 µm.

DISCUSSION

Effect of Vernier zone residues on antibody characteristics are often neglected[10]. Here, we showed that Y49 on variable light chain have significant effect on both binding affinity and biophysical characteristics. In the literature, there is only one study by Dudgeon, *et al.* which analyzes Y49D mutation and they did not find any conclusive result similar to our results[15]. However, Y49N and Y49K mutants are not studied before according to our knowledge. Although Y49 has no direct contact with VEGF, we speculate that a π stacking interaction is key for success of Y49 mutants which can affect antigen contacting residues via secondary interactions. In WT, there is a π(Y49 on V_L)-π(Y109 on V_H)-anion(D111 on V_H) triple stacking towards HCDR3 which heavily contacts with VEGF (**Figure 1A**). For Y49D, this interaction becomes anion-π-anion stacking which is undesired due to repulsion of two aspartates. This might explain why our results and Dudgeon, *et al.* could not obtain any protein of Y49D, probably due to structural destabilization and misfolding during expression. However, we were able to obtain and characterize Y49N and Y49K mutants. Y49N showed almost 3-fold increase in affinity while some of its biophysical characteristics were deteriorated. Dalkas, *et al.* found that there is statistically higher presence of cation/amino-π interactions for favorable conformational epitope-paratope interactions[16] and our finding supports this statement for Y49 position. Since zebrafish shows high pharmacologic similarity with humans[17], and have been used successfully for for anti-angiogenesis screening[18] of chemicals and antibody therapeutics[14] and its we tested the biological efficacy of our most promising mutant, Y49N, in zebrafish models. We found that both WT and Y49N treatments led to significant defects in SIV formation similar to findings of Zhang, *et al.* for bevacizumab[14]. We have not seen any change in the main branch length (data not shown) as this branch already forms before 2dpf before the antibody treatment . The branch pattern of the dorsal branches were severely affected. The number of branches could not be calculated due to complex and disordered structure, however the length of dorsal branches were found to be significantly shorter upon treatment. We have observed and induction in the ventral sprouts upon WT and Y49N treatment, which could be due to a compensation attempt although the difference was insignificant (data not shown). While calculating the SIV area we have included the dorsal branches and ventral sprouts (when present), we have found a highly significant suppression of angiogenesis by WT and Y49N variants.

CONCLUSION

In this study, we aimed to develop a next-generation anti-VEGF scFv antibody fragment for cancer treatment. We found that one of Vernier zone residues, Y49 on variable light chain, is a promising target for antibody engineering. Recent literature usually neglects importance of Vernier zone, but this study highlights key roles of Vernier zone residues for biobetter antibody development. Promising mutations resulted from this study can be generalized to other antibodies used in various cancer treatments.

Acknowledgements

We would like to thank Izmir Biomedicine and Genome Center (Start-up grant), TUBITAK (Project number: 119Z161) and YOK (Council of Higher Education) 100/2000 fellowship program for funding our research group. We thank Emine Gelinci for her technical help with zebrafish experiments. We thank Nazlı Eda Kaleli, Murat Karadag and Dilara Karadag for their valuable input in experimental processes.

REFERENCES

1. Kaplon, H. and J.M. Reichert, Antibodies to watch in 2019. mAbs, 2019. 11(2): p. 219-238.
2. Nelson, A.L., Antibody fragments: hope and hype. MAbs, 2010. 2(1): p. 77-83.
3. Bradbury, A.R., S. Sidhu, S. Dubel, and J. McCafferty, Beyond natural antibodies: the power of in vitro display technologies. Nat Biotechnol, 2011. 29(3): p. 245-54.
4. Bannas, P., J. Hambach, and F. Koch-Nolte, Nanobodies and Nanobody-Based Human Heavy Chain Antibodies As Antitumor Therapeutics. Frontiers in Immunology, 2017. 8(1603).
5. Redman, J.M., E.M. Hill, D. AlDeghaither, and L.M. Weiner, Mechanisms of action of therapeutic antibodies for cancer. Mol Immunol, 2015. 67(2 Pt A): p. 28-45.
6. Sitohy, B., J.A. Nagy, and H.F. Dvorak, Anti-VEGF/VEGFR therapy for cancer: reassessing the target. Cancer Res, 2012. 72(8): p. 1909-14.
7. Yancopoulos, G.D., S. Davis, N.W. Gale, J.S. Rudge, S.J. Wiegand, et al., Vascular-specific growth factors and blood vessel formation. Nature, 2000. 407(6801): p. 242-248.
8. Lee, S.H., D. Jeong, Y.S. Han, and M.J. Baek, Pivotal role of vascular endothelial growth factor pathway in tumor angiogenesis. Ann Surg Treat Res, 2015. 89(1): p. 1-8.
9. Folkman, J., Angiogenesis: an organizing principle for drug discovery? Nat Rev Drug Discov, 2007. 6(4): p. 273-86.
10. Dondelinger, M., P. Filee, E. Sauvage, B. Quinting, S. Muyldermans, et al., Understanding the Significance and Implications of Antibody Numbering and Antigen-Binding Surface/Residue Definition. Front Immunol, 2018. 9: p. 2278.
11. Almagro, J.C. and J. Fransson, Humanization of antibodies. Front Biosci, 2008. 13: p. 1619-33.
12. Studier, F.W., Protein production by auto-induction in high density shaking cultures. Protein Expr Purif, 2005. 41(1): p. 207-34.
13. Lawson, N.D. and B.M. Weinstein, In vivo imaging of embryonic vascular development using transgenic zebrafish. Dev Biol, 2002. 248(2): p. 307-18.
14. Zhang, J., B. Gao, W. Zhang, Z. Qian, and Y. Xiang, Monitoring antiangiogenesis of bevacizumab in zebrafish. Drug Des Devel Ther, 2018. 12: p. 2423-2430.
15. Dudgeon, K., R. Rouet, I. Kokmeijer, P. Schofield, J. Stolp, et al., General strategy for the generation of human antibody variable domains with increased aggregation resistance. Proc Natl Acad Sci U S A, 2012. 109(27): p. 10879-84.
16. Dalkas, G.A., F. Teheux, J.M. Kwasigroch, and M. Rooman, Cation-pi, amino-pi, pi-pi, and H-bond interactions stabilize antigen-antibody interfaces. Proteins, 2014. 82(9): p. 1734-46.
17. Howe, K., M.D. Clark, C.F. Torroja, J. Torrance, C. Berthelot, et al., The zebrafish reference genome sequence and its relationship to the human genome. Nature, 2013. 496(7446): p. 498-503.
18. Chavez, M.N., G. Aedo, F.A. Fierro, M.L. Allende, and J.T. Egana, Zebrafish as an Emerging Model Organism to Study Angiogenesis in Development and Regeneration. Front Physiol, 2016. 7: p. 56.

OP-14

NANOBODIES AS NEW THERAPEUTICS IN CANCER TREATMENT: CAMELIZATION OF AN ANTI-VEGF NANOBODY THROUGH ANTIBODY ENGINEERING APPROACHES

Nazlı Eda Kaleli[1,2], Sibel Kalyoncu[1]

[1]Izmir Biomedicine and Genome Center, Izmir, Turkey

[2]Izmir International Biomedicine and Genome Institute, Dokuz Eylul University, Izmir, Turkey

Most antibody therapeutics are based on full-length IgG form, but new formats, especially antibody fragments, have gained attention over the last decade. Nanobody is an antibody fragment existing as a single domain antibody, which consists of only variable heavy chain (V_H). Although V_H does not exist without variable light chain (V_L) in humans, camelids naturally have such single domain antibodies. Camelid nanobodies are superior than conventional IgGs in terms of physicochemical properties. Removal of V_L causes exposure of hydrophobic residues on V_H-V_L interface, resulting in undesired biophysical properties in human/humanized antibodies. Nanobodies have high potential to be used as new-generation cancer therapeutics due to having many advantages, such as smaller size (15 kDa), improved solubility, and flexibility. Since nanobodies can diffuse into tumor or tissue better than conventional antibodies, they increase efficacy of cancer treatment. Aim of this study is to engineer a biobetter anti-Vascular Endothelial Growth Factor (VEGF) nanobody based on camelid V_H (camelization) for cancer therapy. Our camelization based mutations on framework-2 region have showed better biophysical properties in terms of yield, stability and aggregation/solubility. Interestingly, affinity of engineered nanobodies have also substantially increased.

Keywords: Antibody, antibody fragment, nanobody, cancer, anti-VEGF, antibody engineering, framework-2, camelization, biobetter

INTRODUCTION

To date, US Food and Drug Administration (FDA) and European Medicines Agency (EMA) have approved over 80 therapeutic antibodies, most of which are full-length antibodies [1]. Since antibody engineering is pursuing a better understanding, there is a current trend inclining to working on antibody fragments; especially nanobodies, which are becoming very popular due to their many superior physicochemical features [2]. Nanobodies are single domain heavy chain antibodies (V_HH) lacking constant regions and light chain. V_HHs are derived from *Camelidae* family members such as camel, lama and vicugna [3]. Superior features of nanobodies make them ideal candidates for both therapeutic and diagnostic applications [4-6]. Some of their advantages can be summarized as; (i) smaller size (15 kDa), (ii) robustness, (iii) improved thermal stability and solubility, (iv) recognition of hidden epitopes, (v) better tissue or tumor penetration that are cryptic for full-format antibodies (they even pass blood-brain barrier [7]), (vi) enhanced target specificity, (vii) low immunogenicity [8].

V_H domain (human counterpart of V_HH) can only be found as in complex with V_L domain in human immune repertoire. Lack of V_L would result in exposure of hydrophobic V_H-V_L interface surface. Hydrophobic and exposed V_H residues tend to interact with each other leading aggregation [9]. In order to generate a human nanobody, one needs to engineer hydrophobic V_H domain through "camelization" [5, 10]. The most remarkable property of V_HH is containing entirely hydrophilic V_H-V_L interface which accounts for the superior stability and solubility over a V_H [11]. Hydrophilic framework-2 (FW2) region of V_HH consists of hallmark residues located at 42, 49, 50 and 52 positions according to Kabat numbering (**Figure 1A**). Especially, amino acids at position 49 and 50 are always charged residues that reduce exposed hydrophobic area in V_HH [12]/.

Vascular Endothelial Growth Factor (VEGF) is an angiogenesis-promoting factor and it is overexpressed by many solid cancer cell types. VEGF is also known to have key role in tumor development/enlargement [13]. VEGF overexpression is highly associated with metastatic potential, such as cellular migration ability and neo-vascularization [14]. Anti-VEGF treatment is currently one of the most successful cancer treatment strategy [15]. However, novel and improved anti-VEGF therapeutics are needed for more effective cancer treatment. In this study, we aim to develop a next-generation anti-VEGF nanobodies through protein engineering based on camelization approaches.

Here, we showed that there is a drastic change in both antigen binding and biophysical characteristics, when FW2 residues of anti-VEGF nanobody are camelized. Two mutations (L45R and W47G) improved binding affinity, stability and aggregation features of designed nanobody. This study shows that camelization on any human/humanized antibody can be performed to obtain next-generation, biobetter nanobodies for improved cancer treatment.

MATERIALS AND METHODS:

Expression and purification: A pET17-b expression plasmid encoding anti-VEGF V_HH (design based on bevacizumab) was used (GenScript). Mutant variants were generated by QuikChange Lightning Site-Directed Mutagenesis Kit (Agilent). Plasmids were transformed into competent *E.coli* strain BL21 (DE3) pLysS using heat-shock (42°C, 45 sec). The transformed cells were plated and ten colonies were picked from a single plate and inoculated into Luria-Bertani (LB) broth containing appropriate antibiotics. The cultures were grown overnight at 37°C shaking thoroughly. Inoculum was transferred into auto-induction media and allowed to grow at 18°C, 200 rpm for 48 h [16]. Cultures were centrifuged to remove the cell pellets. Protein containing supernatant was incubated with HisPur Ni-NTA resin for 2 h at 4°C shaking vigorously. Mixture was loaded into 10 ml vacuum column and purified by affinity chromatography. Purified protein was buffer-exchanged into PBS (pH 7.4) through membrane filtration. Purity was analyzed on 12% SDS-Page and concentration was determined by NanoDrop 2000 (280 nm).

Enzyme-linked immunosorbent assay (ELISA): 96-well plates were coated with VEGF (1.5 ng/ml) at 4°C for overnight. Wells were blocked with 10% (w/v) skimmed milk in PBS at room temperature for 6-8 h. Varying concentrations of protein samples (0-1000 nM) were added into wells in triplicates. The plate was incubated at 4°C for overnight. Primary (mouse anti-FLAG-M2 IgG) and secondary antibody (anti-mouse IgG HRP conjugated) with dilution of 1:5000 or 1:10000 was incubated at room temperature for 1 hour each. 1-Step Ultra TMB (3,3',5,5'-tetramethylbenzidine) substrate was added and reactions were quenched with 2 M H_2SO_4. Readings were taken by Thermo Varioskan flash plate reader at 450 nm. Apparent binding affinity (dissociation constant, K_d) was calculated based on Hill equation fit.

Equilibrium denaturation: Protein-Guanidinium Chloride (GdmCl) mixtures containing final protein concentration of 75 µg/mL and GdmCl concentrations ranging from 0 to 6 M were incubated at 10°C for overnight. Intrinsic fluorescence (Ex. 280 nm) was measured by Thermo Varioskan flash plate reader from 300 to 400 nm. Fluorescence ratio ($F_{345\ nm}$/ $F_{325\ nm}$) was used to plot unfolding curve and chemical melting point (C_m) was calculated based on Hill equation fit.

Aggregation kinetics: Protein aliquots (20 µM) were incubated at 60°C and 65°C in a thermal cycler with heated lid. Separately, protein aliquots (0.5 mg/ml) were incubated at 65°C shaking at 200 rpm on a thermomixer. At various time points, a single aliquot was centrifuged at 17,000x g for 10 minutes at 4°C and protein concentration of soluble fraction was measured using NanoDrop. Assuming the loss of protein to be aggregate fraction, the data was fitted to a single exponential function: y = a (1-exp (-b x)) where a is final amplitude, b is apparent aggregation rate constant (k_{app}) and x is time.

RESULTS AND DISCUSSION

Nanobody formats of humanized antibodies display poor biophysical properties due to its exposed hydrophobic interface mainly consisting of framework-2 region (**Figure 1A**). In this study, we remedied two hallmark residues in framework-2 region (L45R and W47G) through camelization in order to improve both biochemical and biophysical characteristics and embrace nanobody format of our previously humanized anti-VEGF antibody. Those camelization based mutations have showed overall better biochemical and biophysical properties (**Figure 1, Table 1**). Protein yield of L45R and W47G increased about 18-fold and 13-fold compared to WT (**Table 1**). WT has very low expression levels, probably due to its exposed hydrophobic V_H-V_L interface, even single mutations on this region improved expression levels drastically.

Interestingly, binding affinity of engineered nanobodies for VEGF has substantially increased (**Figure 1C, Table 1**). While affinity of W47G increased more than 5-fold, that of L45R increased about 2-fold. Although mutation sites are far away from Complementarity Determining Regions (CDR) which are responsible for antigen binding, there is a drastic effect on binding affinity. This shows that camelization approaches based on V_H-V_L interface might not only improve biophysical characteristics but also binding affinity.

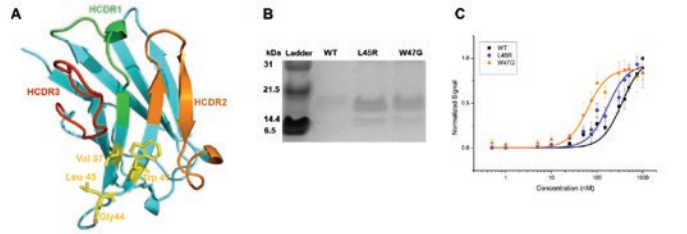

Figure 1. Nanobody variants used. **(A)** 3-D structure of variable heavy chain of bevacizumab (PDB ID: 1BJ1). Hypervariable CDR loops and hallmark residues were highlighted; HCDR1: green, HCDR2: orange, HCDR3: red and FW-2 residues, yellow sticks) **(B)** SDS-PAGE analysis, and **(C)** ELISA results of nanobody variants (n=3).

Table 1. Biochemical and biophysical characterization of V_HH WT, L45R, W47G nanobodies.

Protein	Yield (mg/L culture)	C_m (M)	k_{app} (s^{-1})	K_d (nM)
WT	0.06	N/A	N/A	349.1
L45R	1.11	2.26	0.00433	172.7
W47G	0.80	2.17	0.00838	62.9

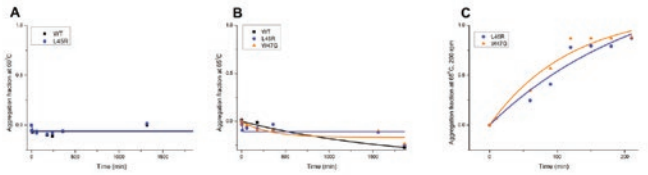

Figure 2. Aggregation kinetics of WT, L45R, W47G nanobodies. **(A)** Aggregation profiles at 60°C, **(B)** 65°C, **(C)** 65°C and mechanical stress at 200rpm.

Another important biophysical characteristic that is important for developability of antibody therapeutics is solubility/aggregation profile [17]. If antibody is aggregation-prone, it should be detected in early stage development because it would be a huge problem during process/formulation and after injection (aggregated proteins might become toxic) [18]. Nanobodies are known to be more stable compared to many other antibody formats [2]. In this study, our nanobody variants could not be aggregated and remained stable with only thermal stress at 60°C and 65°C (**Figure 2A, B**) for over a day. In order to make them aggregated to obtain aggregation kinetics data, we also applied mechanical stress by shaking them at 200 rpm in addition to thermal stress at 65°C (**Figure 2C**). Although we could not get any conclusive result for WT due to its low protein level, which was not enough for this particular assay, we found that both L45R and W47G have low k_{app} values which emphasizes their aggregation-resistant profile (**Table 1**). Stability of our nanobody variants were tested by chemical denaturation experiments with GdmCl (**Figure 3**). Chemical denaturation profile and C_m values of L45R and W47G mutants were similar to each other (**Table 1**) [12]. It is known that chemical and thermal unfolding processes correlate in terms of thermodynamics [19], so our finding supports this statement by having similar aggregation kinetics and chemical equilibrium data for L45R and W47G.

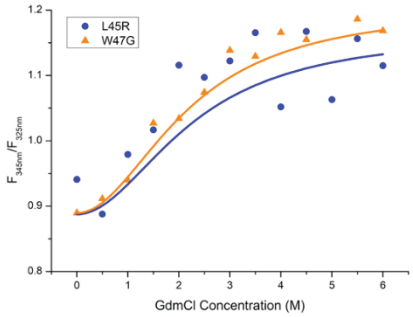

Figure 3. Chemical denaturation of L45R and W47G nanobodies.

Both L45R and W47G mutations convert a highly hydrophobic amino acid into a highly charged (L45R) and less hydrophobic amino acid (W47G), this might help reduce hydrophobic index of V_H-V_L interface. This explains increase in solubility and decrease in aggregation kinetics by blocking hydrophobic effect [20]. The results of this study is very encouraging in terms of development of stable and high affinity nanobodies based on camelization approach. Our work shows that nanobody format of any humanized antibody can be generated successfully to be used as next-generation cancer therapeutics.

Acknowledgement

We would like to thank Izmir Biomedicine and Genome Center (Start-up grant), TUBITAK (Project number: 119Z161) and YOK (Council of Higher Education) 100/2000 fellowship program for funding our research group. We thank Merve Arslan, Murat Karadag and Dilara Karadag for their valuable input in experimental processes.

REFERENCES

1. Kaplon, H. and J.M. Reichert, Antibodies to watch in 2019. mAbs, 2019. 11(2): p. 219-238.
2. Bannas, P., J. Hambach, and F. Koch-Nolte, Nanobodies and Nanobody-Based Human Heavy Chain Antibodies As Antitumor Therapeutics. Frontiers in Immunology, 2017. 8(1603).
3. Muyldermans, S., Nanobodies: Natural Single-Domain Antibodies. Annual Review of Biochemistry, 2013. 82(1): p. 775-797.
4. De Meyer, T., S. Muyldermans, and A. Depicker, Nanobody-based products as research and diagnostic tools. Trends Biotechnol, 2014. 32(5): p. 263-70.
5. Schumacher, D., J. Helma, A.F.L. Schneider, H. Leonhardt, and C.P.R. Hackenberger, Nanobodies: Chemical Functionalization Strategies and Intracellular Applications. Angew Chem Int Ed Engl, 2018. 57(9): p. 2314-2333.
6. Wang, Y., Z. Fan, L. Shao, X. Kong, X. Hou, et al., Nanobody-derived nanobiotechnology tool kits for diverse biomedical and biotechnology applications. International journal of nanomedicine, 2016. 11: p. 3287-3303.
7. Bélanger, K., U. Iqbal, J. Tanha, R. MacKenzie, M. Moreno, et al., Single-Domain Antibodies as Therapeutic and Imaging Agents for the Treatment of CNS Diseases. Antibodies, 2019. 8(2): p. 27.
8. Mitchell, L.S. and L.J. Colwell, Comparative analysis of nanobody sequence and structure data. Proteins, 2018. 86(7): p. 697-706.
9. Tanha, J., P. Xu, Z. Chen, F. Ni, H. Kaplan, et al., Optimal design features of camelized human single-domain antibody libraries. J Biol Chem, 2001. 276(27): p. 24774-80.
10. Riechmann, L. and S. Muyldermans, Single domain antibodies: comparison of camel VH and camelised human VH domains. J Immunol Methods, 1999. 231(1-2): p. 25-38.
11. Goldman, E.R., J.L. Liu, D. Zabetakis, and G.P. Anderson, Enhancing Stability of Camelid and Shark Single Domain Antibodies: An Overview. Frontiers in Immunology, 2017. 8(865).
12. Vincke, C., R. Loris, D. Saerens, S. Martinez-Rodriguez, S. Muyldermans, et al., General strategy to humanize a camelid single-domain antibody and identification of a universal humanized nanobody scaffold. J Biol Chem, 2009. 284(5): p. 3273-84.
13. Lee, S.H., D. Jeong, Y.S. Han, and M.J. Baek, Pivotal role of vascular endothelial growth factor pathway in tumor angiogenesis. Ann Surg Treat Res, 2015. 89(1): p. 1-8.
14. Katayama, Y., J. Uchino, Y. Chihara, N. Tamiya, Y. Kaneko, et al., Tumor Neovascularization and Developments in Therapeutics. Cancers (Basel), 2019. 11(3).
15. Sitohy, B., J.A. Nagy, and H.F. Dvorak, Anti-VEGF/VEGFR therapy for cancer: reassessing the target. Cancer Res, 2012. 72(8): p. 1909-14.
16. Studier, F.W., Protein production by auto-induction in high density shaking cultures. Protein Expr Purif, 2005. 41(1): p. 207-34.
17. Rouet, R., K. Dudgeon, M. Christie, D. Langley, and D. Christ, Fully Human VH Single Domains That Rival the Stability and Cleft Recognition of Camelid Antibodies. J Biol Chem, 2015. 290(19): p. 11905-17.
18. Kohli, N., N. Jain, M.L. Geddie, M. Razlog, L. Xu, et al., A novel screening method to assess developability of antibody-like molecules. MAbs, 2015. 7(4): p. 752-8.
19. Wang, Q., A. Christiansen, A. Samiotakis, P. Wittung-Stafshede, and M.S. Cheung, Comparison of chemical and thermal protein denaturation by combination of computational and experimental approaches. II. J Chem Phys, 2011. 135(17): p. 175102.
20. Jiang, L., S. Cao, P.P. Cheung, X. Zheng, C.W.T. Leung, et al., Real-time monitoring of hydrophobic aggregation reveals a critical role of cooperativity in hydrophobic effect. Nat Commun, 2017. 8: p. 15639.

OP-15

HOLOGRAPHIC IMAGING OF CELL PROLIFERATION

Rahmetullah Varol[1*], Gizem Aydemir, Aslıhan Karadağ, Ecenur Meço, Sevde Ömeroğlu, Enes Oruc, Yasemin Başbınar, Gökhan Bora Esmer, Hüseyin Üvet

[1]Department of Computer Engineering, Boğaziçi University, İstanbul, Turkey

[2]Department of Mechatronics Engineering, Yıldız Technical University, İstanbul, Turkey

[3]Institute of Oncology, Dokuz Eylul University, İzmir, Turkey

[4]Chemical Engineering Department, Gebze Technical University, Kocaeli, Turkey

[5]Department of Electrical and Electronics Engineering, Marmara University, İstanbul, Turkey

INTRODUCTION: In this study we aim to demonstrate the use of holographic imaging as a method for observing biological processes as a means to gain a better understanding through the depth information of the sample.

METHOD: To this end we conducted an experiment where the proliferation of ONCO-DG1 cells were observed over a 48-hour period using a Mach-Zehnder interferometer. A total of eight samples with initial cell counts between 2000-10000 were observed and the total cell counts were reported for 6, 12, 24 and 48-hour periods. We used a modified watershed segmentation technique for segmenting and counting individual cells.

MATERIAL: We compared the cell counts obtained from the holographic images with cell counts obtained via capacitive cell cytometry methods from similar samples. We observed that the holographic cytometry method achieves high sensitivity and specificity against manually annotated samples. Moreover, holographic method gives a depth information which could be used to assess the growth pattern of each individual cell in addition to the proliferation of the whole sample.

RESULT: The results indicate that the holographic imaging method presents clear advantages over standard light microscopy techniques for assessing the proliferation and growth of 2D cell cultures. Through holographic imaging methods we can measure the localized proliferation patterns and single cell growth pattern for better understanding the dynamics of the proliferation process.

Keywords: holographic imaging cell proliferation

INTRODUCTION

Imaging of biological specimens by means of classical optical techniques presents challenges due to their highly transparent nature [1]. Interferometric techniques extract the phase information from the observed sample to obtain quantitative depth measurements [2]. In particular digital holographic microscopy techniques have been gaining popularity due to its high accuracy and non-destructive nature. Use of DHM for imaging of live cells has been demonstrated through numerous application such as analysis of human hepatocytes [3] or observation of mouse cortical neurons [2].

In this study, we investigate the use of DHM for observing the cell proliferation patterns of in-vitro tumor cells. In particular we culture 8 samples with 1000 through 8000 ONCO-DG1 cells inside 480μL micro-wells and holographically reconstruct the well in 6-hour intervals. Using the acquired depth maps, we report the results for our noise reduction, cell segmentation and cell counting algorithms.

MATERIALS AND METHODS

Sample Preparation

We used 480μL micro-wells for culturing each of the samples. The wells were fabricated by replica molding from an SU-8 (MicroChem)/silicon master based on a ratio of 10:1 to curing agent. The master mold was produced by ultraviolet (UV) lithography. After pouring PDMS on a mold, the mixture was degassed in a vacuum chamber for air bubble removal and cured at 80°C for 1 hour in the oven. The devices were then cut out by a razor blade; the fluidic connection ports were punched, and bonding to a glass slide was done after oxygen plasma of both surfaces and conformal contact (Harrick Plasma cleaner/sterilizer, 4 mbar, 120 s).

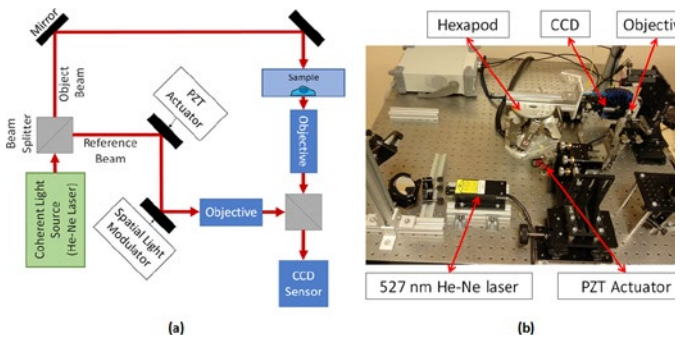

Figure 1: Schematic diagram of the setup and (b) its experimental counterpart.

Holographic Imaging Technique

For almost all cell manipulation tasks, the morphological structure of the manipulated cells is a critical parameter. Cell morphology is an important determinant of the cell genotype and determines many of its characteristics including its surface adhesion behavior its intra cellular signaling pathway regulation and its membrane permeability. It is also a stronger indicator of the class a cell belongs to, compared to classical light microscopy techniques [4]. We investigate the use of morphological information in cell transportation operations. Assessment of the cell shape and cell-surface adhesion helps better understand how to direct the actions of the manipulator and how to lift and carry the without compromising its integrity.

To obtain depth maps from the sample we use a phase shifting in-line Mach-Zehnder interferometer, as shown in Figure 1, in which the phase shifting is achieved by a high-frequency piezo actuator. Mach-Zehnder interferometry is based on the interference of a object wave which contains the wavefield transmitted from the observed sample and a reference wave which contains the wavefield of the original coherent light source. The coherent light source used in this study is a 527 nm He-Ne laser. The interferogram obtained as such is recorded by a CCD sensor. Using the complete set of interferograms obtained in equal intervals throughout a whole period of the wavefield is used to solve for the phase of the observed sample. This information in turn allows us to compute the depth information. The intensity distribution of a given interferogram can be written as

$$L_j(x,y) = A_o^2(x,y) + A_r^2 + 2A_o(x,y)\,A_r \cos[\theta_o(x,y) - \delta]$$

Where A_o and A_r are the object and reference wavefields respectively. The phase information of the sample can be reconstructed by translating the reference wave and solving the set of linear equations that form taking the Fresnel transformation of the complex wavefield that is recorded via an image sensor. In this study we follow this approach using a PZT actuator for shifting the phase of the reference wave.

Holographic Data Processing

Image Stitching: Since the field of view of an imaging system (including ours) is rarely large enough to view the whole sample, we developed a depth based stitching algorithm that composes a depth map of the whole sample by combining together smaller patches. To this end we coupled the sample holder to a 6-axis Hexapod and moved the sample in the XY axis in a stepwise fashion while recording the interferogram at each step. The depth maps, reconstructed from these interferograms are then stitched together using the method described in [5].

Cell Segmentation: After acquiring a depth map for the whole sample, we used a marker-controlled Watershed transform based segmentation algorithm [6] to segment the parts of the map that contain a single cell or a cell group.

Cell Counting: For each segmented section, we use a volumetric prediction method to get an approximate count of the cells within each region. The cell counting algorithm is based on calculating the mean volume of singular cells by clustering the lower end of the segmented volume values and dividing the volume of each segment with this base value. This gives us an approximation to the cell count inside that region.

RESULTS

We prepared four different samples with a known morphology for the assessment of our noise reduction algorithm, using micro spheres with 100μm diameter. We use the known morphology as ground truth and calculate the SNR values for raw and processed maps as follows,

$$SNR = 10 \cdot \left[\frac{\sum_0^{n_z-1} \sum_0^{n_y-1} [r(x,y)]^2}{\sum_0^{n_x-1} \sum_0^{n_y-1} [r(x,y) - t(x,y)]^2} \right]$$

where $r(x,y)$ is the reference depth map and $t(x,y)$ is the noisy depth map. SNR values are compared for, four different images are compared for different σ values are compared in Table 1. The reconstruction obtained from Sample 1 and Sample 2 at 0 and 48-hour marks are given in Figure 2.

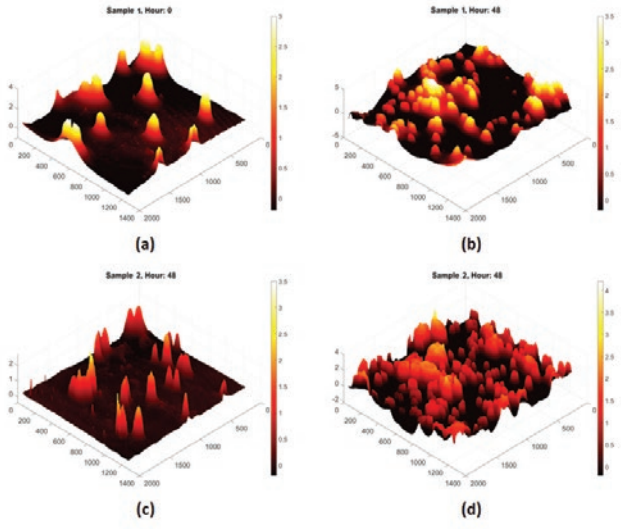

Figure 2: Holographic reconstructions of some example samples. (a) Sample 1 at its initial condition and (b) after 48 hours. (c) Sample 2 at its initial condition and (d) after 48 hours.

For the cell segmentation algorithm, we used manually annotated segmentations as ground truth and compared them with automatically segmented regions using the intersection over union, sensitivity and specificity metrics which are given in Table 2. The method used for calculating these metrics is as

$$Sensitivity = \frac{TP}{TP + FN}, \qquad Specificity = \frac{TN}{TN + FP}$$

where *TP, TN, FP* and *FN* refer to true positive, true negative, false positive and false negative respectively.

	Reference 1	Reference 2	Reference 3	Reference 4
Raw SNR	29.95	28.25	29.21	22.49
Filtered SNR	37.07	36.82	37.82	35.25

Table 1: SNR values of raw and filtered depth maps for reference samples.

	Sample 1 @ 0h	Sample 1 @ 48h	Sample 2 @ 0h	Sample 2 @ 48h
Sensitivity	90.27%	87.45%	90.89%	89.12%
Specificity	91.08%	88.67%	92.03%	91.02%

Table 2: Sensitivity and specificity values for two samples at 0 and 48-hour marks.

CONCLUSIONS

In this study we investigated the use of digital holographic microscopy method for cell cytometry. In particular we developed some depth processing algorithms which could be used for cell segmentation and cell counting. We also reported the performance of these algorithms against manually annotated samples. The results indicate that the DHM method achieves high sensitivity and specificity for the cell segmentation task. Also, we show that the volumetric information obtained from the depth map of the cell culture can be used to acquire a more accurate cell count prediction for regions in which individual cells can't be segmented It is clear that the DHM method will play a critical role in the future for cell culture studies where the morphological structure of the sample is important.

Acknowledgements

This work is funded by The Scientific and Technological Research Council of Turkey (TUBITAK) under the project number 116E743.

REFERENCES

1. Jacques SL. Optical properties of biological tissues: a review. Physics in Medicine \& Biology 2013. 58(11), p.R37.
2. Marquet P, Rappaz B, Magistretti PJ, Cuche E, Emery Y, Colomb T, and

Depeursinge C. Digital holographic microscopy: a noninvasive contrast imaging technique allowing quantitative visualization of living cells with subwavelength axial accuracy. Optics Letters 2005. 30, 468-470.
3. Carl D, Kemper B, Wernicke G, and Bally G. Parameter-optimized digital holographic microscope for high-resolution living-cell analysis. Applied Optics 2004. 43, 6536-6544.
4. Hejna M, Jorapur A, Song JS, Judson RL. High accuracy label-free classification of single-cell kinetic states from holographic cytometry of human melanoma cells. Scientific Reports 2017. 7(19), 11943.
5. Brown M, and Lowe DG. Automatic panoramic image stitching using invariant features. International Journal of Computer Vision 2007. 74.1, 59-73.
6. Beucher S. Watersheds of functions and picture segmentation. ICASSP 1982. Paris, France, pp. 1928-1931.

OP-16

DISCOVERY OF METHYLATION BASED IMMUNE-ESCAPE MECHANISMS IN RARE CANCERS

Kemal Turhan[1*], Serbulent Unsal[1*], Bunyamin Kasap[3*], Nihat Burak Zihni[1], Zeliha Aydın Kasap[1], Aybar Can Acar[2]

[1]Karadeniz Technical University, Trabzon. [2]Middle East Technical University, Ankara. [3]Kanuni Training And Research Hospital, Trabzon, Turkey

* These authors are equally contributed to study

INTRODUCTION: Tumors should escape from immune system to survive. Studies showed that DNA methylation has role in negative regulation of immune system (a.k.a immune-escape) which can be controlled with demethylation agents. Patients with rare cancers suffered from low number of drugs since for most of them drug development is non-trivial and non-profitable. Enlightment of methylation based immune-escape mechanisms are important since regulation of DNA methylation is possible with approved drugs. Aim of this study is creating a bioinformatics pipeline and apply it to ten rare cancer type to reveal common and type specific immune-escape mechanisims rooted from abnormal methylation patterns.

MATERIAL&METHODS: The developed pipeline starts with gathering data from TCGA and normalization. After that, differentialy methylated and expressed genes inferred. Candidate genes clustered according to their semantic similarity for enrichment and network perturbation analysis. Finally, statistically significant pathways and functions analysed and filtered manually based on literature.

RESULTS: In this study, type specific and common genes and pathways revealed for rare and reported with statistical and literature based evidence which might be used for new targets to therapies.

CONCLUSIONS: We discussed that new bioinformatics pipelines are important for rare cancers since known efforts are mostly focused to prevalent cancers. In this study we propose a new end-to-end bioinformatics pipeline and validate its efficiency by using literature results.

Keywords: Cancer, Methylation, Immune-escape

INTRODUCTION

Negative regulation of immune-system (immune-escape) is one of the key characteristics of the tumors [1]. This trait of the tumors also decrease success rate of the immunotherapy which is one of the most promising solutions to treat cancer. Hence, in the last decade, immune-escape has been one of the most studied phenomena for the cancer treatment. Negative regulation of the immune-system can be triggered through genetic or epigenetic alterations [2,3]. From an evolutionary point of view, epigenetic alterations are more common than the genetic alterations in the tumors since there are many mutation control and repair mechanisms are available in the cell [4]. Rare cancers are important since many people suffer from them. However, research and funding aims rare cancers are significantly lower than the common tumor types [5]. Since, funding bodies calculates return on investment numbers, it might be understandable but this does not change the fact that 4,400,000 people diagnosed with rare cancers only in EU [6].

If epigenetic roots of the immune-escape could be discovered these epigenetic changes might be reversed using known epigenetic regulatory drugs [7]. In this study we created a methylation analysis pipeline and investigate the abnormal epigenetic patterns which are supported by the differential expression patterns in ten rare cancer types.

The pipeline we created is an end-to-end workflow starts from the data download continues with the data preprocessing, differential methylation and expression analysis, calculating gene similarity according to the known immune-escape proteins and cluster them to increase specificity of the enrichment and pathway perturbation analysis. We then investigate on each gene and pathway in the literature to discover their relation with possible immune-escape activity.

MATERIALS AND METHODS

We use data from TCGA project and download it from the Genomic Data Commons (GDC) Data Portal. Methylation analysis data is produced by the "Infinium HumanMethylation450 BeadChip" covers gene regions with sites in the transcription start sites (TSS) , 5'UTR, first exon, gene body, and 3'UTR. In transcriptome profiling the downloaded data was preporcessed by the GDC according to "HTSeq - FPKM-UQ" workflow that can be summarized as "Quality Filtering", "Fragment Count", "Count Normalization" and "Upper Quartile Normalization" steps.

After this step the differentially methylated probes discovered. We only aim the distal probes (probes at maximum 2kb distance of the TSS) because we would like to discover down/up regulation of the proteins through binding of transcription factors at TSS which depends DNA methylation patterns. Since the number of the normal samples are not equal to the tumor samples in TCGA and there is no grouping is done based on tumor subtype, we choose unsupervised method for differential methylation analysis. In this method, DNA methylation beta values of the tumor and the normal samples ranked and the lowest %20 bound is selected for both types on each probe for the hypomethylated probes (highest %20 is selected). Afterwards, these values are tested using the one tailed t-test to see if there is a significant difference. This method could discover differences between tumors and normal samples even if the tumor can be composed by different subtypes.

To create a relationship between genes and the differentially methylated probes nearest 10 upstream and 10 downstream genes selected for the testing. Inverse relation between genes and probes are tested with Mann Whitney U test and the multiple test correction is applied using a permutation test. For the permutation based test a number of random probes selected and their p-values counted to find what percentage of these random probes could generate equal or lower p-value. This analysis serves for finding differentially methylated genes which methylation levels are significantly correlated with their gene expression levels. The empirical p-values are calculated in this step and introduced in the results. These genes are saved and used in further steps but we also use them to enlighten methylation based immune-escape mechanisms through literature search. ELMER [8] package is used for these analysis. The next step is clustering these genes based on the biological role that we investigate which is immune escape for this study. We first investigate literature to gather genes involved in immune-escape. We used these genes to define a basis and then measured semantic similarity relative to this basis. The semantic similarity is defined using GO term similarity (all "MF","BP" and "CC" aspects included). Similarity calculation is based on feature vectors. These vectors are calculated based on semantic distance to each prototype gene. Use of prototype genes creates a non-orthogonal basis for protein vectors. Detailed information on this process can be found in GoSim package which is used in this step [9].

After semantic similarities calculated between all candidate genes we apply the hierarchical clustering. With this clustering we aim to create the clusters that includes genes similar to specific immune-escape functions. The quality of clusters controlled using the silhouettes.

The final step in the computational analysis is enrichment and pathway analysis. There are three different approach exits in the literature. The first one is the over-representation analysis which can be defined as a hyper-geometric test which reveals enriched pathways or ontological entities. As other methods established on statistical tests, a p-value threshold is needed to use for this method which means a pathway that is slightly over the threshold will annotated as insignificant even if it has a high biological significance. Moreover, the method evaluates each gene and pathway without their interactions which might be exists in the biological context. The second approach is the functional class scoring that evaluates functionally related genes to reveal related abnormalities even though they each have little changes in their expression values. This method also does not consider interactions between genes and pathways. The third approach is pathway analysis methods which does not have these shortcomings [10]. We choose pathfindeR which is a pathway analysis method [11]. The method searches for active subnetworks which are well-defined phenotype-associated sets of interacting genes. The steps of the method can be summarized as; (1) Relating the differential genes to subnetworks. (2) Filtering the subnetworks. (3) Doing the enrichment on filtered subnetworks. This process is visualized in Figure 1 (taken from [11] with permission).

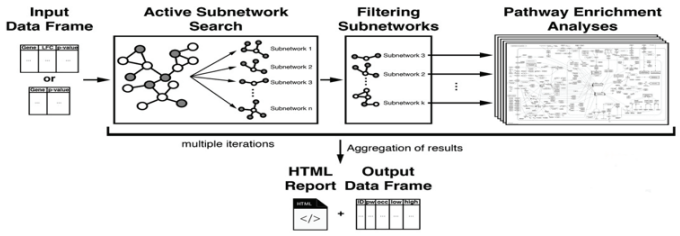

Figure 1. Overview of the pathfindeR method.

RESULTS

We investigate abnormal methylation patterns for the ten rare cancer types which are, acute myeloid leukemia, cholangiocarcinoma, lymphoid neoplasms, diffuse large b-cell lymphoma, mesothelioma, thymoma, uveal melanoma, testicular germ cell tumors, pheochromocytoma and paraganglioma, esophageal carcinoma, thyroid carcinoma. One of the results of our analysis is on downregulation of the SLC38A3 in cholangiocarcinoma cells which is caused by hypermethylation (p-value: 0.00099).

SLC38A3 (Sodium-coupled neutral amino acid transporter 3) acts role in the sodium coupled amino acid transport in or out of the cell and also has a role in synaptic connections and the nitrogen metabolism. In the nitrogen metabolism, if SLC38A3 inhibited nitrogen-oxide (NO) synthesis will be decreased [12]. Moreover, it is claimed that the NO molecule helps transformation of the M2 macrophages to the M1 macrophages. Since M2 macrophages are immune suppressant and M1s are tumor killer we hypothesized that the SLC38A3 might be a part of the immune-escape system of cholangiocarcinoma which is needed to be investigated in detail. On the other hand, this does not mean high NO doses can be associated with the good prognosis. On the contrary it is showed that in the colorectal cancer high levels of the NO has been associated with the bad prognosis and low survival rates [13]. One other interesting result is observed in the cholangiocarcinoma is on LGALS3 (Galectin 3). Our findings showed that expression levels of the LGALS3 is decreased because of hypermethylation (p-value: 0.00099). This protein contributes metastasis in the tumor invasion but more importantly it has a role in the immune-escape in melanoma. Galectin 3 synthesized from melanoma cells causes anergy at tumor specific cytotoxic T lymphocytes. Moreover, it perturbates function of T lymphocytes even causes apoptosis of these immune cells [14]. All these findings indicates the role of LGALS3 in immune-escape.

CONCLUSION

Revealing the molecular mechanisms underneaths tumor immune-escape will have potential to trigger new therapies. DNA methylation is one of these mechanisms and can be reversed in a non-trivial manner using known agents/drugs. Use of the computational analysis methods might speed up the process of enlightenment of the DNA methylation based immune-escape. This is important for all cancers but especially for rare cancers which gets low research funding. Our pipeline might be a starting point for this process. We tried to develop a neat approach which can be implemented easily and understandable by not only computational biologists but also medical experts.

Results of the pipeline, after a careful literature inspection, validates that some of the immune-escape mechanisms might be caused by abnormal DNA methylation patterns. Our results might be used as new targets for cancer therapies. However, we also discuss contrary findings which shows the task we aim is non-trivial and needs more effort. All computational and statistical analysis results in the scientific studies should be validated with experimental results and our study is not an exception. We hope that our study and studies similar to this study will be a starting point for more complex computational methods and studies which reveals more information on rare cancers.

CONFLICT OF INTEREST

The author(s) declare(s) that there is no conflict of interest regarding the publication of this article.

REFERENCES

1. Beatty GL, Gladney WL. Immune escape mechanisms as a guide for cancer immunotherapy. Clinical Cancer Research 2015; 21(4):687-92.
2. Fernández-Morera JL, Calvanese V, Rodríguez-Rodero S, Menéndez-Torre E, Fraga MF. Epigenetic regulation of the immune system in health and disease. Tissue Antigens 2010; 76(6):431-9.
3. Akbay EA, Koyama S, Carretero J, Altabef A, Tchaicha JH, Christensen CL, et al. Activation of the PD-1 pathway contributes to immune escape in EGFR-driven lung tumors. Cancer Discovery 2013; 3(12):1355-63.
4. Selby CP, Sancar A. Mechanisms of transcription-repair coupling and mutation frequency decline. Microbiol. Mol. Biol. Rev.1994; 58(3):317-29.
5. NIH Research Portfolio Online Reporting Tools (RePORT). Categorical Spending.https://report.nih.gov/categorical_spending.aspx (Last accessed: September 2019)
6. Pillai RK, Jayasree K. Rare cancers: challenges & issues. The Indian Journal Of Medical Research 2017;145(1):17.
7. Szyf M. The DNA methylation machinery as a target for anticancer therapy. Pharmacology & therapeutics 1996 ;70(1):1-37.
8. Silva TC, Coetzee SG, Gull N, Yao L, Hazelett DJ, Noushmehr H, et al. ELMER v. 2: An R/Bioconductor package to reconstruct gene regulatory networks from DNA methylation and transcriptome profiles. Bioinformatics 2018; 35(11):1974-7.
9. Fröhlich H, Speer N, Poustka A, Beißbarth T. GOSim–an R-package for computation of information theoretic GO similarities between terms and gene products. BMC bioinformatics. 2007 Dec;8(1):166.
10. Khatri P, Sirota M, Butte AJ. Ten years of pathway analysis: current approaches and outstanding challenges. PLoS computational biology 2012; 8(2): e1002375.
11. Ulgen E, Ozisik O, Sezerman OU. pathfindR: An R Package for Comprehensive Identification of Enriched Pathways in Omics Data Through Active Subnetworks. Frontiers in Genetics 2019; 10:858.
12. Dikalova A, Fagiana A, Aschner JL, Aschner M, Summar M, Fike CD. Sodium-coupled neutral amino acid transporter 1 (SNAT1) modulates L-citrulline transport and nitric oxide (NO) signaling in piglet pulmonary arterial endothelial cells. PloS one 2014; 9(1) : e85730.
13. Kashfi K, Vannini F. Nitric Oxide and Cancer: To Inhibit or To Induce iNOS: That Is the Question?. In: Morbidelli L, Bonavida B editors. Therapeutic Application of Nitric Oxide in Cancer and Inflammatory Disorders. Academic Press, 2019 : 93-111.
14. Radosavljevic G, Volarevic V, Jovanovic I, Milovanovic M, Pejnovic N, et al. The roles of Galectin-3 in autoimmunity and tumor progression. Immunologic research 2012 ; 52(1-2):100-10.

OP-17

IMMOBILIZATION OF CTCS ON SILANE-MODIFIED SURFACES

Sevde Omeroglu[1], Hanife Ecenur Meco[2], Aslıhan Karadag[2], Gizem Aydemir[3], Rahmetullah Varol[4], Muhammed Enes Oruc[1], Yasemin Basbinar[2], Gökhan Bora Esmer[5], Huseyin Uvet[3]

[1]Gebze Technical University, Chemical Engineering Department, Kocaeli, Turkey

[2] Dokuz Eylul University, Translational Oncology Department, Izmır, Turkey

[3]Yildiz Technical University, Mechatronics Engineering Department, Istanbul, Turkey

[4] Bogazici University, Computer Engineering Department, Istanbul, Turkey

[5] Marmara University, Electrical And Electronics Department, Istanbul, Turkey

In this paper, we report the holographic imaging method, algorithms used and the results obtained during an experiment in which dynamic cell cultures were treated with TGF_beta and subsequently underwent epithelial-mesenchymal transition (EMT). The primary motive of this study is to show the advantages of using quantitative phase imaging methods where the observation of the morphological transformation of the sample is important. During the EMT phase, tumor cells lose their adhesive nature and morph into a mesenchymal state in which they start migrating through the bloodstream into different parts of the body as circulating tumor cells. Observation of the transformation of surface structure in 3D during the EMT phase is critical for better understanding of the factors that trigger it since many of its precursors manifest itself in cell morphology. Accurate depth information obtained through quantitative phase imaging methods could play a key role in understanding the dynamics of this complex process. The goal of this work is to immobilize of CTCs (Circulating Tumor Cells) on glass substrates for holographic imaging. We formed a thin, stable layer of silane on a glass substrate using APTES ((3-Aminopropyl)triethoxysilane) solution. The APTES solution coated on glass surfaces is suitable for optical imaging and enables single-cell analyses. We conducted experiments on HCT-116 cell lines for APTES silaned surface structures. Using our segmentation method we show that modified surface structures increase the ability of CTCs to cling to a flat surface and hinders its mesenchymal characteristic. The demonstrated application clearly shows that holographic imaging techniques present valuable information that gives insights into the physiological underlyings of behavioral patterns cancer cells typically undergo.

Keywords: CTC immobilization, Holographic imaging, Surface functionalization.

INTRODUCTION

The methods developed for the analysis and imaging of circulating tumor cells (CTCs) have gained more attention by many researchers. The fact that CTC cells cannot be immobilized on surfaces has led researchers to investigate the interaction of cells between surfaces.In many studies, immobilization of cells on surfaces is by means of antibodies. Dixit et al. formed the APTES self-assembly monolayer on polymeric surfaces, allowed the immobilization of antibodies by covalently and optimized the system for enzyme-linked immunoassay [1]. Gunda et al. used glutaraldehyde as a cross-linker for biomolecule immobilization to the silane layer formed by APTES on a silicone surface [2]. Specifically, APTES monolayers are used for modification of glass surfaces to enhance the immobilization of cells and are a highly effective method for analysis in cell culture studies. The surface concentration of the APTES layer is very important for all applications. APTES films should be optimized for the type of biomolecule to be used and the ambient conditions [3]. As CTC studies continue to evolve, label-based CTC detection studies have become limiting. Digital holographic microscope provides a more appropriate characterization label-free technique and highly efficient for the analyses [4].

The aim of this work is to immobilize of CTCs on glass substrates using APTES solution and imaging by the digital holographic microscope. The characterization of the surfaces was made by contact angle measurement. In future studies, we plan to perform various analyzes on immobilized cells that can be visualized by digital holographic microscopy.

MATERIALS AND METHODS

Surface Modification

Glass substrates (2 x 2 cm2) were immersed in isopropyl alcohol-acetone-isopropyl alcohol respectively and ultrasonicated for 15 min. The glass substrates were rinsed with deionized water and each substrate dried under a nitrogen stream. Oxygen plasma treatment were applied on pre-cleaned glass substrates to provide the activation of the -OH group on the surface with plasma cleaner equipment (PDC-002-HPCE Harrick Plasma, Ithaca, NY, USA) for 2 min at 450 mTorr and high power level. The glass substrates were then immersed into a freshly prepared 2% (v/v) APTES solution in water for 24 h. After removing from the solution, the samples were rinsed with diyonized water and dried in an oven at 100 °C for 1h.

Cell culture

The human colon cancer cell lines HCT-116 were cultured in McCoy's medium, MDA-MB-231 breast cancer cell lines were grown and maintained in DMEM. TGF-ß (Transforming growth factor beta) was applied to HCT-116 and MDA-MB-231. The both cell lines were kept at 37 °C in a humidified incubator containing 5% CO2.

Contact angle measurement

Water contact angles were measured on the pure glass surface, O2 plasma-treated glass surface, 2% APTES-coated glass surface using the sessile-drop method to analyze the change in the surface energy of the glass substrate. The static water contact angle was measured at room temperature using KSV cam 200 contact angle meter . A 5 uml droplet was deposited on the surface and the image was recorded 3 s after the drop. Contact angles for each surface were repeated three times and the average values were reported.

Digital holographic microscopy

Holographic images were acquired using a custom inline phase shifting Mach-Zehnder interferometer equipped with a 437 nm, 5mW, HeNe laser source. Exposure time was 250um and magnification rate was 10x. Phase_shifting is achieved through the use of a high frequency piezo actuator, driven in 500 steps per second. We developed an algorithm for real_time holographic reconstruction using a continuously shifting piezo actuator and a high speed CCD camera. 3D reconstruction is achieved by taking multiple images while shifting the reference phase and solving the set of linear equations that arise by combining the complex wavefield equations of each image.

RESULTS

Normally, CTCs are not morphologically suitable for immobilization on glass surfaces. APTES solution was used to immobilize the CTCs to the glass surface. The amine functional group of APTES possible the covalently bond of CTCs on surfaces. In the current work, self-assembly monolayer of APTES was obtained with a concentration of 2% (v/v) APTES-ethanol and silanization time of 24 h. The amine group of the APTES enables the unification of the CTCs to glass substrates and the Si-O functional group of the other end of the APTES reacts with the glass surface. When APTES silane molecules are completely adsorbed on the –OH activated on the glass substrate by oxygen plasma treatment, silanization can be achieved a full coating on the glass substrate.

Contact angle measurement was used for the physical characterization of the APTES modified surfaces. The contact angle of water was measured on three different areas of the glass substrate for each step of the modification. The measured water contact angles are shown in Figure 1. Oxygen plasma treatment activates by forming -OH functional groups on glass surfaces and the activated surfaces become highly hydrophilic. After the silanization process, self-assemble monolayer with charged amine groups made the surface more hydrophobic than the references substrate and contact angle of modified glass surfaces was found 66.4°. Contact angle values obtained as a result of operations on glass surfaces can be accepted as an indicator of changes in surface properties on glass surfaces.

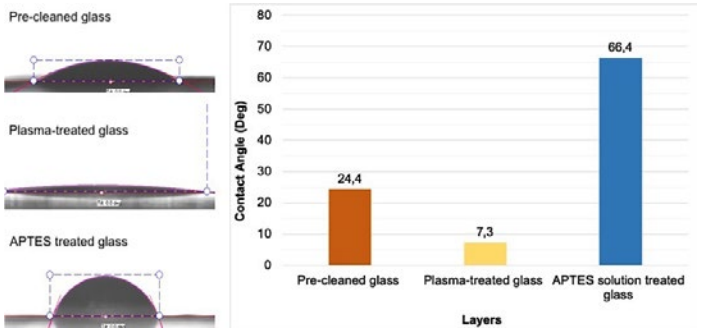

Figure 1 : Water contact angles showing wetting behavior of each step. Contact angles values for pre-cleaned glass, plasma-treated glass and 2 wt% APTES solution treated glass are 24.4°, 7.3°, and 66.4°, respectively.

Before and after immobilization, the CTCs on the surface were visualized by the digital hologram system. DHM images of the cells on the APTES modified glass

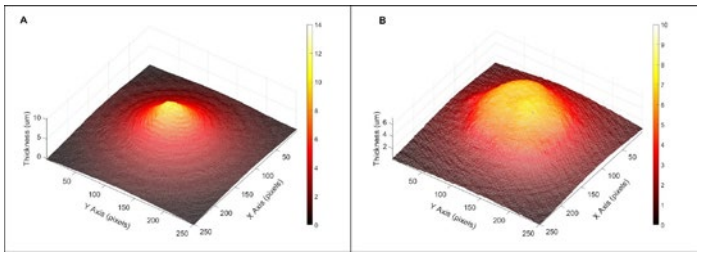

Figure 2: Holographic images of CTCs on the modified glass surfaces, (A) non-immobilized CTC at an initial time and (b) immobilization of CTC after 24 hours

CONCLUSIONS

In this study, we successfully immobilized CTCs that non-adhesive on the substrate on APTES surface-modified glass surfaces. We observed that the immobilized cells were spread over a larger area and lower than non-adhesive cells by the DHM system. The present silane formation method using (3-aminopropyl) triethoxysilane (APTES) on glass substrates is modified to produce a stable and thin silane layer for the immobilization of CTC. The glass samples were characterized of surface modification after every step by contact angle measurement system. The values of contact angles for pre-cleaned glass, plasma-treated glass and 2 wt% APTES solution treated glass are 24.4°, 7.3°, and 66.4°, respectively. İmmobilized CTCs can be used to study of cancer and metastasis analyses wtih the DHM.

Acknowledgements

This work is supported by The Scientific and Technological Research Council of Turkey (TUBITAK) with 116E743 project.

REFERENCES

1. Dixit C., Vashist S., MacCraith B., O'Kennedy R., Multisubstrate-compatible ELISA procedures for rapid and high-sensitivity immunoassays, Nat. Protoc. 6, 2011, 439–445.
2. Gunda, Kumar N. S., Singh M., Norman L., Kaur K., Mitra S. K., Optimization and characterization of biomolecule immobilization on silicon substrates using (3-aminopropyl) triethoxysilane (APTES) and glutaraldehyde linker, *Applied Surface Science*, 2014, *305*, 522-530.
3. Xiang S., Xing G., Xue W., Lu C., Lin J. M., Comparison of two different deposition methods of 3-aminopropyltriethoxysilane on glass slides and their application in the ThinPrep cytologic test. *Analyst*, 2012, *137*(7), 1669-1673.
4. Singh, D. K., Ahrens, C. C., Li, W., Vanapalli, S. A., Label-free, high-throughput holographic screening and enumeration of tumor cells in blood. Lab on a Chip, 2017, 17(17), 2920-2932.

OP-18

PROLIFERATIVE ACTIVITY OF HUMAN GLIOMA CELL LINES: EFFECTS OF VOLTAGE-GATED SODIUM CHANNEL BLOCKERS

Sıla Ulutürk[1,2*], Josephine von Kempis[1], Scott P. Fraser[1] and Mustafa B.A. Djamgoz[1,3]

[1]Imperial College London, Department of Life Sciences, London SW7 2AZ, U.K. [2]The LIMES Institute, Bonn University, 53115 Bonn, Germany; [3]Biotechnology Research Centre, Cyprus International University, Haspolat, Nicosia, TRNC.

*Corresponding author.

INTRODUCTION

Gliomas are the deadliest of all cancers and there is great unmet need in their clinical management [1]. Voltage-gated ion channels (VGICs) are well known to be important for membrane potential generation, ionic homeostasis and electrical signalling. Recently, VGICs have been shown to control cellular proliferation, migration, apoptosis, differentiation, invasion, secretion, gene expression and adhesion in cancer cells [e.g. 2-4]. In particular, strongly metastatic cells have been shown to express functional voltage-gated sodium channels (VGSCs) which promote invasive behaviour *in vitro* and metastasis *in vivo* [3,5-7]. These effects of the VGSCs occur, at least partially, via Na^+/H^+ exchanger activation [8]. VGSCs generate two kinetically distinct inward Na^+ currents: transient (I_{NaT}) and persistent (I_{NaP}). The latter increases under hypoxic conditions which occur commonly in growing tumours [9]. Hence, I_{NaP} blockers, such as ranolazine, have been suggested to be potential anti-metastatic drugs [9]. Indeed, ranolazine has been shown to suppress *in vitro* invasiveness of human breast cancer cells [10], colon cancer cells [11] and breast cancer metastasis *in vivo* [5].

Previous work showed that VGSC mRNA expression overall in gliomas correlated positively with malignancy grade except in high-grade gliomas where it was reduced [12]. The main aim of the current study was to determine the potential effects of ranolazine and the more recently developed analogue, eleclazine, on glioma cell proliferation under normoxic and hypoxic conditions.

MATERIALS AND METHODS

The human glioma cell lines U87, LN229 and LN18 were cultured by standard methods in RPMI medium. Hypoxia was induced by exposing the cells to 1% O_2 for 48 hours. Eleclazine (15 μM) was prepared in the culture medium with a maximum of 0.15% DMSO as a supplementary solvent. Ranolazine (10 μM) and TTX (1 μM) were dissolved directly in medium. Cell viability was determined by trypan blue dye exclusion assay. Cell proliferation was quantified colorimetrically by MTT assay. This confirmed (i) the linearity of the relationship between cell number and absorbance (Figure 1a); (ii) that hypoxia did not affect the calibration (Figure 1b); and (iii) that the relationship did not change during the course of the treatments (Figure 1c). Quantitative data were analysed with GraphPad Prism. Shapiro Wilk W test was used for normality test. Parametric data were presented via charts and any differences were tested by Student's t test for significance. Non-parametric data was tested with Mann-Whitney Rank Sum test. Statistical significance was defined as p-value <0.05 (*) and p<0.01 (**).

RESULTS AND DISCUSSION

Experiments were initiated on human glioblastoma U87, LN229 and LN18 cell lines. Most data were obtained from U87 cells adopted as a model.

VGSC protein expression in glioma cell lines

All three cell lines expressed VGSC protein (Figure 2a-c). Negative controls (omission of the primary antibody) confirmed the authenticity of the staining. There was some heterogeneity in the expression and only some 80 % of U87 cells stained and expression in plasma membrane was apparent. Treatments with eleclazine and ranolazine for 48-hour had no effect on the VGSC expression (Figure 2d). Trypan blue exclusion assays showed that the various treatments (ranolazine, eleclazine and TTX) were not toxic to the cells (data not shown).

Gliomas are known to express VGSCs *in vitro* and *in vivo* and this has been confirmed here for three different cell lines [13]. The VGSC expression seemed very stable since it did not change after treatment of the cells with the various blockers. As regards the subtype(s) of VGSC expressed, evidence points to Nav1.1-Nav1.3, Nav.1.5-Nav1.7 [14].

Effect of hypoxia

Exposing the U87 cells to 1% O_2 for 48 hours decreased the cells' proliferative activity by about 10% (Figure 3a). There was no effect on cell viability (data not shown). It is well known that growing tumours develop internal hypoxia [15]. The effect of hypoxia on tumour cell proliferation has been studied. In gliomas, hypoxia inducible factor-1, which is the main mediator of the hypoxia response, regulates many genes including some that induce proliferation [16]. As regards carcinomas, hypoxia (1% O_2) was shown to inhibit colon cancer cell proliferation time dependently, reaching 48% over 72 hours [11].

Effects of VGSC blockers on proliferation

Ranolazine had no effect on proliferation under normoxia and hypoxia (data not shown). In contrast, treatment with eleclazine caused significant reduction in proliferation by 19 % under normoxia and 9 % under hypoxia (Figure 3b&c). The highly specific VGSC blocker, TTX had no effect on proliferative activity under both normoxia and hypoxia (data not shown). It was concluded, therefore, that the inhibitory effect of eleclazine was not mediated by VGSC activity (at least in full). Under normoxic conditions, VGSC activity has been found consistently to promote the *in vitro* invasiveness of a variety of carcinoma cell lines without changing their proliferative activity, i.e. proliferation and invasion can be controlled independently. *In vivo*, however, silencing VGSC expression in a breast cancer xenograft has been shown also to produce an anti-proliferative effect [6]. In the current study, also, since TTX did not affect proliferation, we can conclude that VGSC activity is not involved in the primary growth of gliomas. On the other hand, silencing VGSC (Nav1.5) expression in the astrocytoma U251 cell line decreased proliferation [17].

Of the two pharmacological agents used, ranolazine (even at 10 μM) did not affect proliferation, consistent with its main mode of action being inhibition of I_{NaP} [18]. In colorectal cells, also, ranolazine did not affect proliferation [11]. In contrast, eleclazine significantly decreased cellular proliferation. The mechanism(s) of this effect is not clear at present but it is likely to be more than I_{NaP} inhibition since the effect was smaller in hypoxia. One possibility is that eleclazine, like ranolazine, depending on concentration (also) inhibited a K^+ channel [18]. K^+ channels are well known to promote cellular proliferation [19].

CONCLUSION

At the concentrations used, ranolazine (10 μM) and eleclazine (15 μM) differ in their effects on glioma cell proliferation and may also differ from carcinomas. Further work is required to determine (i) the precise modes of action of eleclazine, at a range of concentrations, on tumour, including glioma, cells; and (ii) the effects of eleclazine on metastatic cell behaviours.

REFERENCES

1. Esparragosa I, Diez-Valle R, Tejada S, Gallego Perez-Larraya J. Management of diffuse glioma. Presse Med 2018; 47(11-12 Pt 2): e199-e212.
2. Brackenbury WJ. Voltage-gated sodium channels and metastatic disease. Channels (Austin) 2012; 6(5):352-361.
3. Fraser SP, Diss JKJ, Chioni AM, Mycielska ME, Pan H, Yamaci RF, et al. Voltage-gated sodium channel expression and potentiation of human breast cancer metastasis. Clin Cancer Res 2005; 11 (15):5381-89.
4. Djamgoz MBA. Biophysics of cancer: cellular excitability ('CELEX') hypothesis of metastasis. J Clin Exp Oncol 2014. doi:10.4172/2324-9110. S1-005.
5. Driffort V, Gillet L, Bon E, Marionneau-Lambot S, Oullier T, Joulin V, et al. Ranolazine inhibits NaV1.5-mediated breast cancer cell invasiveness and lung colonization. Mol Cancer 2014; 13:264.
6. Nelson M, Yang M, Dowle AA, Thomas JR, Brackenbury WJ. The sodium channel-blocking antiepileptic drug phenytoin inhibits breast tumour growth and metastasis. Mol Cancer 2015; 14:13.
7. Mao W, Zhang J, Körner H, Yong J, Ying S. The emerging role of voltage-gated sodium channels in tumor biology. Front Oncol 2019; 9: 124.
8. Brisson L, Gillet L, Calaghan S, Besson P, Le Guennec JY, et al. Na(V)1.5 enhances breast cancer cell invasiveness by increasing NHE1-dependent H (+) efflux in caveolae. Oncogene. 2011; 30(17):2070-6. doi: 10.1038/onc.2010.574.
9. Djamgoz MBA, Onkal R. Persistent current blockers of voltage-gated sodium channels: clinical opportunity for controlling metastatic disease. Recent Pat Anticancer Drug Discov 2013; 8(1):66-84.
10. Lee A, Fraser SP, Djamgoz MBA. Propranolol inhibits neonatal Nav1.5 activty and invasiveness of MDA-MB-231 breast cancer cells: Effects of combination with ranolazine. J Cell Physiol 2019; 234(12):23066-23081.
11. Guzel RM, Ogmen K, Ilieva KM, Fraser SP, Djamgoz MBA. Colorectal cancer invasiveness in vitro: Predominant contribution of neonatal Nav1.5 under normoxia and hypoxia. J Cell Physiol 2019: 234:6582-93.
12. Schrey M, Codina C, Kraft R, Beetz C, Kalff R, Wölfl S, Patt S. Molecular characterization of voltage-gated sodium channels in human gliomas. Neuroreport 2002;13(18):2493-8. DOI: 10.1097/01.
13. Pollak J, Rai KG, Funk CC, Arora S, Lee E, Zhu J, et al. Ion channel expression patterns in glioblastoma stem cells with functional and therapeutic implications for malignancy. PLoS One 2017; 12(3): e0172884.
14. Wang J, Ou SW, Wang YJ. Distribution and function of voltage-gated sodium channels in the nervous system. Channels (Austin) 2017; 11, 534-554.

15. Muz B, de la Puente P, Azab F, Azab AK. The role of hypoxia in cancer progression, angiogenesis, metastasis, and resistance to therapy. Hypoxia (Auckl) 2015; 3:83-92.
16. Monteiro AR, Hill R, Pilkington GJ, Madureira PA. The role of hypoxia in glioblastoma invasion. Cells 2017; 6(4). pii: E45.
17. Xing D, Wang J, Ou S, Wang Y, Qiu B, Ding D, Guo F, Gao Q. Expression of neonatal Nav1.5 in human brain astrocytoma and its effect on proliferation, invasion and apoptosis of astrocytoma cells. Oncol Rep. 2014;31:2692-700.
18. Antzelevitch C, Belardinelli L, Zygmunt AC, Burashnikov A, Di Diego JM, Fish JM, et al. Electrophysiological effects of ranolazine, a novel antianginal agent with antiarrhythmic properties. Circulation 2004; 110(8):904–10.
19. Serrano-Novillo C, Capera J, Colomer-Molera M, Condom E, Ferreres JC, Felipe A. Implication of voltage-gated potassium channels in neoplastic cell proliferation. Cancers (Basel) 2019; 11(3): 287.

Fig.1

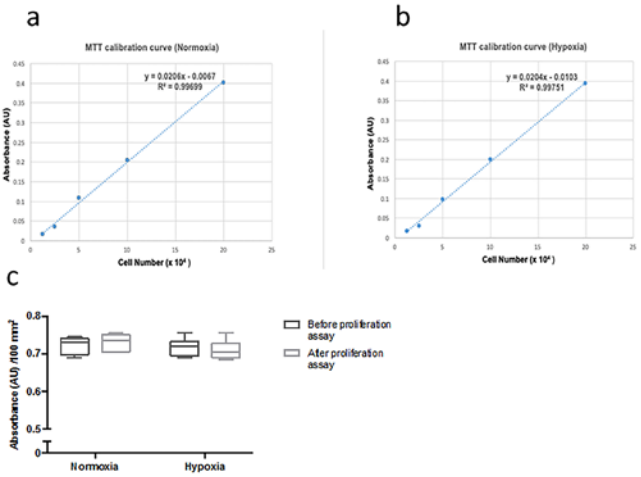

Figure 1. Calibrations of the colorimetric MTT assay under different experimental conditions. Standard curves for the U87 cell line showing that absorbance at 570 nm (arbitrary units: AU) increased linearly with cell number. (a) normoxic cells; (b) and hypoxic cells. (c) Data showing that the calibration did not change during given experiments under normoxia and hypoxia. For (c), $2x10^4$ cells were seeded. There was no significant change (n=3).

Fig.2

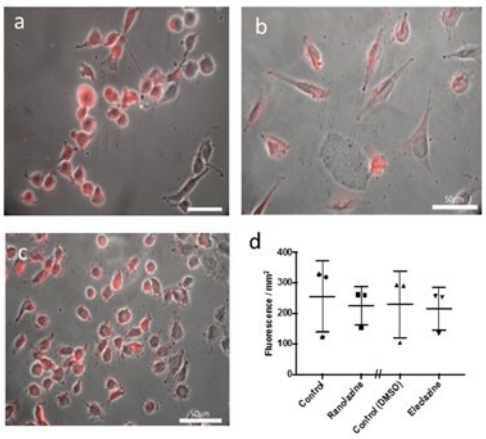

Figure 2. VGSC expression in human glioma cell lines. Expression was determined by immunocytochemistry using a polyclonal pan-VGSC antibody as the primary. The secondary Ab was goat anti-rabit IgG Alexa Fluor® 568. The following cell lines were studied: U87 (a), LN229 (b) and LN18 (c). (d) Data showing pharmacological treatment (10 μM ranolazine and 15 μM eleclazine) did not affect the VGSC immunofluorescence of U87 cells under normoxia (n=3).

Fig.3

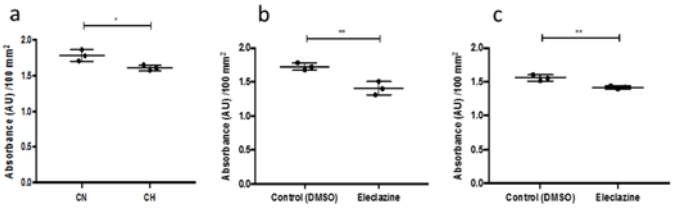

Figure 3. Effects of treatments on U87 cell proliferation. (a) Effect of hypoxia (1% O_2, 48 hours); CN, control normoxia, CH, control hypoxia. (b) and (c), effects of treatments with eleclazine (15 μM) for 48 hours under normoxia (b) and hypoxia (c). Data (non-parametric) are shown as median values and interquartile ranges (n=3). (*) $p<0.05$. (**) $p\leq 0.01$.

OP-19

OPTIMIZATION OF PATIENT-DERIVED COLORECTAL CANCER ORGANOIDS PROTOCOLS FOR PERSONALIZED DRUG SCREENINGS

Tolga Sever[1*], Ezgi Daskin[1], H. Koray Misirlioglu[1], Gizem Calibasi-Kocal[2], Sulen Sarioglu[3], Aras Emre Canda[4], Yesim Tuncok[5], Ilhan Oztop[6], Ender Ellidokuz[7], Omer H. Yilmaz[8], Yasemin Basbinar[1]

[1]Dokuz Eylül University, Institute of Health Sciences, Department of Translational Oncology, İzmir, Turkey

[2]Dokuz Eylül University, Institute of Oncology, Department of Translational Oncology, İzmir, Turkey

[3]Dokuz Eylül University, Faculty of Medicine, Department of Surgical Medical Sciences, Department of Medical Pathology, İzmir, Turkey

[4]Dokuz Eylül University, Faculty of Medicine, Department of Surgical Medicine, Department of General Surgery, İzmir, Turkey

[5]Dokuz Eylül University, Faculty of Medicine, Department of Internal Medicine, Medical Pharmacology, Department of Clinical Toxicology / Clinical Pharmacology, İzmir, Turkey

[6]Dokuz Eylül University, Institute of Oncology Department of Clinical Oncology, İzmir, Turkey

[7]Dokuz Eylül University, Faculty of Medicine, Department of Internal Medicine, Department of Gastroenterology, İzmir, Turkey

[8]The Koch Institute for Integrative Cancer Research at MIT, Associate Professor of Biology.

OBJECTIVES: Recently, the development of technologies to culture intestinal epithelial cells in vitro as different forms of intestinal organoids causes drawing attention in this area. The isolation and culture of colorectal crypts were first demonstrated in the very recent decade with the identification of stem cell marker Lgr5. The growth of crypts into organoids provides an in vitro model for studying the mucosal physiology, colorectal cancer tumorigenesis, and regeneration. In the current study, cancer stem cell isolation, tissue decontamination, organoid freezing and thawing processes, and organoid culture media ingredients have been evaluated. The aim of this investigation is optimization and production of human colorectal cancer organoids.

MATERIAL&METHODS: The colorectal cancerous tissues are collected from Dokuz Eylul University Hospital. Isolation method of cancer cell is performed by EDTA solution and agitation is provided by shaker. Matrigel is used to create optimal 3D structure to grow cancer stem cells up to colorectal tissue. L-WRN cell line has been used to produce secreted factors which are WNT-3A, Rspondin and Noggin in purpose of supporting the development of organoids.

RESULTS: Different parameters have been evaluated to obtain more efficient organoids. The experiment is performed in our laboratory presented that, human colorectal cancer organoids have been generated and manipulated in our laboratory.

CONCLUSIONS: The currency protocol explains how the generation of 3D organoid cultures from cancerous human colorectal tissue is manipulated. The in vitro 3D organoid model is a promising and novel approach which present us more real-like working material.

Keywords: organoid,colorectal cancer

INTRODUCTION

Scientists have been looking for developmental and functional processes of tissues and organs. However, these processes are very complex those cause difficulties to develop a reliable in vitro model system for investigations. [1] Developing 3D cell culture technologies contribute to generating more real-like cell culture models of human diseased and normal tissue tools. Tissue derived adult stem cells could generate self-organizing organ-like structures which are called organoid within a 3D matrix. 3D organoids could be generated by a single leucine-rich repeat-containing G protein-coupled receptor 5 (LGR5)+ stem cell. [2] Stem cells are cultured in appropriate conditions which present the in vivo stem cell niche. [3] Organoids could be maintained long term, could be genetically modified and cryopreserved, and remain genetically and phenotypically stable. This feature let for a high scale of applications in research of cancer.

Organoid cells have connections between cell-matrix and cell-cell interactions, those are the missing issue in traditional 2D models. These linkages are necessary to create in vivo situations. While cell-matrix and cell-cell interactions are lacked, cells possibly lose their distinctive phenotype. Thus, they could show a different response to external stimuli [4–5]. So that organoid technology presents heterogeneous tissue-specific cell organization which is very similar to the real-life structure and functional work material. Up to date, there are vigorous studies have been performed in this area and generation of intestinal, cerebral, inner ear, liver, pituitary gland, gastric, retina, kidney, lung, breast, heart organoids have been generated by the usage of stem cells.[1] Although it is small in size, organoids are a novel and promising technology for regenerative and developmental researches due to their advantages in stability, manipulation and long-term cultivation.[6-7-8] Organoids are more attractive than animal models since they are more recapitulate native human tissue.[9, 10] Moreover, the ethical issue for animal models is making difficulties for researches. So, the organoid technology is more suitable and reliable models for individualized medicine studies as well.

In this study, we have performed the development of colorectal cancer organoid generation and maintenance protocols for further studies such as personalized medicine.

MATERIALS AND METHODS

Production of WRN Factors

L-WRN (CRL-3276) cell lines were obtained from American Type Culture Collection (ATCC). Cells were split 1:10 in culture media (10% FBS in high glucose DMEM) and seeded 13 mL cell suspension into T-75 flasks. Flasks were incubated for 3 or 4 days or until the cells become over-confluent and a number of cell aggregates come off. Media was removed and flasks were rinsed with 10 mL media and rinse were discarded. 13 ml of fresh media was added to flasks and cells were incubated for 24 hours. After 24 hours of incubation, L-WRN conditioned media was containing signaling factors Wnt3a, R-spondin-3, and Noggin (WRN). Media was removed to a centrifuge tube. Fresh media was added to flasks. Conditioned medium was centrifuged at 2000 x g for 5 minutes and the supernatant was removed from the pellet. Conditioned medium was stored at 4°C. This was the first batch of media. 2nd, 3rd and 4th batches of WRN media were collected in every 24 hours. All batches were added to the same bottle after centrifugation. After the 4th batch, an equal volume of Advanced DMEM was added to the bottle (different final concentrations), well mixed and media was aliquoted into 50 mL centrifuge tubes and stored at -20°C.

Human Tissue Materials

Surgically resected colon tissues or colonoscopic biopsy samples were obtained from 8 patients from the Dokuz Eylül University Hospital, Gastroenterology Department. 5 of 8 of colorectal cancer material were obtained via surgery and the rest of them were obtained via colonoscopic biopsy. Tissue samples were collected from three different parts of cancer tissue which are outer, middle and inner parts. Tissue materials were transported in transfer media at +4 °C degree.

Stem Cell Isolation

Tissues were washed three times with DPBS. They were gently washed with an antibiotic solution for one hour. Then, the tissues were washed three times with DPBS. Tissues were centrifuged at 40g for 10 minutes and the supernatant was removed. 5mM EDTA in DPBS was added to the pellet and washed for 60 minutes in +4°C. EDTA was removed via washing with DPBS. Then, 10 ml of DPBS added on tissues and vigorously washed. Isolated cancer stem cells were centrifuged at 300g for 2 minutes. The supernatant is removed from the pellet which has isolated cancer stem cells.

Organoid Culturing

Isolated stem cell pellets were resuspended with human organoid growth media and counted on hematocytometer. The suitable ratio of Matrigel was added and the suspension was seeded to 48-well plate. The suspension was incubated for 5 minutes at room temperature and 15 min at 37 °C. Finally, 300µL of Human Organoid Growth Media was added to each well and placed in an incubator.

RESULTS

Development of Human Colorectal Cancer Culture System

In the current experiment, cancer stem cells are isolated from colorectal cancerous tissue and embedded within Matrigel and per well includes approximately 500 cancer stem cells. After organoid culture medium has been added into each well, the plate is incubated in suitable conditions. Imaging of organoid is performed under Fluorescent microscopy day by day. As it is illustrated in figure 1, the development of human colorectal cancer organoids is observed.

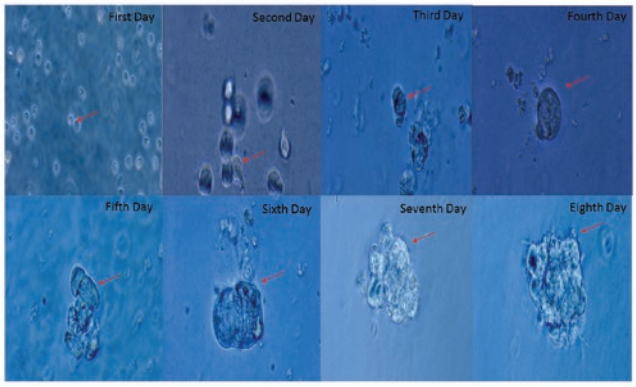

Figure 1. The image is prepared for illustration of human colorectal cancer organoid cultures development in the time course. They are taken by the fluorescent microscope.

DISCUSSION

In this study, some parameters were changed for the effective production of human colorectal cancer organoid, and consequently, the changes were evaluated. First, tissue size is an important parameter. As the size of the tissue increases, the number of isolated stem cells increases. Stem cell density should be high for the formation of human colorectal cancer organoid. Thus, as the tissue grows, the yield of the organoid formation increases. [3]

Second, the depth of the layer from which the tissue is removed is an important parameter. Very few stem cells were isolated from the outermost tissue and no organoid growth was observed. Organoid development was observed in the middle and innermost layers. The organoid formed from the tissue from the innermost layer is more effective than the organoid formed from the tissue from the middle layer.

The time in the EDTA isolation step is another important parameter. It was observed that when stem cell isolation was made from long-term EDTA tissue, the cells died, and when short-term, stem cells were not isolated. The isolation step time is optimized to 60 min.

WRN media percentage is a crucial parameter for optimizing organoid growth media. 50% is the best percentage for the generation of organoids.

The parameters have been evaluated and the most efficient protocol is determined for forming human colorectal cancer organoid for personalized medicine studies for further.

ACKNOWLEDGMENT

The investigation is supported by Dokuz Eylül University, Scientific Research Projects Coordination Unit with 2018.KB.SAG.039 project number.

CONFLICT OF INTEREST

The authors declare no conflict of interests.

REFERENCES

1. Ninouk Akkerman and Libert H.K. Defize. 3D tissue and organ cultures revolutionize the study of development, disease, and regeneration. Doi: 10.1002/bies.201600244 (2017).
2. Sato T1, Vries RG, Snippert HJ, van de Wetering M, Barker N, Stange DE, van Es JH, Abo A, Kujala P, Peters PJ, Clevers H. Single Lgr5 stem cells build crypt-villus structures in vitro without a mesenchymal niche. 10.1038/nature07935. Epub 2009 Mar 29.
3. Toshiro Sato,, Daniel E., Stange Marc, Ferrante Robert G.J.Vries Johan H.van Es Stienekevan den Brink Winan J.van Houdt ApolloPronk// Joostvan Gorp Peter D.Siersema HansClevers 2011. Long-term expansion of epithelial organoids from human colon, adenoma, adenocarcinoma, and Barrett's epithelium.Gastroenterology 141, 1762–1772 .
4. Weaver VM, Petersen OW, Wang F, Larabell CA, et al. 1997. Reversion of the malignant phenotype of human breast cells in three-dimensional cutlure

and in vivo by integrin blocking antibodies. J Cell Biol 137: 231–45.
5. Shannon JM, Mason RJ, Jennings SD.1987.Functional differentiation of alveolar type II epithelial cells in vitro: effects of cell shape, cell-matrix interactionsandcell-cellinteractions.BiochimBiophysActa931:143–56.
6. Turner DA,Glodowski CR,Alonso-Crisostomo L, Baillie-Johnson P, et al. 2016. Interactions between nodal and wnt signalling drive robust symmetry breaking and axial organisation in gastruloids (Embryonic organoids). bioRxiv, 1–31. doi: 10.1101/051722
7. Turner DA, Glodowski CR, Alonso-Crisostomo L, Baillie-Johnson P, et al. 2016. Interactions between nodal and wnt signalling drive robust symmetry breaking and axial organisation in gastruloids (Embryonic organoids). bioRxiv, 1–31. doi: 10.1101/051722
8. Yin X, Mead BE, Safaee H, Langer R, et al. 2016. Engineering stem cell organoids. Cell Stem Cell 18: 25–38.
9. Lancaster MA, Renner M, Martin C-A, Wenzel D, et al. 2013. Cerebral organoids model human brain development and microcephaly. Nature 501: 373–91.
10. Willyard C. 2015. Rise of the organoids. Nature 523: 520–2.

OP-20

EVALUATING THE EFFECT OF KC7F2, THE HIF-1A INHIBITOR, ON GLUCOSE METABOLISM IN U87MG GLIOMA CELL LINE

[1]Zaka Abbaszade, [1]N Pınar Özateş, [1]Vahidreza Karamad, [1]Bakiye Göker Bağca, [1]Cansu Çalışkan Kurt, [1]Ali Haydar Kayğusuz, [1]Fatma Söğütlü, [1]Selin Çeşmeli, [1]Alican Kuşoğlu, [1]Cumhur Gündüz, [1]Çığır Biray Avcı
[1]Ege University Faculty of Medicine, Medical Biology Department, İzmir, Turkey

Glioblastom Multiforme (GBM) is the most invasive and malignant member of the IV grade of the subclass Astrocytoma according to the last assessment of the 2016 WHO report. Due to the resistance to treatment and weak response, as well as the topographical structure of the blood brain barrier, which is a major part of malignant brain tumors, treatment is also difficult due to the severe clinical manifestation, and new treatment methods and new therapeutic agents are needed. Conventional treatment methods are surgical resection, radiotherapy and chemotherapy. Median survival time is 12.5 months in patients. Glucose metabolism is a complex energy producing machine that generates energy and stores it as ATP and provides energy for all cellular processes. A glucose molecule produces 38 molecules of ATP after full glycolytic catabolism. According to Otto Warburg's numerous studies and basic hypothesis, cancer metabolism is completely different from normal cells. Cancer cells tend to the anaerobic phenotype only by performing the first glycolytic step without entering the mitochondrial step. As a result, these cells produce lactic acid and make the secretions and micro-media even more acidic in aerobic conditions. This phenomenon is attributed to the Warburg hypothesis and either as anaerobic glucolysis. Although glycolysis enzymes are the primary actors of this phenotypic expression, some genetic and epigenetic factors are no exception. For this reason, we experimentally used KC7F2 active ingredient to target cancer metabolism. As a result of our experience, we observed that the effect of the KC7F2 suppresses aerobic glycolysis and has significant effects on several metabolism genes.

INTRODUCTION

Glioblastoma multiforme [GBM; WHO astrocytoma grade IV] is the most common malignant primary brain tumor in adults. It grows rapidly and a high degree of invasiveness and angiogenesis is observed. Glioblastoma multiforme cells are polygonal with acidophilic cytoplasm and indeterminate cellular boundaries. [Schultz et al. 2005]. Glioblastoma multiforme is characterized by high proliferative activity [Schröder et al. 1991]. When GBM leaks into the surrounding tissue, complete resection is impossible and in this case radiotherapy is not always efficient [Karcher et al. 2006]sGBM. The blood-brain barrier makes treatment more difficult and tumor cells in hypoxic regions are resistant to radiotherapy [J. E. Chang et al. 2007]. Cancer metabolism refers to changes in pathways of cellular metabolism that are specific to cancer cells compared to most normal tissue cells. Metabolic changes in cancer cells are multifaceted [Warburg, Wind, and Negelein 1927] and aerobic glycolysis, as a result of reduced oxidative phosphorylation, increases the formation of biosynthetic intermediates, providing the basis for cell growth and proliferation [Warburg 1925]. [KORNBERG, LIEBERMAN, and SIMMS 1955] Hypoxia-inducible Factor [HIF] is particularly important in the realization of this process. Tumor HIF-1α is an indicator of aggressive disease and poor patient prognosis in cancer patients. Seahorse XFp technology is capable of measuring two main energy production pathways, mitochondrial respiration and glycolysis simultaneously. This method is used in studies on cellular functions, cell activation, proliferation, differentiation and etiology of disease. In this study, we aimed to investigate the metabolic effects of KC7F2, a HIF-1α inhibitor, on the U87MG glioblastoma cell line and especially on the glycolytic pathway.

MATERIALS AND METHODS

Gene Expression Analysis

Changes in gene expression levels of IC_{50} dose of KC7F2 active agent were evaluated by comparing with control cells. For this purpose, IC_{50} dose of KC7F2, 19 µM, active agent was applied to the cells. Cells without active agent as control group were also treated under the same conditions. After 48 hours, RNA was isolated from cells using RNeasy Plus Mini Kit. Complementary DNA synthesis was performed using the RT2 First Strand Kit [Qiagen]. In order to correlate these metabolic effects with changes in molecular level on glycolysis metabolism, changes in gene expression levels were determined with Light-Cycler 480 Instrument II [Roche].

Seahorse Xf Metabolic Analysis

Metabolic analysis was performed through Seahorse XFp analyzer to evaluate the effect of KC7F2 on glycolytic metabolism. In this study, Seahorse XFp Cell Energy Phenotype Test Kit [Seahorse XFp Energy Phenotype Test Kit] was used to determine the effects of IC_{50} dose of KC7F2 active agent on the U87MG cell line at 72 hours. The test measures the three basic parameters of cell energy metabolism [Basic Phenotype, Stressed Phenotype and Metabolic Potential] and determines the metabolic behavior of the cell by determining the mitochondrial respiration and glycolysis rate under basal and stressful conditions. Seahorse XFp technology is capable of simultaneously measuring mitochondrial respiration and glycolysis, the two main ways of generating energy in cells. Glycolytic metabolism rate is determined by the accumulation of lactic acid, the end product of glycolytic respiration in the cell, and the formation of acidic microenvironment in the cell, and the reduction of PH value in the cell around the lactic acid by decreasing the pH value and calculating the correlation of this pH value with glycolysis rate. The rate of mitochondrial metabolism is based on the real-time reflectance of the amount of O_2 present in the microenvironment by measuring the rate of uptake. To determine its effects on both metabolism and expression, the IC_{50} of KC7F2, which we found in our previous study, was applied to U87MG cells. Non-treated cells were used as control group.

RESULTS

Investigation of The Effect of KC7F2 Agent on Gene Expression

Phosphoribosylpyrophosphate synthetase 1 [PRPS1] is an enzyme that catalyzes the first step in nucleotide biosynthesis to synthesize phosphoribosylpyrophosphate [PRPP] from adenosine triphosphate [ATP] and ribose-5-phophate [R5P] [KORNBERG, LIEBERMAN, and SIMMS 1955]. There are three isoforms encoded by the PRS1, PRPS2 and PRPS1L1 genes including PRS-I, PRS-II and PRS-1L1. A study conducted by Li C. et al. demonstrated that suppression of PRPS1 in glioma stem cells reduced the tumor formation capacity [Li et al. 2016]. In our study, we found that KC7F2 suppressed the expression of PRS1L1 by two fold compared to control group, suggesting the agent plays a role in tumor suppression.

PYGL is one of three isoforms of glycogen phosphorylase [GP]. The activity of these enzymes can be modulated by post-translational modification and allosteric effectors [ATP, AMP and G6P] [Lawrence and Roach 1997]. A study in more than 2000 cases has shown that PYGL is upregulated in various types of cancer, including clear cell renal carcinoma, papillary renal cell carcinoma, seminoma, and brain cancer, compared to normal tissues. Studies indicated that PYGL has important functions for glioma cells survival since the enzyme is pivotal for pentose phosphate pathway, in addition, the depletion of PYGL reduced tumor formation in vivo [Winter et al. 2007]. In our study, we showed that PYGL gene expression level reduced two folds in KC7F2 treated cells compared to control group.

Aldolases are a class of essential enzymes that play an important role in glucose processing. There are 3 members of the aldolase family: ALDOA is found in muscle cells, ALDOB, predominantly in the liver and aldolase C [ALDOC] in the brain which is responsible for repair of damaged tissue. In our study, it was observed that ALDOC gene expression level decreased significantly in KC7F2 treated cells compared to controls. A recent study revealed that high expression of ALDOC correlates with favorable prognosis in GBM patients [Y.-C. Chang et al. 2019].

Table 1. Gene expression analysis of U87MG cell lines after KC7F2 treatment

Genes	Fold Change [log 2]	P value
ALDOC	-23.6538	1E-06
PYGL	-2.1199	8.4E-05
PRPS1L1	-2.0335	0.00414

Seahorse XFp Metabolic Analysis

KC7F2 application has been observed to change the metabolism profile from glycolytic respiration to mitochondrial respiration in U87MG cells. Considering the central role of HIF-1α in cancer glycolysis, the fact that the HIF-1α inhibitor we use causes such a change in metabolism profile supports our prediction. Extracellular acidification rate of the cells treated with KC7F2 decreased around 4 fold comparing control group. In stress conditions, that difference increased to 5 fold. Oxygen consumption rates of the cells treated with KC7F2 increased 350 fold comparing control group.

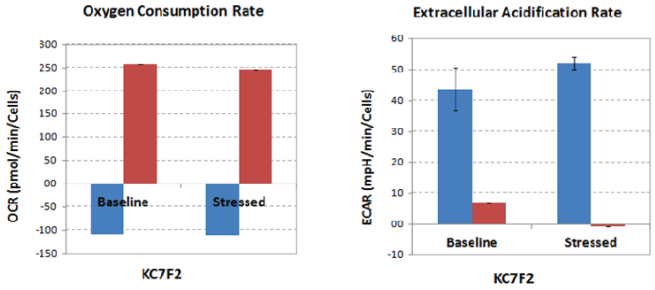

Figure 1. Seahorse XFp metabolic analysis results of U87MG cells after KC7F2 treatment

DISCUSSION

Recent studies have revealed that aldolase family members have abnormal expression or translocation that helps signal transduction in tumor progression. The suppression of PRPS1L1 expression on different cancer cell types has been determined in different studies which is in agreement with our data. Studies have shown that decreased expression of PYGL, the catabolic enzyme, results in accumulation of glycogen associated with low proliferation and low survival induction [Favaro et al. 2012]hypoxia induced an early accumulation of glycogen, followed by a gradual decline. Concordantly, glycogen synthase (GYS1. These data increase the likelihood that PYGL has an essential activity for glycogen degradation in HIF-1α over expressed cells. The data we obtained supports this idea.

Warburg has revealed that metabolic mechanism, among all other known mechanisms for cancer cells, is of great importance in the process of cancer, and numerous studies on this subject prove the importance of this theory. In our study, the effect of HIF-1α inhibition on cancer metabolism was investigated by applying KC7F2 to U87MG cells to reveal the expression changes of metabolism pathway genes.

CONCLUSION

In this study, the effect of HIF-1α inhibitor on metabolism was evaluated, suggesting that the data obtained from both metabolic and gene expression profiles would contribute to the studies to be done in this regard.

ACKNOWLEDGEMENTS

CONFLICT OF INTEREST

No potential conflict of interest was reported by the authors.

REFERENCES

1. Chang, Julie E, Deepak Khuntia, H Ian Robins, and Minesh P Mehta. Radiotherapy and Radiosensitizers in the Treatment of Glioblastoma Multiforme. "*Clinical Advances in Hematology & Oncology*" *:* 2007. *H&O* 5 [11]: 894–902, 907–15.
2. Chang, Yu-Chan, Hsing-Fang Tsai, Shang-Pen Huang, Chi-Long Chen, Michael Hsiao, and Wen-Chiuan Tsai. "Enrichment of Aldolase C Correlates with Low Non-Mutated IDH1 Expression and Predicts a Favorable Prognosis in Glioblastomas." *Cancers*. 2019. 11 [9]: 1238.
3. Favaro, Elena, Karim Bensaad, Mei G. Chong, Daniel A. Tennant, David J.P. Ferguson, Cameron Snell, Graham Steers, et al. "Glucose Utilization via Glycogen Phosphorylase Sustains Proliferation and Prevents Premature Senescence in Cancer Cells." *Cell Metabolism*. 2012. 16 [6]: 751–64.
4. Karcher, Sibylle, Hans-Herbert Steiner, Rezvan Ahmadi, Saida Zoubaa, Gergely Vasvari, Harry Bauer, Andreas Unterberg, and Christel Herold-Mende. "Different Angiogenic Phenotypes in Primary and Secondary Glioblastomas." *International Journal of Cancer*. 2006. 118 [9]: 2182–89.
5. KORNBERG, A, I LIEBERMAN, and E S SIMMS. "Enzymatic Synthesis and Properties of 5-Phosphoribosylpyrophosphate." *The Journal of Biological Chemistry*. 1955. 215 [1]: 389–402.
6. Lawrence, J C, and P J Roach. "New Insights into the Role and Mechanism of Glycogen Synthase Activation by Insulin." *Diabetes* 46. 1997. [4]: 541–47.
7. Li, Chen, Zhongjie Yan, Xuhua Cao, Xiaowei Zhang, and Liang Yang. "Phosphoribosylpyrophosphate Synthetase 1 Knockdown Suppresses Tumor Formation of Glioma CD133+ Cells Through Upregulating Cell Apoptosis." *Journal of Molecular Neuroscience* 60. 2016. [2]. Springer US: 145–56.
8. Schröder, R, K Bien, R Kott, I Meyers, and R Vössing. "The Relationship between Ki-67 Labeling and Mitotic Index in Gliomas and Meningiomas: Demonstration of the Variability of the Intermitotic Cycle Time." *Acta Neuropathologica* 82. 1991. [5]: 389–94.
9. Schultz, Stacey, Gregory S Pinsky, Nancy C Wu, Marc C Chamberlain, A Sonali Rodrigo, and Sue E Martin. "Fine Needle Aspiration Diagnosis of Extracranial Glioblastoma Multiforme: Case Report and Review of the Literature." *CytoJournal* 2. 2005. [1]: 19.
10. Warburg, O. "The Metabolism of Carcinoma Cells." *The Journal of Cancer Research* 9. American Association for Cancer Research Journals: 1925. [1] 148–63.
11. Warburg, O, F Wind, and E Negelein. "THE METABOLISM OF TUMORS IN THE BODY." *The Journal of General Physiology* 8. 1927. [6]. The Rockefeller University Press: 519–30.
12. Winter, S. C., F. M. Buffa, P. Silva, C. Miller, H. R. Valentine, H. Turley, K. A. Shah, et al. "Relation of a Hypoxia Metagene Derived from Head and Neck Cancer to Prognosis of Multiple Cancers." *Cancer Research* 67. 2007. [7]: 3441–49.

OP-21

PEPTIDE LINKER CHARACTERISTICS OF AN ANTI-VEGF SCFV ANTIBODY AFFECTS BOTH ITS BIOPHYSICAL PROPERTIES AND EFFICACY IN CANCER

Murat Karadağ[2], Merve Arslan[2], Dilara Karadağ[1], Sibel Kalyoncu[1]

[1]Izmir Biomedicine And Genome Center, Izmir, Turkey

[2]Izmir Biomedicine And Genome Center; Dokuz Eylul University, Izmir, Turkey Biomedicine And Genome Institute, Izmir, Turkey

OBJECTIVES: Single-chain variable fragment (scFv) is one of the most useful antibody fragments for therapeutic and diagnostic applications due to its small size and availability of protein engineering approaches. scFv is a fusion protein of variable domains of the heavy (VH) and light chain (VL) of immunoglobulins, where they are linked by a flexible peptide linker. Solubility, stability, and affinity are important characteristics in antibody engineering, we hypothesize that the linker between VH and VL can be engineered to improve biophysical characteristics of the entire antibody. Anti-Vascular Endothelial Growth Factor (VEGF) antibodies are important antiangiogenic drugs used in cancer treatment. In this study, we varied both the length and amino acid composition of the linker of an anti-VEGF scFv to see whether it would affect key biophysical characteristics and drug efficacy.

MATERIAL&METHODS: Recombinant DNA constructs were prepared for anti-VEGF scFvs with differences in linker sequences. Bacterial expression was performed by an autoinduction condition. Expressed scFvs were purified through affinity chromatography and biophysically characterized based on affinity, solubility, and stability. Produced scFvs were administrated to zebrafish models in order to observe angiogenic efficacy.

RESULTS: Preliminary results show that more flexible linker caused increased production yield, stability and affinity of antibodies. We realized that flexibility is more important than the content of the linker. Interestingly, scFvs also showed different efficacies based on our preliminary zebrafish study.

CONCLUSIONS: This study emphasizes the importance of linker engineering in antibody fragment design and demonstrates that linkers might play an active role from early to late stage development stages.

Keywords: Antibody; Antibody fragments; Single chain variable fragment (scFv); Linkers; Cancer; Angiogenesis; Vascular Endothelial Growth Factor (VEGF)

OP-22

FDG PET/CT METABOLIC PARAMETERS CAN PREDICT THE RECURRENCE IN PATIENTS WITH N0 LUNG ADENOCARCINOMA

Ahmet Yanarateş
University Of Health Sciences, Izmir Dr. Suat Seren Chest Diseases And Surgery Training And Research Hospital, Department Of Nuclear Medicine, Izmir, Turkey

OBJECTIVES: The purpose of this study was to investigate the value of metabolic parameters detected on PET/CT in the diagnosis of recurrent disease in patients with histopathologically lung adenocarcinoma without lymph node metastasis.
MATERIAL&METHODS: Forty-nine patients with adenocarcinoma of the lung without lymph node metastasis and who underwent curative surgery were included in the study. Maximum standardized uptake value (SUVmax), metabolic tumor volume (MTV) and total lesion glycolysis (TLG) values of primary tumor detected on pretreatment PET / CT were calculated. Metabolic PET parameters of patients with recurrence and disease-free cases were compared with t test. A receiver operating characteristic curve was plotted to determine the optimal cutoff value.
RESULTS: The study included 49 patients (mean age 64 ± 5.1 years) with a diagnosis of lung adenocarcinoma (28 male, 21 female). Recurrent disease was detected in 18 of 49 patients during 36 ± 7.4 months follow-up. SUVmax (p: 0.012), MTV (p: 0.004) and TLG (p: 0.002) values of patients with recurrent disease were significantly higher than those without disease. The optimal cut off values were determined 8.70, 17.63 and 42.52 for SUV max, MTV and TLG, respectively.
CONCLUSIONS: High metabolic pretreatment PET parameters may predict recurrence in patients with early-stage lung adenocarcinoma undergoing curative surgery. Therefore, in patients with high metabolic parameters, risk of recurrence should be kept in mind and patients should be evaluated for adjuvant treatment after curative surgery to reduce the recurrence rate.
Keywords: PET/CT, lung adenocarcinoma, SUVmax, MTV, TLG

OP-23

VOLUMETRIC PET/CT PARAMETERS PREDICT OVERALL SURVIVAL IN STAGE 3A NON-SMALL CELL LUNG CANCER

Emine Budak
University Of Health Sciences, Izmir Dr. Suat Seren Chest Diseases And Surgery Training And Research Hospital, Department Of Nuclear Medicine, Izmir

OBJECTIVES: The present study evaluates the prognostic value of metabolic F18-FDG-PET/CT parameters in patients with stage IIIA non-small cell lung cancer(NSCLC).
MATERIAL&METHODS: Eighty patients who underwent curative surgery with or without neoadjuvant therapy and were histopathologically diagnosed as stage 3A NSCLC with N1 or N2 lymph node metastasis were included in this study. All patients had pretreatment PET/CT imaging. Maximum standardized uptake value(SUVmax), metabolic tumor volume(MTV) and total lesion glycolysis(TLG) of primary tumor and whole body (primary tumor+regional lymph nodes) were measured for each patient. Overall survival(OS) curves were drawn using the Kaplan-Meier method. The relationship of PET parameters with OS was evaluated using the Cox proportional hazard model. A receiver operating characteristic curve was plotted to determine the optimal cutoff values.
RESULTS: The study included 80 patients (35 female, 45 male, 62±2.3 mean age) with stage 3A NSCLC. The mean follow up time was 32±1.7 months. Of the total sample, 60 died at the time of the analysis. Higher MTV and TLG values of both primary tumor (HR= 1.3, P=0.023 for MTV and HR= 1.2, P=0.032 for TLG) and whole body (HR= 1.7, P=0.012 for MTV and HR= 1.5, P=0.020 for TLG) were significantly associated with poorer OS. SUVmax of neither primary tumor nor whole body was not predictor of prognosis.
CONCLUSIONS: The volume-based PET parameters (MTV and TLG) better reflecting the tumor burden were found to be more predictive for OS than SUVmax in patients with stage 3A NSCLC. Patients with high MTV and TLG values should be evaluated for adjuvant therapy.
Keywords: MTV, non small cell lung cancer, overall survival, PET/CT, SUVmax, TLG

OP-24

MEASUREMENT OF HER2/NEU ONKOGEN AMPLIFICATION AND P53 TUMOR SUPRESSOR GENE DELETION QUANTITATITEVELY WITH REAL TIME PCR IN THE PATIENTS OF BREAST CANCER AND ITS COMPARISON WITH PROGNOSTIC FACTORS

Gözde Ülfer
İstanbul Medipol University, faculty Of Medicine, department Of Biochemistry, İstanbul, Turkey

OBJECTIVES: In this study HER2/neu oncogene and p53 tumor suppressor gene which have been important for the prognosis in breast cancer were investigated. The study was made retrospectively on 50 patients. In all of the patients histological type of the tumor, tumor grade, size of the tumor, lymph node invasion, estrogen receptor (ER) and progesterone receptor (PR) results evaluated by immunohytochemistry (IHC) were previously known. Presence of HER2/neu oncogene amplification and p53 tumor suppressor gene deletion which are today routinely detected by immunohystochemistry (IHC) methods, were measured by the method RT-PCR, assaying gene copy number quantitatively. The relationship between HER2/neu oncogen amplification and p53 tumor suppressor gene deletion were assayed and compared with histopathological prognostic factors.
MATERIAL&METHODS: The Sections obtained from tumor paraffinized blocks were prepared on microscopeslides and then DNA of the tumor tissues were isolated.DNA samples obtained from 50 patients were studied in "LightCycler" device by RT-PCR technique by an appropriate PCR programme to detect HER2/neuonkogene amplification and p53 tumor suppressor gene deletion.
RESULTS: In patients the correlation of HER2/neu oncogene amplification and p53 tumor suppressor gene deletion which were both measured by RT-PCR methods was found insignificant (p>0, 05).There was also no significant correlation between HER2/neu oncogene amplification and p53 tumor suppressorgene deletion with tumor's grade, tumor's size, lymphnode invasion, ER and PR status (p>0.05). IHC and RT-PCR method were compared and it was found significant(p<0.05).
CONCLUSIONS: But presence of high grade tumor was detected in patients who have HER2/neu oncogene amplification and p53 tumor suppressor gene deletion together.
Keywords: HER2/neu Onkogen, p53 Tumor Supressor Gene, Real Time PCR

OP-25

CANCER ASSOCIATED FIBROBLASTS INFLUENCE THE MACROPHAGE POLARIZATION IN BREAST CANCER

Gurcan Gunaydin
Hacettepe University, Department of Basic Oncology, Ankara

OBJECTIVES: Monocytes differentiate into M1/M2-macrophages. Tumor-associated-macrophages resemble M2-macrophages. Identification of mechanisms affectting macrophage-plasticity in cancer-microenvironment may provide crucial information concerning diagnostic and therapeutic strategies against cancer. Thus, this study aims to determine the effects of cancer-associated-fibroblasts(CAFs) on macrophage-polarization in breast-cancer.
MATERIAL&METHODS: Collagenase/Hyaluronidase were used to isolate normal-fibroblasts(NFs)/CAFs;from patients undergoing reduction-mammoplasty or total-mastectomy. Immunocytological-examinations were performed to investigate differential-expressions of surface-markers such as ykrk7-SMA, vimentin;to distinguish CAFs/NFs. Conditioned-mediums(CMs) were obtained from CAFs/NFs. Magnetic-bead-based-selection-protocols were utilized to isolate CD14+ monocytes and CD4+ T-cells from PBMCs (from healthy-volunteers). Flow-cytometry was performed for CD206, CD163. CFSE-labelled CD4+ T-cells (CD3/CD28-magnetic-bead-activated) were utilized to investigate the functional effects of CAF/NF-educated-monocytes on CD4+ T-lymphocytes. Migration-assays with Transwell-chambers were used to determine the effects of CAFs/NFs on monocyte-recruitment. Western-blot was utilized to examine E-cadherin, vimentin protein-expressions. Transwell-inserts were used to analyze MDA-MB-231 breast cancer-cell-invasion.
RESULTS: CAFs expressed ykrk7-SMA unlike NFs. CAFs effectively recruited monocytes. MCP-1 or SDF-1 cytokines might be responsible from this recruitment, because MCP-1 or SDF-1 inhibition thorugh MCP-1 or CXCR4 (a-chemokine-receptor-specific for SDF-1) blocking-antibodies, significantly reduced monocyte-migration. CAF-educated-cells' expressions of CD163, CD206 (associated-with M2-macrophages) were higher than NF-educated-cells. CAF-educated-monocytes suppressed T-cell-mediated immune-responses. CAF-

educated-monocytes increased breast-cancer cell-invasion, unlike NF-educated-monocytes. CAF-educated-monocytes increased vimentin-expression; decreased E-cadherin-expression in breast-cancer-cells. Finally, CAFs differentiated M1-macrophages to M2-like-macrophages, since CD163-expression significantly increased in M1-macrophages due to CAFs.
CONCLUSIONS: CAFs differentiated monocytes to M2-like pro-tumoral macrophages phenotypically and functionally; unlike NFs. CAFs were very effective in recruiting monocytes. Monocyte-chemotactic-protein-1 (MCP-1) and stromal-cell-derived-factor-1 (SDF-1) may prove to be crucial monocyte chemotactic cytokines, which are secreted from stromal-cells.
Keywords: breast cancer, cancer-associated-fibroblasts, monocytes, macrophages, tumor microenvironment

OP-26
A TMB EXPERIENCE IN A PATIENT DIAGNOSED WITH EWING SARCOMA

Nadide Cemre Randa
Antalya Training And Research Hospital, Medical Genetics, Antalya

OBJECTIVES: We performed 'tumor mutation burden (TMB)' analysis to determine if immunotherapy could be given to our patient (30 years old, white male) who was diagnosed as Ewing sarcoma.
MATERIAL&METHODS: DNA extracted from both peripheral blood and tumor biopsy tissues. WES analysis performed with both DNA samples. All variants (Benign/Likely benign/VOUS/Likely Pathogenic/Pathogenic) counted in excel file from both DNA samples. TMB was calculated according to definitions in the literature.
RESULTS: TMB was calculated as 27. Our patient has been receiving immunotherapy for 2 months. We are waiting for oncologists' evaluation results to assess drug response.
CONCLUSIONS: Checkpoint blockade therapies induce immune responses against cancer cells. Recently, several immune checkpoint inhibitors approved by the FDA and their targets are cytotoxic T lymphocyte-associated antigen 4 (CTLA-4) and programmed cell death 1 (PD-1) or its ligand PD-L1. Immunotherapy has potential to treat all cancers and offers the possibility for long-term control of cancer. Due to its treatment potential, so many studies has been done and there are still many on-going clinical trials. For example, 2250 clinical trials are evaluating PD-1/L1 immune checkpoint inhibitors, an increase of 748 trials over the past year. 240 drug targets are being evaluated in the current landscape, 75 more than a year ago. The TMB score must be calculated before making an immunotherapy decision. According to clinical trials, there is a correlation between TMB score and drug response. In spite of all these developments, since it is a very new method, standardization and harmonization between centers is required for calculation of TMB.
Keywords: Immune Check Point Inhibitors, Immunotherapy, Tumor Mutation Burden

OP-27
EVALUATING THE METHYLATION STATUS OF RB1 GENE PATIENTS WITH RETINOBLASTOMA

Ozge Sukruoglu Erdogan[1], Betul Celik[1], Seref Bugra Tunçer[1], Seda Kılıç[1], Demet Akdeniz[1], Sema Büyükkapu Bay[2], Samuray Tuncer[3], Rejin Kebudi[2], Hulya Yazici[1]
[1]Istanbul University, Oncology Institute, Department Of Basic Oncology, Division Of Cancer Genetics, Istanbul, Turkey
[2]Istanbul University, Oncology Institute, Division Of Pediatric Hematology-oncology, Istanbul, Turkey
[3]Istanbul University, Istanbul Medical Faculty, Department Of Ophthalmology, Istanbul, Turkey

OBJECTIVES: The most frequently diagnosed malignant ocular tumor of infancy and childhood is Retinoblastoma. Due to the mutation on the q14 on chromosome 13 causes the retinoblastoma. There are two types of basic gene mutations: genetic and sporadic. This cancer is initiated by RB1 mutation, responsible for the cell cycle regulation and genome stability in the cells of the retina in children under 5 years old. The retinoblastoma comprises about 40% inherited mutations, 10% of germline mutations of RB1 inherited from an affected parent, and 30% from de-novo germline mutations.
MATERIAL&METHODS: Methylation of the RB1 gene on promoter region is unknown. The results obtained by MLPA analysis and sequence analysis were investigated for RB1 gene methylation in patients without RB1 mutation. The methylation determination is done with OneStep qMethyl-PCR Kit using a Real-Time PCR system. Methylation changes were investigated in peripheral blood samples of 60 patients with retinoblastoma, 18% of the patients (11/60) had bilateral and 82% of patients (49/60) had unilateral disease and 52 healthy controls.
RESULTS: The mean methylation levels of 60 retinoblastoma patients and 52 healthy controls were 35% and 34%, respectively. Mann Whitney U test was compared between the patient and healthy controls and no statistically significant difference was detected between the two groups ($p = 0.882$).
CONCLUSIONS: The promoter methylation levels in RB1 gene patients having familial history was believed to be large deletion and duplication and small indel absence mutations in the RB1 gene are not effective especially in the etiology of heritable retinoblastoma.
Keywords: Retinoblastoma, RB1 gene mutation, Promoter Methylation

OP-28
TRPV1 CHANNELS: POTENTIAL TARGET IN THE CHEMOTHERAPEUTIC PAIN

Bilal Çiğ
Süleyman Demirel Üniversitesi Tıp Fakültesi Biyofizik, Isparta, Turkey

OBJECTIVES: The transient receptor potential subfamily Vanilloid member 1 (TRPV1), also known as the capsaicin receptor, responds to chemical and thermal stimuli as the molecular transducer of nociceptive signals (Julius and Basbaum, 2001). This channel was first discovered in mouse DRGs by activation of high temperature and hot chili pepper component (capsaicin) (Caterina et al, 1997). In addition to capsaicin and high temperature (> 43?C), extracellular cations can be activated by different stimuli such as lipids, low pH (<5.9), oxidative stress causing pain perception (Tominaga et al., 1998).
MATERIAL&METHODS: Numerous studies on inflammation and nerve damage have shown that it increases TRPV1 mRNA and protein levels in DRG neurons. In this context, TRPV1 may contribute to the development of mechanical and thermal hyperalgesia in neuropathic pain due to the use of chemotherapeutic drugs (Chukyo et al., 2018).
RESULTS: Chemotherapy induced peripheral neuropathy (CHIN), which is a highly debilitating symptoms without effective treatment, impairs quality of life by affecting 50% of patients treated with many commonly used chemotherapy drugs.
CONCLUSIONS: The etiology of painful neuropathy due to chemotherapy remains unclear. Existing analgesic drugs may provide partial analgesic effects in some patients, but have not completely relieved pain. Therefore, instead of symptomatic treatment, mechanism-based approaches are needed by exploring the molecular mechanisms of this type of pain. Thus, the discovery of new therapeutic agents against painful neuropathy caused by chemotherapy is an urgent issue. In this presentation, we will discuss the roles of TRPV1 cation channels in chemotherapy-induced neuropathic pain.
Keywords: TRPV1; Capsaicin; Chemotherapy; Pain; Neuropathy

OP-29
THE EFFECTS OF HYPERFORIN ON PROLIFERATION RATE AND SOCE IN HUH-7 HUMAN HEPATOCELLULAR CARCINOMA CELLS

Damla Getboğa, Mine Kocabıyık, Yasemin Eraç
Ege University, Department of Pharmacology, İzmir, Turkey

OBJECTIVES: The purpose of our study was to investigate the effects of hyperforin which is the specific activator of the transient receptor potential canonical 6 (TRPC6) channel on proliferation rate and store-operated calcium entry (SOCE) in Huh-7 human hepatocellular carcinoma cell line.
MATERIAL&METHODS: The effects of hyperforin on the proliferation of Huh-7 cells were examined with real-time cellular analysis (xCELLigence). In addition, following hyperforin incubation, sarcoplasmic/endoplasmic reticulum Ca²ykrk15 ATPase blocker cyclopiazonic acid (CPA)-induced changes in intracellular Ca²ykrk15 levels were monitored in fura-2 loaded Huh-7 cells. Real-time quantitative RT-PCR was performed to determine TRPC1 and TRPC6 mRNA levels.

RESULTS: 1 µM hyperforin did not inhibit the proliferation rates of Huh-7 cells at 10000 cells/well. However, higher concentrations of hyperforin (5 µM and 10 µM) caused a significant decrease in proliferation rate. CPA-induced SOC was significantly increased in hyperforin incubated Huh-7 cells compared to control cells. According to the PCR results, hyperforin significantly increased TRPC1 mRNA levels. Although not statistically significant, TRPC6 mRNA levels were apparently increased with hyperforin incubation.
CONCLUSIONS: These results showed that the antiproliferative effects of hyperforin are dependent on concentration. Furthermore, hyperforin may have a role in activation and regulation of store-operated Ca²ykrk15 entry in hepatocellular carcinoma cells.
Keywords: Calcium, Cancer, Hepatocellular carcinoma, Proliferation, TRPC6

OP-30

THE EFFECT OF INFILTRATION PATTERN OF T CELLS ON SURVIVAL OUTCOMES IN METASTATIC PANCREATIC CANCER PATIENTS

Derya Kıvrak Salim[1], Canan Sadullahoğlu[2],
[1]University Of Health Sciences, Antalya Education And Research Hospital, Medical Oncology Department Antalya
[2]University Of Health Sciences, Antalya Education And Research Hospital, Pathology Department Antalya, Turkey

OBJECTIVES: Present study aims to determine the effect of T cell infiltration pattern on survival outcomes in metastatic pancreatic cancer patients.
MATERIAL&METHODS: Metastatic pancreatic cancer patients who had adequate tumor tissue samples for immune-histochemical analysis were included in the study. Immunohistochemistry was performed for markers of (CD8, CD4, CD25, FOXP3) T cell subsets on deparaffinized tissue sections. Intratumoral and peritumoral distribution of T cells were counted.
RESULTS: Peritumoral CD4+ and CD8+ T cell density were higher than intratumoral densities whereas CD25+ and FOXP3+ Treg cell densities were comparable in number in both areas. Intratumoral CD4+ T helper cell density >16.8 is associated with improved overall survival (p <0.001). Intratumoral CD8+ cytotocic T cell density >19.6 is also associated with better overall survival (p=0.018). Intratumoral or peritumoral FOXP3+ Treg densities did not differ on overall survivals (p=0.179, p=0.330 respectively). Peritumoral CD8+ T cell density did not effect on overall survival and progression free survival (p=0.99, p=0.16 respectively) whereas CD4+ T helper cell density >41.8 had improved overall survival and progression free survival (p=0.003, p=0.011 respectively). Multivariate analysis showed that intratumoral CD4+ T cell density <16.8 had increased death risk (HR 3.27; 95%CI, 1.17 to 9.15; p=0.024) and CD8+ T cytotoxic cell gradient <0.47 had increased progression risk (HR 2.43; 95%CI, 1.3 to 4.55; p=0.005).
CONCLUSIONS: FOXP3+ Treg distribution did not differ in intra or peritümoral area. Lower intratumoral CD4+ T cell density and lower CD8+ T cytotoxic cell gradient showed bad prognostic significance.
Keywords: pancreatic cancer, T cell response, survival, treatment response

Figure 1

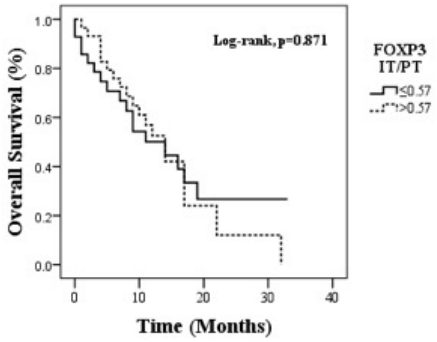

FOXP3 gradient and OS

Table 1 Patient Demographics

Age, median(min-max)	66(47-86)
Gender (Male/Female)	37(59.7)/ 25(40.3)
ECOG PS, median(min-max) <2 ?2	1(0-3) 43(69.4) 19(30.6)
Tumor size, median(min-max)	3(1-9.5)
LVI, n(%)	49(80.3)
PNI, n(%)	57(93.4)
Grade, n(%) 1 2 3	1(1.6) 54(88.6) 6(9.8)
PT, median(min-max) CD4PT CD8PT CD25PT FOXP3PT	41.8(0-181) 47.4(0-122) 6.1(0-52.8) 2.9(0-62.8)
IT, median(min-max) CD4IT CD8IT CD25IT FOXP3IT	16.8(0-216) 19.6(0-100) 4.3(0-33) 2.2(0-27)
Gradient CD4 IT/PT CD8 IT/PT CD25 IT/PT FOXP3 IT/PT	0.39(0.04-2.3) 0.47(0.04-1.76) 0.79(0.1-5.75) 0.57(0-14)

LVI: lymphovascular invasion, PNI: perineural invasion, PT: Peritumoral infiltration, IT: Intratumoral infiltration

OP-31

CHEK2 MUTATION IN BREAST/OVARIAN CANCER

Şeref Buğra Tunçer, Demet Akdeniz Ödemiş, Seda Kılıç, Özge Şükrüoğlu Erdoğan, Betül Çelik, Gözde Kuru Türkcan, Yasemin Gider, Mukaddes Avşar, Hülya Yazıcı
Istanbul University, Oncology Institute, Department Of Basic Oncology, Division Of Cancer Genetics, Istanbul, Turkey

OBJECTIVES: The germline mutations in some genes are associated with the development of certain types of cancer and the most common type of these is hereditary breast/ovarian cancer caused by germline mutations in the breast cancer susceptibility genes BRCA1 and BRCA2. CHEK2 often considered to be a third specific gene in breast and ovarian cancer, is being investigated in many societies such as Europe, America and Russia, whether it is related to the pathogenesis of breast and especially ovarian cancer.
MATERIAL&METHODS: A total of 1196 patients, including 1080 patients with breast cancer and 116 patients with ovarian cancer, were included in this study. Demographic, environmental, family history and reproductive characteristics of all patients were taken into account. Patients were screened for BRCA1, BRCA2 and CHEK2 1100delc mutation by multiple ligation-dependent probe amplification test.
RESULTS: In this study, the mean age of diagnosis of breast cancer patients was 41, while the average age of ovarian cancer patients was 50, 1. In the study population, BRCA1, BRCA2 and CHEK2 1100delc mutations were screened and all patients were found negative for BRCA2 gene and CHEK2 1100delC mutation.
CONCLUSIONS: According to many studies conducted on screening of breast and ovarian cancer patients with familial history, CHEK2 1100delC mutation rates for many populations in ovarian cancer are given as well as helps the awareness of in breast cancer and emphasized the importance of cancer development. As a result of our study to determine the CHEK2 1100delC mutation rate in Turkish society, it was decided that this mutation was very rare for our society.
Keywords: CHEK2 mutation, breast cancer, ovarian cancer

OP-32

NEW CANDIDATE GENE THAT MAY BE EFFECTIVE IN AGGRESSIVE TUMOR PROGRESSION IN RETINOBLASTOMA

Demet Akdeniz Odemis[1], Seref Bugra Tuncer[1], Rejin Kebudi[2], Betul Celik[1], Gozde Kuru Turkcan[1], Seda Kilic Erciyas[1], Ozge Sukruoglu Erdogan[1], Mukaddes Avsar[1], Sema Buyukkapu Bay[2], Samuray Tuncer[3], Hulya Yazici[1]
[1]Istanbul University, Oncology Institute, Department Of Basic Oncology, Division Of Cancer Genetics, İstanbul, Turkey
[2]Istanbul University, Oncology Institute, Division Of Pediatric Hematology-oncology, İstanbul, Turkey
[3]Istanbul University, Istanbul Medical Faculty, Department Of Ophthalmology

OBJECTIVES: Various molecular changes in Fibroblast Growth Factor Receptor 4 gene that is known with its oncogenic transformation activity are known to result with different gene variants. To investigate the potential candidate variant of c.1162G>A that is known to have a role in cancer progression and retinal development in the tumor development and progression in patients diagnosed with retinoblastoma who had no RB1 gene mutation.
MATERIAL&METHODS: c.1162G>A variant was bi-directionally sequenced using the Sanger sequencing in 49 retinoblastoma patients with no mutation in RB1 gene, in their first degree 13 healthy relatives, and in 146 individuals who were matched for sex and age in the control group.
RESULTS: c.1162G>A variant was found positive in about 55% of patients, and mutation was detected in 54% of healthy relatives of the patients in our study. Mutation was detected in 48% individuals in the evaluation of the c.1162G>A mutation in healthy controls. Although c.1162G>A allele frequency was detected as 30% in general population in different databases, we demonsrated the frequency as 50% in Turkish population in our study.
CONCLUSIONS: c.1162G>A allele was significantly higher in patients who were diagnosed with retinoblastoma before the month 24, and in advanced stage patients. In conclusion, these results suggested that c.1162G>A polymorphism might have a role in aggressive tumor progression, and in tumor development.
Keywords: retinoblastoma, Fibroblast Growth Factor Receptor 4 gene , mutation

OP-33

THE RELATIONSHIP BETWEEN S100A4 C-TERMINAL REGION AND BREAST CANCER

Seda Kılıç Erciyas, Özge Şükrüoğlu Erdoğan, Demet Akdeniz, Şeref Buğra Tuncer, Betül Çelik, Mukaddes Avşar Saral, Gözde Kuru Türkcan
[1]Istanbul University, Basic Oncology Department, Istanbul, Turkey

OBJECTIVES: The S100A4 gene, a calcium binding molecule, has been reported in the literature to be associated with metastasis. S100A4 gene C-terminal region sequence and total serum calcium levels were investigated in this study.
MATERIAL&METHODS: 141 samples from 117 patients and 16 control samples were examined by C-terminal region sequence analysis method. and total serum calcium levels were measured by quantitative colorimetric method.
RESULTS: Total calcium levels of DCIS group and metastatic group have been found significantly (p<0, 001) lower than the control group. The statistical significance (p<0, 001) have also been found to exist both among the patients with DCIS and patients with metastatic breast cancer. Moreover, serum calcium levels of patients with bone metastasis were found significantly (p<0, 001) higher than the rest of metastasis group.
CONCLUSIONS: The absence of a change in the C-terminal region of the S100A4 gene suggests that the S100A4 gene does not function alone to increase metastatic activity. Therefore, it is necessary to investigate which proteins interact with the S100A4 after calcium binding and the pathway of the interacted molecules. Higher calcium concentration on metastatic breast cancer cases suggest that it cause metastasis by triggering some other impaired pathways in cancer.
Keywords: S100A4, cancer, breast, calcium, mutation

OP-34

INVESTIGATION OF METABOLITE LEVELS IN TCA CYCLE AND GLYCOLYSIS IN COLON CANCER CELL LINES

Esra Bulut Atalay[1], Hülya Ayar Kayalı[2, 3]
[1]Izmir International Biomedicine And Genome Institute, Dokuz Eylül University, İzmir, Turkey
[2]Izmir Biomedicine And Genome Center, İzmir, Turkey
[3]Dokuz Eylül University, Department Of Chemistry, İzmir, Turkey

OBJECTIVES: In the present project, the level of some TCA cycle and Glycolysis intermediate products (glucose, ykrk7-ketoglutarate, citrate, succinate, fumarate, malate, and pyruvate) will be investigated in primary (Caco-2) and metastatic character (SW620) colorectal cancer cell lines and the obtained data will be compared with colon epithelial cell line (CCD18Co). Besides, the transformation of 2-Hydroxyglutarate (2HG) from ykrk7-ketoglutarate with the mutant IDH enzyme was also investigated and the results were compared between colon cancer cell lines at different stages and epithelial cell line, as well.
MATERIAL&METHODS: Metabolites were extracted from cells by the freezing-thawing method and their levels were determined by an HPLC system with Alltech OA-1000 column on the UV detector.
RESULTS: Significant differences were observed especially in the levels of citrate and 2HG metabolites between cancer and epithelial cell lines. The citrate metabolite level in the SW620 is 340.6 ppm, while the CCD18Co is 24.4 ppm. Besides, the 2HG metabolite was synthesized and immediately transferred to the nutrient medium in CCD18Co while it was deposited in the cancer cells.
CONCLUSIONS: Metabolites emerge as essential components of communication between the mitochondria and the nucleus. They can be increased or decreased by the effect of genetic changes. Thus, it activates tumorigenesis and directs the cell to cancer. With this project, for the first time, the determination of metabolite levels in colon cancer cell lines were studied. When the results of the project are evaluated, 2HG metabolites may be a biomarker for early detection of colon cancer.
Keywords: Colon Cancer, Glycolysis, Metabolite, TCA cycle

OP-35

INVESTIGATION OF CELL POPULATIONS IN AN {IN VITRO} INTRATUMORAL HETEROGENEITY MODEL OF SOLID TUMORS

Öykü Gönül Geyik[1], Darawalee Wangsa[2], Thomas Rıed[2], Zeynep Yüce[1]
[1]Dokuz Eylul University, Medical Biology And Genetics Department, İzmir, Turkey
[2]National Institutes Of Health, National Cancer Institute, Bethesda, Md, USA

OBJECTIVES: In our study we aimed to generate an in vitro intratumoral heterogeneity model by florescent tagging isogenic subclones derived from the same cancer cell line and co-culturing these clone by which we could investigate the phenotypic behaviours of these clones subsequent to exposure to various therapeutic treatments. We aimed to identify genetic variations that lead to drug resistance in tumors.
MATERIAL&METHODS: Isogenic diploid and tetraploid cell lines were established from the colon cancer DLD1 cell line via FACS-sorting and confirmed by genetic analyses. These subclones were tagged with different florescent plasmid vectors and mixed in equal proportions to co-culture. Genetic properties of clones were determined by chromosome number count, aCGH, miFISH, and SKY. Then various chemotherapeutics (5-fluorouracil, oxaliplatin, irinotecan, paclitaxel ve gemcitabine), radiotherapy, and hypoxia treatments were performed on this co-culture model in order to determine the effects of the therapeutics on cell behaviours (viability, proliferation, migration, invasion, and dedifferentiation). Thus we could designate specific genetic variations could be related to therapy resistance.
RESULTS: Experiments on genetic properties showed that 4N clones have higher number and variety of genomic alterations than 2N clones. Population studies indicated that 4N and 2N clones respond differently both under normal conditions and with therapeutics. Results led us speculate that these responses could be related to specific genetic properties of the clones.
CONCLUSIONS: Addressing the genetic characteristics-especially the ones with relevance to therapy resistance-of different cell clones in the tumor would enable us to target these regions and play a crucial role in improving survival rates of cancer patients.
Keywords: intratumoral heterogeneity, therapy resistance, colorectal cancer